Thermodynamic Model and Initial Experimental Investigation of Air Dehumidification through Electrically Charged Vapor Capturing Electrostatic Droplets

by

Stefano Morcelli

A thesis submitted to the Graduate Faculty of
Auburn University
in partial fulfillment of the
requirements for the Degree of
Master of Science

Auburn, Alabama
May 7, 2022

Keywords:
Dielectrophoresis, Dehumidification, Electrically Charged Droplets, Electrospray, Vapor Capturing

Approved by:
Lorenzo Cremaschi, Chair, Professor of Mechanical Engineering
Sushil Bhavnani, Associate Department Chair of Mechanical Engineering
Nicholas Tsolas, Assistant Professor of Mechanical Engineering

Abstract

The removal of water vapor from the air to reduce relative humidity is a well known indoor environmental comfort requirement. Common dehumidification approaches require a substantial amount of energy and usually involve the cooling of atmospheric humid air below its dew point or the use of absorbent/adsorbent materials to extract water vapor out of the air. More recently, researchers investigated the effect of electrostatic forces for enhancing water vapor condensation with the goal to reduce the energy consumption associated with dehumidification. However, the studies are limited, and there is a lack of correlations that can predict the dehumidification rate.

In this thesis, a broad theoretical investigation to study the electrostatically enhanced condensation processes was carried out. These processes consist of the use of highly charged particles, preferably highly charged water droplets to attract polar water vapor molecules to their surfaces and promote condensation, a phenomenon known as dielectrophoresis. The electrical charge promotes the reduction of the vapor pressure on the droplets' surface with respect to the saturated pressure predicted by the Kelvin equation on curved surfaces and, consequently, the equilibrium between evaporation and condensation is shifted towards condensation.

This investigation resulted in the development of a thermodynamics model, which was able to predict an effective size range of the charged droplets for optimal dehumidification, under ideal conditions. The range resulted in about 2 to 4 μm in diameter, while the electrical charge was kept to the maximum limit predicted by the Rayleigh model. A sensitivity analysis on the variation of the size and the charge of the charged droplets was also performed. In terms of dehumidification rates, when six electrospray heads, i.e. the maximum number of heads tested in the experimental campaign, were considered, the model predicted very limited rates, way lower than the target of this research, i.e. a

dehumidification rate in terms of relative humidity of 5 % with an air flow rate of 5 cfm. While ways to increase this rate existed, their implementation proved difficult for this initial investigation.

According to the requirements predicted by the model, the use of electrosprays appeared the most suitable solution for the production of small but highly charged droplets. The electrospray features and operational modes were studied in detail and an electrospray assembly was designed to be tested in this initial experimental investigation.

For this initial investigation, an experimental system was designed and built to validate the thermodynamics model and with the goal to achieve a dehumidification rate of 5 % in terms of relative humidity with an air flow rate of 5 cfm. The experimental system consisted of a wind tunnel test apparatus, dew point sensors, thermocouples for temperature measurements, pressure sensors and other devices. The experimental system was equipped with a computerized data acquisition and storage system. The system was suitable to evaluate the air water content differential before and after the test section where the electrospray heads were installed. The air water content differential was evaluated in terms of the $\frac{\Delta\omega}{\omega_1}$ ratio, to eliminate the dependence on the dry bulb temperature along the test apparatus.

This work presented initial experimental data for electrostatically enhanced dehumidification processes. Working parameters, such as air and water flow rates, high voltage potentials and polarity, deionized water types with different electrical conductivity, were varied to find the best combination for an improved dehumidification.

With the set up used and the conditions considered, it was never possible to achieve a 5 % dehumidification rate with 5 cfm. In general, the dehumidification rate was always limited and lower than 1 % for all the air flow rates considered and mainly within the uncertainty of the dew point sensors. These results confirmed the already limited predictions of the thermodynamics model, for ideal conditions and the interesting and promising results obtained in some experimental investigations available in the open literature were not achievable in this thesis. The more probable reasons were the higher air flow

rates considered and the complete absence of the use of cooling power, which was mainly implemented to facilitate the vapor condensation.

Acknowledgments

I would like to thank Auburn University and my advisor Dr. Lorenzo Cremaschi for the opportunity to study and conduct research in the United States of America and for the invaluable support I received.

I would like to thank my committee members, Dr. Sushil Bhavnani and Dr. Nicholas Tsolas, and all the members of the research group for their help and support. A special thank you to Joshua and Christian for being friends also outside the lab.

I would like to thank the U.S. Department of Energy's Office of Energy Efficiency and Renewable Energy (EERE) for supporting my research through the Building Technologies Program Award Number DE-EE0009161.

I would like to thank all my family for pushing me to reach something I once thought impossible. Thank you to my dad Erio, the biggest supporter of this adventure, thank you to my sister Laura for her kind words and thank you to my aunts Enrica and Silvana for their English lessons. A special thank you to my mom Catia and my grandfather Antonio for inspiring me by example. Thank you also to my adventure companion Jessica for her invaluable help and kindness.

I would like to thank Dr. Luca Molinaroli, Maxa Air Conditioning and Polytechnic University of Milan for the knowledge and skills they passed to me.

I would like to thank also the Auburn University Sailing Club and its members for making this experience at Auburn University even more remarkable.

Grazie! Thank you!

Table of Contents

List of Tables

List of Figures

Nomenclature

ρ	bulk density liquid	$(\frac{kg}{m^3})$
k	Boltzmann's constant	$(\frac{J}{K})$
N_A	Avogadro's number	$(\frac{1}{mol})$
e	elementary charge	(C)
ε_0	vacuum permittivity	$(\frac{F}{m})$
q	number of elementary charge	(-)
σ	surface tension	$(\frac{N}{m})$
M	molecular weight liquid	$(\frac{kg}{m^3})$
ε_l	relative permittivity bulk liquid	(-)
α	polarizability vapor molecule	$(F * m^2)$
μ_0	permanent dipole moment	$(C * m)$
h_m	mass transfer coefficient	$(\frac{m}{s})$
Q	liquid volume flow rate	$(\mu l/min)$

ρ	997.7	$(\frac{Kg}{m^3})$	k	$1.380649 * 10^{-23}$	$(\frac{J}{K})$
α	$1.61304000 * 10^{-40}$	$(F * m^2)$	ε_0	$8.85418781 * 10^{-12}$	$(\frac{F}{m})$
e	$1.60217662 * 10^{-19}$	(C)	σ	0.07298	$(\frac{N}{m})$
μ_0	$6.18494 * 10^{-30}$	$(C * m)$	ε_l	73.15	$(-)$

Chapter 1: Introduction

1.1 Motivation of Research

The removal of water vapor from the air to reduce relative humidity and improve thermo-hygrometric comfort is a well-known requirement in the heating, ventilation, and air conditioning (HVAC) industry. The most common approach involves the cooling of atmospheric humid air below its dew point temperature and the condensation of the water vapor from the air by passing the moist air through cooled coils. This approach is usually high energy-consuming because of the low temperatures involved. Another known method of removing water vapor from the air is to pass the humid air through an absorbent material that eventually becomes saturated. Also adsorbent materials, such as zeolites and silica gel, may be used for this purpose. These materials are characterized by a limited capacity of water removal and, once saturated, must be discarded or recycled by heating, consuming a significant amount of energy, before reuse. In addition, the implementation of these materials always causes augmented pressure losses in the overall ventilation system. All of the above processes require substantial amounts of energy showing how humidity is a leading environmental factor penalizing the energy performance of HVAC systems.

In order to overcome this main drawback, innovative solutions have to be developed to drastically reduce the energy for dehumidifying the air. Recently, researchers investigated the effect of electrostatic forces for enhancing water vapor condensation and improve heat and mass transfer. In this contest, electrostatically enhanced condensation may be a viable possibility to improve the overall dehumidification process if economical solutions can be provided to remove the water from the air flow and if it can be scalable to air flow rates typical to residential or light commercial applications, i.e. air flow rates higher than 200 cfm. However, the studies available so far were limited, and there was a lack of

correlations that can predict the dehumidification rate as function of the main operating parameters. Also, the findings from the literature focused mainly on small flow rates on the order of 1-2 cfm.

Electrostatically enhanced condensation mainly consists of the use of highly charged particles, preferably highly charged water droplets, to attract polar water vapor molecules to their surfaces, by generating a gradient electric field all around the charged droplets. When water molecules are placed in a gradient electric field, such polar molecules experience a dielectrophoresis force, which moves the molecules and produces a vapor concentration gradient. When the vapor density exceeds the saturation level, nucleation occurs, effectively wiping out the humidity from the air. The high electric charge of the very small water droplets, used as nucleation centers, decreases the pressure of the vapor, which is in equilibrium with the water droplets. Consequently, the equilibrium between evaporation and condensation is shifted towards condensation. The vapor phase near the droplets is then depleted, which is compensated for by the dielectrophoresis flow and vapor diffusion. The charged water droplets' growth and dehumidification are then promoted, without cooling down the air stream below the dew point or increase the pressure losses of the overall system.

In order to further contextualize how the electrostatically enhanced condensation may reduce the energy consumption associated with the dehumidification processes, Fig. 1 shows an illustrative thermodynamics process, where the proposed system is compared to the conventional cooling and dehumidification A/C system.

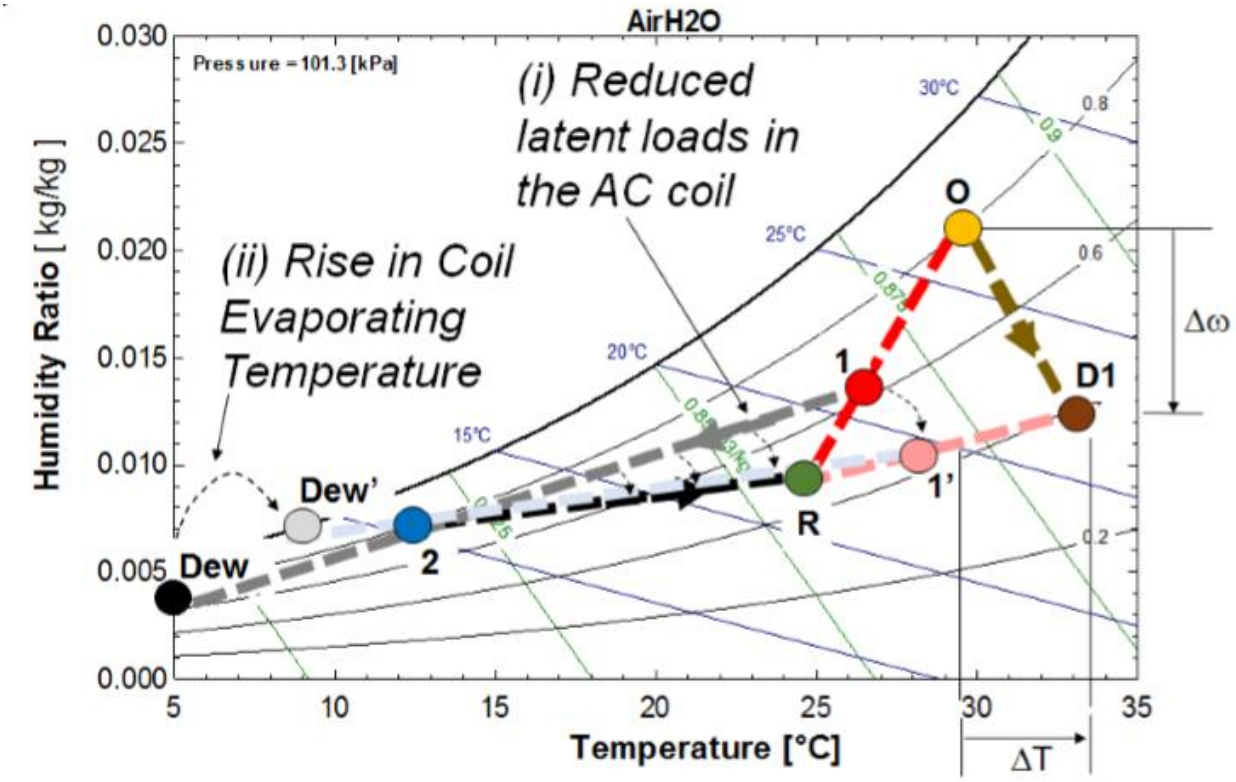

Fig. 1: Example of the cooling and dehumidification process of (a) conventional A/C system (points 0, R, 1, 2, and Dew) and (b) proposed electrostatically enhanced condensation process in a modified A/C system (points 0, R, D1, 1', 2 and Dew')

Avoiding to cool down the atmospheric humid air below its dew point temperature, the electrostatically enhanced condensation process can reduce the cooling coil's latent load and increase the coil evaporating temperature of the A/C unit. This results in the increased energy efficiency of the entire HVAC system, as shown in the comparison of Fig. 1.

The outdoor air (point O) is mixed in the return air (point R) in the conventional A/C system. The coil cools and dehumidifies the air from point 1 to point 2, which represents the design supply conditions. Note that the actual process would be represented by a straight line from point 1 to the saturation curve, followed by a decrease of absolute humidity along the saturation curve and then adiabatic mixing of air due to the coil by-pass factor. The overall cooling and dehumidification process can still be represented by a straight line connecting points 1 to 2 and this line defines the A/C coil sensible to latent heat ratio.

The supply air to the room increases its temperature and humidity from point 2 to point R when it circulates through the room from the supply vents to the return grills, according to the room sensible and latent heat loads.

In the modified A/C system, instead, the outdoor air (point O) is first processed by the innovative electrostatically enhanced device to lead to point D1, drier and warmer, thanks to the action of this device, and is then mixed in the return air (point R). The slight increase in temperature is due to the heat released during the vapor's condensation out of the humid air on the charged droplets. In the psychrometric chart, the new straight line from points 1’ to 2 represents again the cooling and dehumidification process and it clearly indicates a reduction of the latent load that the A/C coil needs to handle. This is shown by a reduction of slope of the aforementioned line if compared to the cooling and dehumidification line in the conventional A/C system. From this point of view, the coil dew point temperature and, consequentially, the evaporating temperature of the coils can be significantly raised, augmenting the COP of the combined system. The overall effect is a higher energy performance for the modified system with respect to the conventional one. As a result, energy savings are promoted and electrostatically enhanced condensation may be a viable way to face the drawbacks associated with dehumidification processes.

The electrostatically enhanced condensation process is then represented by the line connecting points O and D1 in Fig. 1 and it has as a main goal the dehumidification of the outdoor air. As a practical implementation of this process, an Electrospray Vortical Flow eXchanger (EVFX) was envisioned. In this exchanger, electrospray heads were intended to release small highly charged water droplets in optimal velocity-generated air rotating vortexes to attract water vapor and dehumidify the air stream. The charged droplets can then wipe out the humidity from the air, without the high energy consuming requirement to cool down the air stream below its dew point. The larger droplets, grown due to electrostatically enhanced water vapor nucleation and condensation, were effectively removed from the air stream and collected at the outer wall of the exchanger due to the centrifugal force field's action. The collected water was then

re-used in the electrospray heads. As an example, Fig. 2 shows a schematic sketch for the envisioned innovative electrostatically enhanced device. In this device, the humid air is fed radially and the charged water droplets are injected from the outer surface of the device towards its vertical axis. The condensed water is collected at the bottom while drier air is released from the device's central top circular duct.

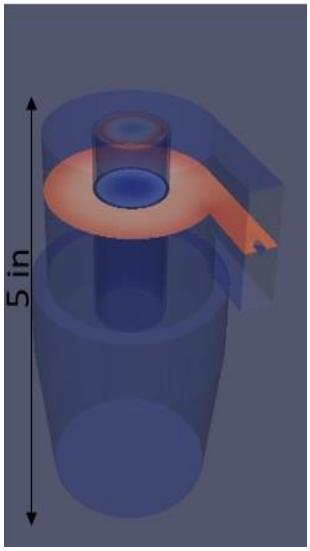

Fig. 2: 3D sketch for envisioned electrostatically enhanced device

The integration of this envisioned device in a conventional A/C system had as overall effect a higher energy performance for the combined system. For example, when applying this approach to buildings in Auburn, AL, U.S.A., and accounting for its temperature bin distribution and high relative humidity during the cooling season, the combined system energy savings over the baseline one were consistent, and estimated between 10 and 20 %. The savings were due to the significant reduction in the humidity of the entering outdoor air, which reduced the latent loads and increased the coils dew point operating temperatures. The additional power consumption due to the fan, pump, and electrospray heads was more than compensated by the reduction of the power consumption in the compressor, due to a higher COP of the A/C unit.

The estimated 10 – 20 % combined system energy savings depended mainly on the ability of the electrostatically enhanced condensation system to provide a dehumidification potential suitable for residential and light commercial applications, where up to 25 % of the loads dehumidifies the air (latent load). In this enhanced system, the energy consumption was mainly associated with the electrical input to power the electrospray heads, used to produce small and highly charged droplets. As it will be seen later in this thesis, the maximum electrospray current per single electrospray head was about equal to 35 μA when a high voltage potential of 20 kV was applied. In this case, the power consumption for single head was equal to 0.7 W. When, instead, lower high voltage potentials were applied or resistors were connected, the power consumption was even lower than the consumption just evaluated. Another source of power consumption was the syringe pump, and its consumption was capped to 12 W for the six (6) syringes pump. However, considering the limited water flow rates delivered by the single syringe in this thesis, a power consumption of about 0.05 W per syringe was expected. This information will be beneficial when the exact number of heads required to reach a target dehumidification rate is known. For instance, in case of 362 heads as predicted by the thermodynamic model to achieve a dehumidification rate of 5 % with 5 cfm, the total power consumption, in the worst case scenario, was equal to 272 W. More likely, the consumption could be even lower if a high voltage potential of 10 kV results enough to dehumidify the air.

1.2 Objectives of Research

The work presented in this MS thesis was conducted as part of a larger research group project. The overarching goal of the group research was to provide the enabling technology required to commercialize electrostatic based water vapor separation systems for decoupling sensible and latent cooling (SSLC) in A/C systems, with the main goal to reduce the energy consumption associated with dehumidification processes. The Electrospray Vortical Flow eXchanger (EVFX) was envisioned for this purpose, for residential and light commercial applications.

This thesis aimed to investigate the potential of the electrostatically enhanced condensation process for humidity control in buildings. In particular, the model developed in this thesis focused to identify a suitable initial diameter range for droplet growth under ideal conditions. The aim was to estimate the maximum droplet growth potential once droplets with appropriate size were injected in the air stream to dehumidify and to predict the number of droplets required to achieve a target dehumidification rate. The model then identified the main controlling parameters, such as droplet size and charge, for an enhanced dehumidification process and provided a brief sensitivity analysis on the effect of the variation of these parameters. Estimating the potential for water vapor condensation on the electrically charged water droplets was a main contribution of the model developed in the present thesis.

During the experimental investigation, a new test apparatus was designed, assembled and calibrated to conduct preliminary proof of concept experiments of air dehumidification. The test apparatus did not implement centrifugal forces for an improved separation of the water droplets from the humid air stream. Rather the focus of this thesis was to model and investigate only the ability of small highly charged droplets to capture and condense water vapor molecules from the humid air. The vapor molecules attraction was supported by dielectrophoresis and diffusion processes. Condensation of water vapor occurred on the surface of the electrically charged droplets. These were the hypotheses that the present thesis aims to verify.

1.3 Research Approach

As a first step, after an extensive literature review, a thermodynamics model that captured this process was developed to explore the controlling parameters of the condensation process. In particular, a suitable range of initial droplet sizes and charge was predicted to maximize dehumidification. The influence of environmental factors, such as air temperature and relative humidity, were also discussed, and the flow rates and the number of electrosprays required to achieve dehumidification were analyzed.

With the results from the thermodynamics model, the most suitable technology for an experimental investigation of electrostatically enhanced condensation process was identified. The electrospray technology was selected to produce the small and highly charged droplets and it was designed and assembled as part of the test apparatus. Its operation was investigated in an experimental facility and safety protocols were developed to prevent hazardous electrical shocks due to the high voltage potentials involved with the technology.

A large experimental facility was used to control the psychrometric conditions of a large recirculating 2ft x 2ft cross section wind tunnel. Some of equipment of this large experimental facility included a chiller and pump module, cooling coils, heaters, humidifiers, and air handling devices. Sensor instrumentation included thermocouples, dew point sensors, mass flow meters, pressure transducers, and visualization devices such as a high speed camera and a high definition CCD camera. The test apparatus was installed within this large wind tunnel.

During the tests, operating parameters were varied in order to validate the previously developed thermodynamics model and identify the best combination of parameters for an improved dehumidification. The finding of this preliminary theoretical and experimental investigation will be essential for an optimal integration of the electrospray technology in the Electrospray Vortical Flow eXchanger (EVFX). As a rule of thumb, the experimental tests aimed to achieve up to 5 % dehumidification rate in terms of relative humidity, with constant air dry bulb temperature and an air flow rate of 5 cfm.

Chapter 2: Literature Review

Electrostatically enhanced condensation was first investigated as enabling technology to produce potable water in remote areas. Only recently, some researchers started investigating its potential in HVAC applications, in particular to dehumidify the air at limited air flow rates. The technology used for these purposes was the electrospray one for the production of small highly charged droplets.

A summary of the relevant work in this important area is provided in this chapter, with particular care of the physics of the phenomenon and the experimental results obtained so far. The main operational features of the electrospray technology are highlighted and some correlations for its characterization are reported. A collection of the main relevant patents in this relatively new field of study are also summarized.

2.1 Condensation on Electrically Charged Nucleus

In 1897, C. T. R. Wilson was among the first ones to note the phenomenon of water vapor nucleation on electrically charged particles. He investigated the nucleation and condensation of water vapor in the presence of dust free air and other gases, noting that water vapor nucleation was enhanced in the presence of electrically charged particles, preferably negatively charged [1, 2]. Afterwards, condensation enhancement on electrically charged particles and influence of the charge sign was further investigated, in particular in relation to the matter of atmospheric physics [3, 4, 5] and the chemical kinetics of nucleation [6]. Researchers, in an attempt to study the phenomenon theoretically, investigated the new equilibrium of electrically charged particle with the nearby vapor phase and, in particular, they focused on the assessment of which process, condensation or evaporation, was more favorable in this thermodynamics condition. They speculated that the evaporation of charged droplets was suppressed because of the increase of the energy barrier for evaporation.

The impact of the charge on the vapor pressure on the small droplets was assessed. Starting from the classic Kelvin equation for neutral droplets, Thomson (1871) [7] developed a new model and equation, known in the literature as classic Kelvin-Thomson equation, for long the basis of nucleation theories on charged particles. He developed this equation accounting for the polarization of water vapor near the electrically charged particle. Later, when the dielectrophoretic phenomenon was discovered and introduced [8], a modified equation, known in the literature as modified Kelvin-Thomson equation, was derived by Yu et al. [9], to account for the dielectrophoretic effect and the drift of dipoles (water vapor) towards the charged particle due to the dielectrophoretic effect. Dielectrophoresis occurs when a polar molecule, such as water, is placed in a non-uniform electric field and, as a consequence, it experiences a force which is directed towards the increased field in the case of positive dielectrophoresis. This force is responsible for the additional potential energy experienced by the vapor molecules near the surface of the liquid droplet surface. The non-uniform electric field induces an enrichment of the water vapor near the charged droplet and, when the vapor density exceeds the saturation level, nucleation occurs. This phenomenon is illustrated in Fig. 3.

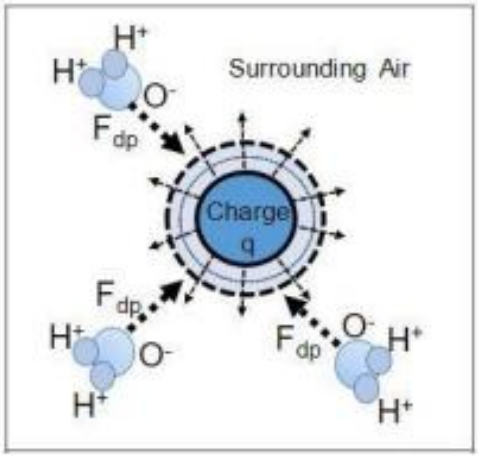

Fig. 3: Attraction of the vapor molecules with a native dipole moment to the charged droplet

A reduction of the chemical potential of the liquid droplets in equilibrium with the vapor phase was predicted, and, as a result, the evaporation of a charged droplet was suppressed. As an additional consequence, the saturation vapor pressure over the charged droplet's surface was reduced if compared with that of a neutral droplet of the same size, and the condensational growth of the droplet was promoted. A complete derivation of the equations to evaluate the saturation vapor pressure over the curved surface of neutral and charged droplets may be found in [9]. Fig. 4 provides the additional factors included passing from the Kelvin model to the modified Kelvin-Thomson one, while details on the equations of each model will be provided in the next chapter.

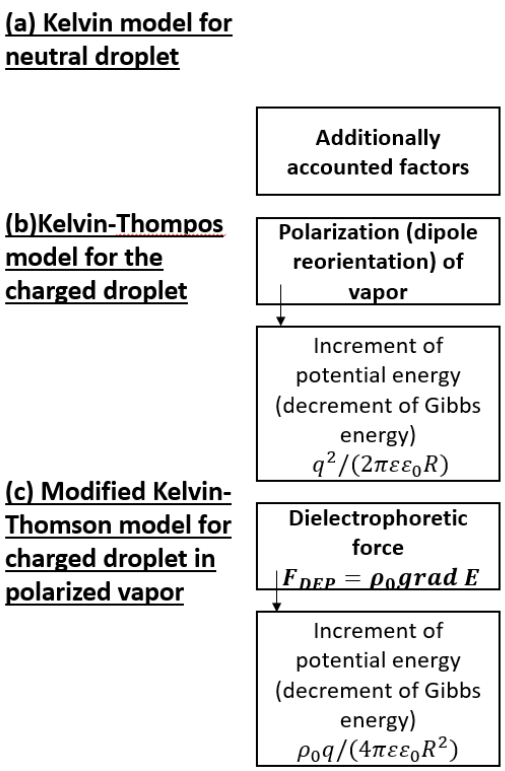

Fig. 4: Additionally accounted factors for the modified Kelvin-Thomson model for charged droplet in polarized vapor

As previously mentioned, the modified Kelvin-Thomson model predicted a reduction of the saturated vapor pressure if compared to the classical Kelvin-Thomson one. This could also be seen as a reduction of surface tension due to the presence of electric forces. This consistent reduction of the saturation vapor pressure, when the droplet size was reduced and the electrical charge increased, may be the theoretically explanation of the suppression of the evaporation from the charged particles that, consequentially, promoted the condensational growth of the droplets.

2.2 Electrostatically Enhanced Condensation – experimental work

Following the broad physics based work on the improved condensation on electrically charged nucleus, [10, 11] successfully demonstrated the generation of water droplets on ions. Afterwards, additional theoretical and experimental work, on water nucleation and condensational growth on ions and electrically charged droplets, was carried out. The main goal was to prove the performance increment due to electrostatically enhanced condensation in a variety of engineering applications, from the condenser of power plants to systems specially designed to harvest water vapor from the air and to dehumidify humid air. A consistent improvement of condensation both by means of the use of ions and electrosprayed droplets was detected and light was shed on the potential of electrostatically enhancement condensation. However, all the experimental work was performed only on laboratory scale systems with limited humid air flow rates, in general lower than 5. As a consequence, experimental results were available only for this restricted condition and no data, to the best knowledge of the author, was available for conditions more suitable for residential or light commercial HVAC systems.

Electrostatically enhanced condensation by ions allowed approximately for a 16 – 20 % improvement in the condensation rate in a cooled multichannel aluminum steam condenser where each channel was equipped with an array of wires, where an 8 kV electrical potential was applied [12]. The condensation rate improvement was dictated mainly by the condensation of water vapor on mobile charge carriers (ions) and by the electrohydrodynamic vapor flow toward the cooled condenser wall. The

16 – 20 % improvement was limited by the charge of a single ion, and better results could be expected with nucleation nuclei with higher electrical charge density, such as the electrosprayed charged droplets. When the potential of charged droplets produced by the electrospray technology was investigated on a similar industrial steam condenser, a significant 57 % improvement in condensation rate was achieved [13]. The key component of this steam condenser configuration was represented by an array of electrospray heads. The electrospray heads employed 21 gauge needles, where a high negative voltage of approximately 8 kV was applied. The distance between the needles and the grounded electrode, corresponding to the cooled condensing wall in this set up, was always maintained at around 8 cm. However, a still significant amount of cooling power had to be provided in the steam condenser.

Together with the applications on industrial steam condensers, an atmospheric water generation system was investigated by the same research group [14, 15]. In contrast with the conventional technologies, which mostly cooled the entire air flow below the dew point temperature, the system proposed consisted of a selective electrostatic separator of moisture from the air followed by an electrospray enhanced steam condenser. The so called moisture separator used corona discharge (ions), directed across the airflow towards grounded mesh electrodes, to separate the moisture from the air thanks to the nucleation of water molecules on the ionized air (ions). The moisture enriched separated flow was then directed towards the condenser where potable water was produced thanks to the combined action of thermoelectric coolers and electrospray heads. This technology represented an energy efficient solution for harvesting of water from an airstream and provided a fivefold improvement in water production if compared to the same prototype without electrostatically enhancement. Also in this case, cooling power was essential and the airflow rate investigated was limited and kept below 2 cfm.

An investigation of the only use of electrosprays to dehumidify an airstream, where moisture absorbing polymer sheet was used to avoid the re evaporation of the collected condensate, was also performed recently [16]. A relative humidity reduction of approximately 5% was measured with a limited

airflow rate of 0.04 cfm when four electrospray heads were used. The conditions of the supply air were 24 $°C$ and relative humidity of 70%, 80 % and 90%. The air temperature remained fairly constant throughout all the process and the 5 % relative humidity decrement was experienced for all the inlet relative humidity.

A review of electrically driven dehumidification technology for air conditioning systems was also published in 2020 [17]. A research progress update on four different kinds of methods proposed in recent literatures, including also the high voltage discharge dehumidification, was given. The research gaps and development prospects of electrically driven dehumidification were also discussed, highlighting how a further improvement in dehumidification rate is essential for the commercial penetration of many of these methods.

2.3 Production of Electrically Charged Particles

Ionized air (ion) enhanced condensation was shown to be successful but limited by the charge of the ion. In contrast to the ionization of air, nucleation centers with higher electrical charge density, such as the charged droplets produced by the electrospray technology were investigated in the literature to show water vapor condensation rate improvement. Indeed, if compared to ions, water droplets can hold a much higher electrical charge if compared to the elementary charge.

Different technologies are available for the production of fine droplets and for their charging [18]. Example of these technologies for the production of small size droplets are mini-foggers, nebulizers, ultrasonic humidifiers, which rely on the use of piezoelectric transducers, condensation aerosol generators and electrosprays. While, to charge the fine droplets, example of methods are electrostatic spraying of liquids, triboelectrification, corona, induction and conduction (electrospray) charging. A detailed comparison of these technologies and their working principles is outside the scope of this thesis work but it is worth to highlight that, among these technologies, electrosprays can accomplish the production of small droplets and their charging simultaneously and it has the potential to produce sub-

micron size droplets. In fact, electrospray atomization is probably the only known procedure capable of dividing a liquid into fairly uniform fragments with dimensions that may be controlled from hundreds of microns down to the nanometer range. Electrosprays were also extensively used in numerous related research work to prove the electrostatically enhanced condensation concept.

2.3.1 Electrospray Technology

Electrosprays represent the best candidate if a precise control of the operating parameters, in particular droplet size and charge, is required. They can be easily implemented applying a high electric field (high voltage) to a metal capillary or needle, usually placed a few centimeters away from a grounded electrode. A summary of all fields of current and potential applications of the electrospray technology may be found in [19]. Electrosprays generate fine droplets with a charge magnitude which is way higher than the one an ion can hold. However, even if electrospraying methods provide flexible control of the size and the charge of the droplets, physical limits, named Rayleigh limit and Paschen limit, restrict the maximum charge the droplets can carry [20]. The Rayleigh limit corresponds to the condition where electrostatic forces exceed those of surface tension, while the Paschen limit corresponds to the condition where localized electrical discharge may occur due to avalanche ionization processes (corona discharge). Equation (1) and (2) can be used to evaluate the theoretical maximum amount of charge a droplet can retain before becoming unstable.

$$q_R = \pi\sqrt{8\varepsilon_0\sigma D^3} \tag{1}$$

$$q_P = 2\pi\varepsilon_0 D V_P \tag{2}$$

where V_P is the voltage value necessary for ionizing collisions.

For a given fluid, the maximum charge a droplet can safely hold increase with the radius, according to both the equations. For small droplets, the Rayleigh limit is usually the most restrictive one and, if

overcome, it leads to the disintegration or fission of the charged droplets. For instance, a highly charged droplet can go through unstable disintegration if the evaporation process on its surface dramatically increases its charge density. Further details on the Coulomb fission, i.e. unstable disintegration, of charged liquid droplets and models to predict the droplet size and charge of the smaller droplets subsequent to the disintegration are available in the literature [21]. However, charged droplets in the context of enhanced condensation and dehumidification decrease the charge density due to the condensational growth. Electrosprayed droplets, therefore, should be charged as much as possible close to the Rayleigh limit, letting the condensational growth to move them away from the limit.

For a given fluid, such as water, to precisely control the size and the charge magnitude, the flow rate and the high voltage applied should be carefully tuned. Moreover, the flow rate and the applied voltage are also responsible for the establishment of one of the many electrospray modes, so widely investigated in the literature [22, 23]. Among all the electrospray modes, each of them characterized by its own process of formation of the meniscus and jet emerging from this meniscus, the so called cone-jet mode appears to be the only one that allows for a monodisperse spray, i.e. a spray characterized by droplets of the same size. This peculiarity makes this mode among the most studied. Monodispersity, indeed, is required in different practical applications and, in the contest of electrically enhanced condensation and dehumidification, it could be a tremendous advantage to facilitate the development of a preliminary model considering that the condensational growth should be the same on each of the same size electrosprayed droplets.

Different liquids and solutions to be electrosprayed were investigated in the open literature. Pure water and water solutions were extensively investigated even if their large surface tension required a very high voltage potential for the establishment of a stable electrospray. [24] focused on sucrose water solution where the liquid electrical conductivity was controlled by adding small amounts of nitric acid to generate monodisperse droplets in the small particles size range (nm range), in the cone jet operational

mode. The system employed in this work was characterized by a platinum capillary tube, with an internal diameter equal to 81 μm, a neutralization chamber and a plate electrode, which was approximately 5 mm away from the tip of capillary tube. Negative high voltage potential was applied to the neutralization chamber and the plate. A sheath flow of CO_2 surrounding the capillary tube prevented possible corona discharges. The size distribution of the electrosprayed droplets was quite monodisperse and the liquid feed rate and the electrical conductivity were changed in order to vary the mean droplet size. Varying the electrical conductivity from 15.6 $\mu/\Omega^{-1}cm^{-1}$ to 8000 $\mu/\Omega^{-1}cm^{-1}$, it was possible to obtain droplets from 40 nm to 1.8 μm in size, with the appropriate liquid feed rate.

Always using deionized water with an electric conductivity of 1.02 $\mu/\Omega^{-1}cm^{-1}$ and a surface tension of $73\ 10^{-3}\ N/m$ as electrosprayed liquid, the generation of electrosprayed water droplets was investigated [25, 26]. Two operational modes were found out to generate droplets monodisperse in size, i.e. the "classical" cone-jet mode and an "unconventional" corona-assisted cone-jet mode. In the latter operational mode, the gas-phase ionization (corona discharge) had a stabilizing effect. The experimental set up was characterized by a stainless steel capillary with an internal diameter of 0.12 mm at high electric potential (10-20 kV) and a grounded electrode placed below, in a perpendicular way, of the capillary emitter, at a distance of 3 cm. The large surface tension of the water required a high voltage potential for the establishment of the cone-jet mode and the voltage was usually higher than the electric breakdown threshold of the surrounding air. For this reason, a CO_2 sheath flow was used to isolate the capillary tip from the air and prevent uncontrolled corona discharge, the main responsible for a polydisperse electrospray. No effects on either the electrospray stability or the droplet size were seen if the CO_2 flow rate was varied between 0.0048 l/min and 1.5 l/min.

Plots highlighting the stability domains, where a stable and monodisperse electrospray could be achieved, were reported for both the operational modes as function of the voltage potential and liquid water flow rate. The voltage, indeed, was a key parameter affecting the stability of the electrospray. In

general, the “classical” cone-jet stability domain was obtained for voltage potential higher than 14 kV and the minimum water flow rate for a monodisperse electrospray was 5.8 $\mu l/min$. At this flow rate, the smallest electrosprayed water droplet in size, i.e. 2.5 μm in radius, was measured. In case finer droplets were required, two possible solutions were proposed. One solution consisted in the increase of the electrical conductivity of the liquid in order to shift the stability domain towards lower water flow rates. With a saline solution of water characterized by 0.005% of NaCl (by weight), the smaller droplet produced had a radius lower than 1 μm. A second solution consisted in the operation of the electrospray in the newly discovered “unconventional” corona-assisted cone-jet mode. This new stability domain was quite different with respect to the “classical” cone-jet mode and it extended to water flow rates more than one order of magnitude smaller, allowing the generation of smaller monodisperse droplets. In addition, it established for much lower voltages.

The total electrical current was also measured at the grounded electrode. The current carried out by the lower voltage domain (corona-assisted cone-jet mode) was larger if compared to the current carried out by the “classical” cone-jet mode, at same flow rates.

The size, as well as the charge of the electrically charged droplets, could be well estimated with numerous available correlations [27, 28] as a function of the flow rate and the properties of the sprayed fluid in the cone-jet mode. The monodispersity of the droplets in this operational mode was essential for the development of these correlations. Among the most experimentally validated for the estimation of the droplet size, there were the scaling equations proposed by [28, 29] and, as proof of the complexity of the problem of mathematical description of electrospraying, both these two equations (3) and (4) were function of specific experimental constants.

$$d = G(\varepsilon)\left[\frac{\epsilon\epsilon_0 Q}{K}\right]^{\frac{1}{3}} \tag{3}$$

$$d = \alpha \left[\frac{\rho \epsilon_0 Q^3}{\pi^4 K \sigma}\right]^{\frac{1}{6}} \quad (4)$$

where Q is the feed flow rate of liquid pushed through the jet [cm^3/s]; K, σ and ϵ are the electrical conductivity, surface tension coefficient and dielectric constant of the liquid (liquid permittivity), respectively; ϵ_0 is the electrical permittivity of vacuum. $G(\epsilon)$ is instead a constant depending on the dielectric constant of the liquid and α is another constant depending on the properties of the fluid. All these equations indicated that the diameter scales with the liquid flow rate, and is inversely proportional to the liquid electrical conductivity to a certain power.

Together with the equations for droplet size, equations for the current carried by electrospray jets were also available in the literature. For liquid with electrical conductivity $K > 10^{-5}$, equation (5) may be use to estimate the electrospray current [30].

$$I = f(\epsilon) \left[\frac{\sigma K Q}{\epsilon}\right]^{\frac{1}{2}} \quad (5)$$

where $f(\epsilon)$ is a function of the dielectric constant of the liquid. For water, the values of $f(\epsilon)$ and $G(\epsilon)$ are equal to 18 and 0.648 respectively. The experimental work [24] carried out with water for a wide range of electrical conductivities confirmed equation (3) and (5).

On average, equation (3) and (5) could be combined together to give the charge over volume ratio of a droplet which is simply given by I/Q. Equation (6), instead, divides the total droplet charge by the maximum charge the droplet can theoretically sustain q_R to estimate how much charge is hold by the droplet if compared to the theoretical limit.

$$\frac{q_m}{q_R} = f(\epsilon) G(\epsilon)^{\frac{3}{2}} / (6\sqrt{8}) \quad (6)$$

Equation (6) predicted that the fraction was not a function of the feed flow rate and, for water, the fraction resulted equal to 0.553. In other words, for a fixed electrosprayed liquid, the fraction was a constant of the Rayleigh's limiting charge. This equation, if compared to one used to predict the sizes, was not as experimentally validated [27, 28]. In general, experiments predicted that charge density was inversely proportional to the droplet diameter and the fraction deviated more from the Rayleigh limit when smaller droplets were produced by decreasing the liquid flow rate [25, 26]. Large droplets were characterized by a lower charge density and were closer to the Rayleigh limit, while small droplets were characterized by a higher charge density but were further from the Rayleigh limit.

2.4 Patents and Inventions

Difference inventions and patents available have some common peculiarities with the system that has to be developed in this overall project. One of this, "Direct contact vortex flow heat exchanger" (US8210506B1), shares the concept that high density liquid droplets can be separated by the centrifugal force of the continuing vortex movement of the gas stream and appropriately removed from the gas steam. This invention deals mainly with direct contact heat exchanging between two fluids, water and air, and the implementation of the process in a suitable heat exchanger characterized by far less weight than a typical heat exchanger. Water droplets, injected in the forced air vortex by conventional spray nozzles, are free to exchange thermal energy and mass (evaporation and/or condensation) and heat transfer performances are improved if compared to indirect heat exchanger. Therefore, this heat exchanger, by means of the vortex movement of the gas stream, provides a viable solution to separate the two heat transfer fluids after mass and heat have been exchanged.

The injection of tiny electrically charged droplets, instead of neutral droplets, in the high humidity forced air vortex in order to enhance water vapor condensation represents a clearly upgrade of this invention. Moreover, the effectiveness of the vortical flow in separating water droplets from the air, also

demonstrated by [31], should avoid the use of strong and energy-consuming electric fields to repel and remove water droplets from the air flow, which is one of the real challenge for scaling up this technology. The integration of these two processes, electrically enhanced condensation by charged droplets and separation of the droplets by the centrifugal force of the vortical flow, is the significant variation and innovation of the system, if compared to the already available one, and should promote the effectiveness and scalability of the dehumidification process.

The scalability is indeed one of the main challenge of available systems that use electrostatic separation methods to dehumidify air. These systems are widely described in already registered patents and, even if they are relatively inexpensive and low energy-consuming systems, they are difficult to be integrated with high flow rate processes.

“Method and apparatus for electrostatic extraction of droplets from gaseous medium” (US 4670026A) is one of the aforementioned systems and it relies on an array of conductive pointed needles at high voltage (corona discharge array) adjacent to a grounded conductive collector to remove water vapor from air. The electric field so produced is responsible for both the coalescence of mist droplets and the charging of the coalesced water droplets on the shank of the needle so that repulsive forces can repel and move the electrically charged droplets towards the conductive collector plate where they are removed from the air flow. Cooling is required in order to dissipate latent heat of condensation of the molecules and to avoid the re-evaporation of the droplets into the air.

A different invention, “Aircraft electronic particle separation system” (US 20150090120A1) has been developed to remove (water) liquid particles in an Environmental Control System (ECS). The main goals of the invention are the comfort of passengers and crew by means of humidity control and the minimization of the system pressure drops and of the maintenance requirements in ECS while maintaining liquid particle separation efficiency. In general, the airstream is subjected to a charging stage, where liquid particles in the airstream are charged by an inner electrode connected to a high voltage electricity source,

and a collecting stage, where liquid particles are centrifugally moved to the periphery of the air stream and removed from the main stream. This system, even if it shares the concept of centrifugal separation, is arranged in two clearly separated stages that can potentially penalize the dimensions of the system and it doesn't rely on charged droplet for the collection and condensation of vapor. In the charging stage, the electric field may cause the air around the electrode system to ionize (when the electric field intensity exceeds the maximum limit that the air stream can sustain, a corona discharge may form) that means that one or more electrons can be removed from the liquid molecules in the airstream. These positive charged molecules are forced radially away from the inner electrode and this may facilitate the agglomeration of liquid particles into larger droplets with range in size from 0.05 μm to 5.0 μm. Increasing the electric field intensity may ionize smaller particles in the airstream and thus help agglomerate also the finer particles. In the collecting stage, a fixed vane imparts a centrifugal motion to the airstream that directs the larger droplets toward the periphery, allowing their removal from the airstream.

"Electrospray vortical flow exchanger" (US 20210093996) represents the envisioned device of this project where the charged droplets are released in a vortical flow exchanger for an enhanced dehumidification of air. The electrospray technology produces the charged droplets, which are then removed by the centrifugal forces. Details on the flow exchanger and fluid dynamics consideration are provided.

Other inventions, instead, are mainly focus on electrostatic precipitators to remove particles (dust) from an air or from a gas stream, and they are significant for the peculiarities they share with the system envisioned in this research work. These inventions are characterized by the use of charged droplets, used to collect dust (not vapor), or by the separation of particles by means of centrifugal forces. With respect to conventional dust collection technologies, such as gravity dust collection, inertial dust collection, filter dust collection and scrubbing, the electrostatic precipitators want to overcome the inability to collect fine particles and to reduce the operational costs and corrosion.

"Wet type dust collector using electrospray and vortex" (US 20190336904A1) relies on electrospray and vortex to promote the removal of dust contained in an exhaust gas. The dust collector has a cyclonic structure and electrospray fine water droplets are generated when high voltage is applied to the dust collector (10-50 kV). The main advantage of this invention is the possibility to produce very small particles by means of electrospray (low water consumption), which are able to collect fine particles of small granular sizes. This increases the removal efficiency of the system.

"Apparatus for removal of particulate matter from gas" (WO2012139642A1) is an additional invention for the removal of particulate matter from gas. It also combines the use of centrifugal action and electrostatic force for particle removal from a gas. A stream of particles is introduced tangentially into a cyclonic separation zone so that the particles experience a centrifugal force (swirling flow) allowing the particles to be collected on the outer wall of the separation zone and removed. However, cyclone separators are not suitable to remove the finer particles, in fact their collection efficiency for particles smaller than 5 μm is extremely low. For this reason, a combination of more technologies should be employed to achieve a good collection efficiency also with respect to finer particles. This invention is, in fact, characterized by an innovative combination of a cyclone and an electrostatic precipitator. In the electrostatic precipitator, the ionization electrode is connected to a high voltage source, preferably of negative polarity, which is capable of providing a corona initiating electrical potential and, as a result, it is capable of ionizing the particulate matter in the gas flowing through it. When the charged particulate matter enters the separation zone, it is separated due to both the centrifugal action and the electric field produced between the charged particulate matter and the grounded cyclone casing. Electrostatic precipitators are considered very effective in the removal of smaller particles and avoid typical problems associated with conventional technologies.

Chapter 3: Thermodynamics Model

Based on the physics and the thermodynamics of the electrostatically enhanced condensation phenomenon, a model was developed to predict the influence of the main operating parameters on condensation and/or dehumidification. In particular, parameters characterizing the water droplets were investigated in detail. The size and the charge of the droplets appeared to be the most influential parameters to control for an enhanced dehumidification process, reason why a suitable technology for their production had to be carefully chosen. Relying on the electrospray technology, the size and the charge of the droplets may be tuned varying the water injection rate, the electrical conductivity of the fluid and/or the high voltage potential applied between the emitter and the electrode. Other parameters, such as the air flow rate and the inlet relative humidity of the air, played an important role in the overall process and they were considered in the model as well.

3.1 Theoretical Background

Considering a water droplet surrounded by humid air, at thermodynamic equilibrium, the chemical potential of the liquid water phase molecule in the droplet is equal to the chemical potential of the vapor water phase molecule near the surface of the droplet. In the case of a neutral droplet, this equality leads to the classic Kelvin equation, represented in equation (7).

$$kTln\left(\frac{p}{p_{sat}}\right) = \frac{2\sigma M}{N_A \rho R} \tag{7}$$

where p is the saturated vapor pressure near the surface of the droplet of radius R and p_{sat} is the pressure of the saturated water vapor above a flat surface at temperature T. On a flat surface, indeed, the curvature of the liquid vapor interface does not play any role, and the saturation vapor pressure is simply given by the water saturation tables.

When the droplet is electrically charged, the chemical potential of the liquid water phase molecule is reduced, and the saturated vapor pressure near the droplet was conventionally calculated by the classic Kelvin-Thomson (CKT) equation, represented in equation (8).

$$kTln\left(\frac{p}{p_{sat}}\right) = \frac{2\sigma M}{N_A \rho R} - \frac{\left((qe)^2 M\right)}{32\pi^2 \varepsilon_0 N_A \rho R^4}\left(1 - \frac{1}{\varepsilon_l}\right) \quad (8)$$

However, this equation considers only the interfacial polarization of water in the droplet and the vapor near the droplet, and it underestimates the reduction of the saturated vapor pressure. In particular, the CKT model does not evaluate the important phenomenon, known as dielectrophoresis, in which a force is exerted on a polar particle when it is subjected to a non-uniform electric field. Indeed, when also the dielectrophoresis is taken into consideration, the chemical potential of the water in the droplet is further reduced, and the saturated vapor pressure may be evaluated by the modified Kelvin-Thomson (MKT) equation, represented in equation (9).

$$kTln\left(\frac{p}{p_{sat}}\right) = \frac{2\sigma M}{N_A \rho R} - \frac{\left((qe)^2 M\right)}{32\pi^2 \varepsilon_0 N_A \rho R^4}\left(1 - \frac{1}{\varepsilon_l}\right) - \frac{\alpha (qe)^2}{32\pi^2 \varepsilon_0^2 R^4} - kTln\left(\frac{\exp\left(\frac{\mu_0 qe}{4\pi\varepsilon_0 R^2 kT}\right) - \exp\left(-\frac{\mu_0 qe}{4\pi\varepsilon_0 R^2 kT}\right)}{2\frac{\mu_0 qe}{4\pi\varepsilon_0 R^2 kT}}\right. \quad (9)$$

The developed thermodynamics model was heavily based on these equations, in particular the modified Kelvin-Thomson (MKT) equation for charged droplets. It was mainly used to estimate the

reduction in the saturated vapor pressure near the water droplet surface, knowing that only with a positive driving potential the condensation or diffusional growth of the droplet can be possible. The vapor pressure far away from the droplet, in the bulk air, had to be higher than the one close to the droplet to have a drift a vapor towards the droplet itself. The drift of water vapor induced an enrichment of vapor near the charged droplet and, when the vapor density exceeded the saturation level, nucleation occurred.

While giving a good estimation of the maximum growth potential of the droplet, this model cannot predict the growth rate itself, i.e. how fast a droplet can grow given certain conditions. Different approaches will be required, as briefly discussed later.

3.2 Vapor Pressure and Driving Potential for Diffusional Growth

As a first step, these equations were used to evaluate the variation of saturated vapor pressure near the surface of the droplet, at fixed electrical charge, as function of the droplet size. In particular, Fig. 5 shows the dimensionless oversaturation ratio $\frac{p}{p_{sat}}$, i.e. the ratio of the saturated vapor pressure near the surface of the droplet and the saturated water vapor pressure above a flat surface at temperature T, evaluated with the Kelvin and the MKT equation. In other words, Fig. 5 shows a comparison of the saturated vapor pressure between a neutral and a charged droplet. For a better readability of the plot, the CKT model was not reported, considering that MKT model represented an upgrade of the previously developed CKT model.

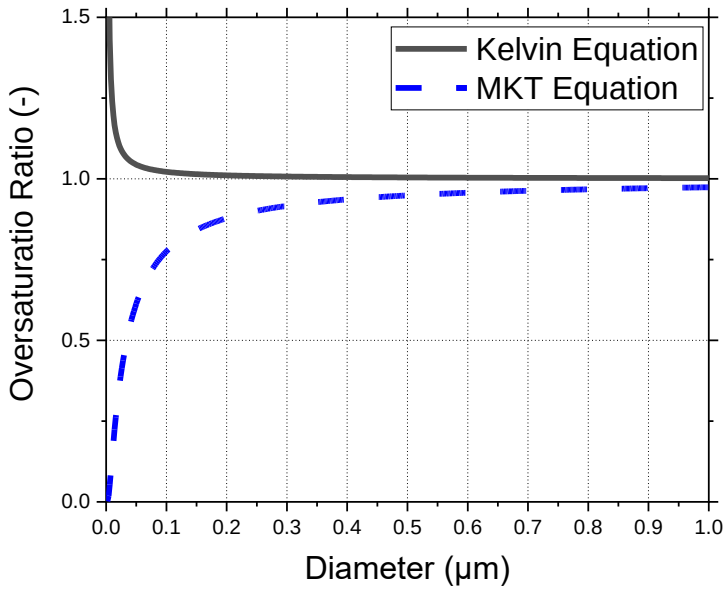

Fig. 5: Oversaturation ratio as a function of the diameter

For the MKT model, the droplet was assumed to be charged to its maximum electrical charge, dictated by the Rayleigh limit, at a temperature of $22°C$ and saturated conditions ($RH = 100\%$). The charge then increased as the diameter of the droplet increased. A significant reduction of the oversaturation ratio compared to the one predicted by the Kelvin equation was evaluated. In particular, for droplets charged to their maximum electrical charge, the MKT equation predicted an oversaturation ratio consistently lower than unity for droplets whose diameter was lower than a few μm. In this range, there were not any energy barriers for droplet growth.

In addition, Table 1 reports the values for the oversaturation ratio, including also the results from the CKT equation. The same electrical charge and ambient air conditions were considered, and the same conclusion from Fig. 5 can be drawn.

Table 1: Oversaturation ratio evaluated with the Kelvin, CKT, and MKT equations

Diameter [μm]	Kelvin Eq. [-]	CKT Eq. [-]	MKT Eq. [-]
0.002	2.93	1.01	0.0015
0.010	1.24	1.00	0.14
0.02	1.11	1.00	0.33
0.2	1.01	1.00	0.88
1	1.00	1.00	0.97
2	1.00	1.00	0.99
10	1.00	1.00	1.00
20	1.00	1.00	1.00

The maximum electrical charge predicted by the Rayleigh limit was only theoretical, and the droplets could practically be charged to only a fraction of this limit. When droplets were charged to a lower charge value, a minor reduction of the oversaturation ratio was predicted by the model. In particular, the oversaturation ratio values resulted more similar to the ones predicted for a neutral droplet as the electrical charge was decreased. For instance, if a single or double electron charged droplet was considered, the oversaturation ratio resulted consistently lower than the unity only when the droplet diameter was lower than 12 nm [12].

The influence of the temperature on the oversaturation ratio, instead, was minor compared to the influence of the droplet size and charge. However, a lower temperature may slightly improve the reduction of the oversaturation ratio, and it may enhance the maximum growth potential of the droplet.

The consistent reduction of the saturated vapor pressure enhanced the droplet growth potential thanks to an increase in the driving potential of diffusion, i.e. the vapor pressure difference. According to the MKT equation, saturated vapor pressure near the surface of the charged droplet decreased as the

droplet size was decreased and the droplet charge increased. For this reason, small and highly charged droplets should be preferred to larger poorly charged droplets, which caused only a limited reduction of the vapor pressure near the droplet. In fact, the condensational or diffusional growth of poorly charged droplets may be sustained by diffusion only when the diameter was in the sub-micron range, where the oversaturation ratio was lower than the unity and a vapor pressure gradient was established. If the vapor pressure gradient was not established, only the dielectrophoretic force F_{dp} might sustain the flow of vapor towards the droplet surface.

The knowledge of the variation of the vapor pressure near the surface and the estimation of the driving potential for diffusion, if the bulk vapor pressure was known, was essential for a further development of the model. With this information, indeed, it was possible to estimate the maximum droplet growth potential. In particular, the model had as main objective the identification of a suitable size range for the droplets to grow, under ideal conditions such as saturated air conditions and droplets charged to their maximum limit. In fact, in the literature, it was not readily available any model to estimate the optimal size for the droplets to grow and consequently to assess which technology was the most suitable to produce the charged droplets. In addition, after estimating a suitable size range, the model also estimated the maximum diameter increment during the growing process and how much vapor the single droplet can condense on its surface due to the volume increase of the droplet. This information allowed to estimate how many droplets were required to achieve a target dehumidification rate. A sensitivity analysis on the main parameters considered in the model was also performed, suggesting that more demanding requirements on the initial size of the droplets were required, when conditions different from the ideal ones were considered. More details on the development of the model are provided in the next paragraphs.

3.2.1 Maximum Droplet Growth Potential

The maximum droplet growth potential was evaluated assuming ideal conditions, such as droplets charged to their maximum limit. Supposing that the oversaturation ratio and the conditions of the bulk air far away from the droplet were known, the difference between the saturated vapor pressure over the surface of the charged droplet and the vapor pressure of the bulk air could be evaluated. According to MKT model, it was clear how the droplet charge and size had a significant impact on the vapor pressure on the droplet surface. Compared to the vapor pressure over a flat surface, the one over the surface of small and highly charged droplets was lower, as shown also in Fig. 5. This phenomenon increased the pressure differential potential for condensational or diffusional growth of the droplets. This differential established the net vapor transport between the bulk vapor and the condensed phase and, when the vapor density exceeded the saturation level close to the droplet surface, nucleation and droplet growth occurred. Droplet growth occurred only when the vapor pressure of the bulk air was higher so that the net vapor transfer was towards the droplet. When the vapor pressure near the droplet surface was considered almost the same as that far away from the droplet, the net transport between the phases, as well as the droplet growth, was reduced.

The minimum requirement to achieve droplet growth by diffusion was shown in equation (10).

$$\frac{p}{p_{sat}} < \frac{RH}{100} \tag{10}$$

where $\frac{p}{p_{sat}}$ is the MKT oversaturation ratio, and RH is the relative humidity, in percentage, of the bulk air, far away from the droplet surface.

If the pressures near the droplet surface and far away from the droplet were equal, the driving potential for diffusion vanished. As an additional driver for the droplet growth, the dielectrophoretic force F_{dp} might be considered. This force may sustain the flow of vapor towards the droplet surface, but the

sphere of influence of the dielectrophoretic force was not clearly assessed in the open literature. In [12], it was speculated that, for droplets charged to the Rayleigh limit, the dielectrophoretic force could sustain the vapor flow towards the surface for droplets with a radius equal or smaller than 120 nm. This meant that larger droplets' growth was supported by diffusion only, for which a pressure gradient was required and then equation (10) had to be satisfied. Considering that highly charged droplets with a radius smaller than 120 nm radius were extremely difficult to achieve by current technologies, a model that accounted for only diffusional growth was developed. The possible enhancement of vapor transport due to the dielectrophoretic force was not taken under consideration, as a conservative assumption.

Additional assumptions were made in the development of the current thermodynamics model. In the scenario of saturated ($RH = 100\%$) bulk air at $22\ ^{\circ}C$, it was conservatively assumed that diffusional growth occurred when the oversaturation ratio was below 0.995, and not 1 as suggested by equation (10). This assumption was made to limit the growth of the droplet calculated by the model by imposing a value of the oversaturation ratio close to and slightly below the asymptotic value of 1. According to this assumption, also when the oversaturation ratio was about 0.99 the droplets were free to grow, in saturated conditions. It should be noticed that this assumption should be further verified.

The thermodynamic model identified the droplet size and charge, together with the relative humidity of the bulk air, as the most influential parameters for droplet growth. The best conditions were characterized by droplets charged to their maximum limit, dictated by the Rayleigh limit, and inlet relative humidity equal to 100%. Considering the droplet size, the model predicted that smaller droplet were characterized by lower values of the oversaturation ratio. Adopting these optimal conditions, the maximum droplet growth potential was later evaluated. Particular care should be spent on the droplet size, as detailed later.

These small and highly charged droplets, in order to grow, were then assumed to be injected and released in a saturated humid air environment. Once released in the saturated environment, all the

droplets were free to grow until the oversaturation ratio reached the assumed value, i.e. 0.995. Afterward, they were conveniently separated from the environment, effectively wiping out the humidity from the air. All the droplets were assumed to be of the same size and charge, for an easier further development of the model. In practice, a distribution for both the size and charge was more realistic, but it represented a deviation from the ideal conditions for the evaluation of the maximum potential.

In this context, the electrical charge of the droplets depended on the initial size of the droplet itself. In particular, the maximum charge a droplet with radius R can hold was given by the Rayleigh limit, as shown again in equation (11).

$$q_{Rayleigh} = 8\pi\sqrt{\varepsilon_0 \sigma R^3} \tag{11}$$

The electrical charge was then fixed by the initial droplet size along all the growing process, and, for this reason, the charge density decreased as the radius increased. The trend of the oversaturation ratio given in Fig. 5 should then be readapted because, in that figure, each droplet was charged to its Rayleigh limit. In other words, for each droplet's diameter the charge was calculated with equation (11), and this value was entered in the MKT model for the evaluation of the dimensionless oversaturation ratio.

Fig. 6 reports an example of droplet growth for initial droplet diameter of 200 nm up to 2 μm, and charged to their maximum limit. Three initial values for the droplet diameter were chosen, i.e. 200 nm, 1 μm, and 2 μm.

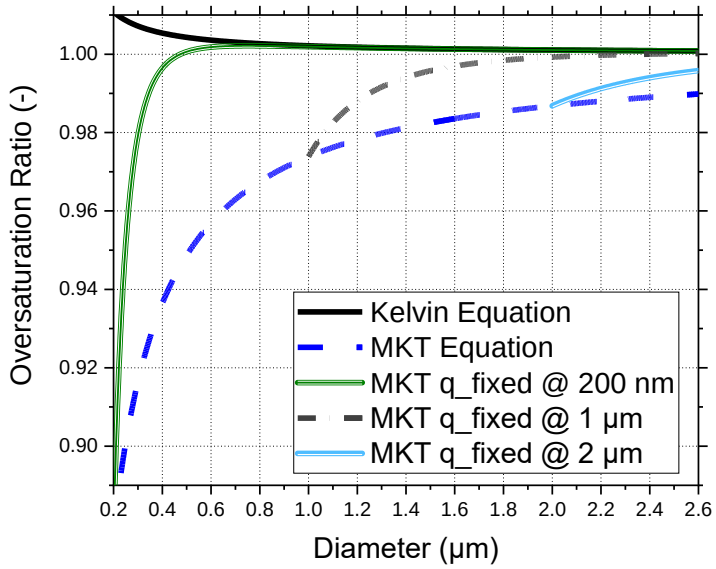

Fig. 6: Oversaturation ratio when the charge q was fixed by the initial diameter of the droplet

The figure shows the difference in trends between undertaking the growing process with droplets at fixed electrical charge compared to droplets always charged to the Rayleigh limit, represented in Fig. 6 by the MKT equation. The possible reduction of the initial charge due to the ions' neutralization when vapor molecules collapse on the droplets or due to electrical corona discharge was not taken into account.

When the electrical charge was fixed by the initial diameter, the oversaturation ratio tended to be asymptotically equal to one for a smaller value of the diameter. This meant that the growth potential was diminished because the pressure difference for diffusion vanished at a smaller radius, and, consequentially, the droplets could grow until a smaller diameter. The suitable initial diameter range for diffusional growth then shifted towards smaller values. Also, droplets with a bigger initial size tended to the unity more gradually, meaning that they can potentially deplete more water vapor than smaller droplets. For this reason, it was not true that the smallest droplet, and consequently the smallest oversaturation ratio, led to the maximum potential. An optimization analysis was then performed to find

out the optimal initial droplet size to lead to the maximum droplet growth potential, i.e. the maximum diameter increment for the droplet.

In order to perform this optimization analysis, the previously mentioned most favourable conditions, i.e. $T = 22°C$, $RH = 100\%$, and $q = q_{Rayleigh}$, were again considered. The droplet electrical charge was kept fixed throughout all the growing process and it was evaluated at the initial droplet size. The maximum diameter increment was simply evaluated through equation (12), as the difference between the electrically charged droplet diameter at which the oversaturation ratio was equal to 0.995 and the initial diameter of the electrically charged droplet suspended in the air and water vapor mixture.

$$Diameter\ Increment = D_{@\frac{p}{p_{sat}}=0.995} - D_{initial}\ [nm] \tag{12}$$

Fig. 7 shows its trend as function of the initial diameter.

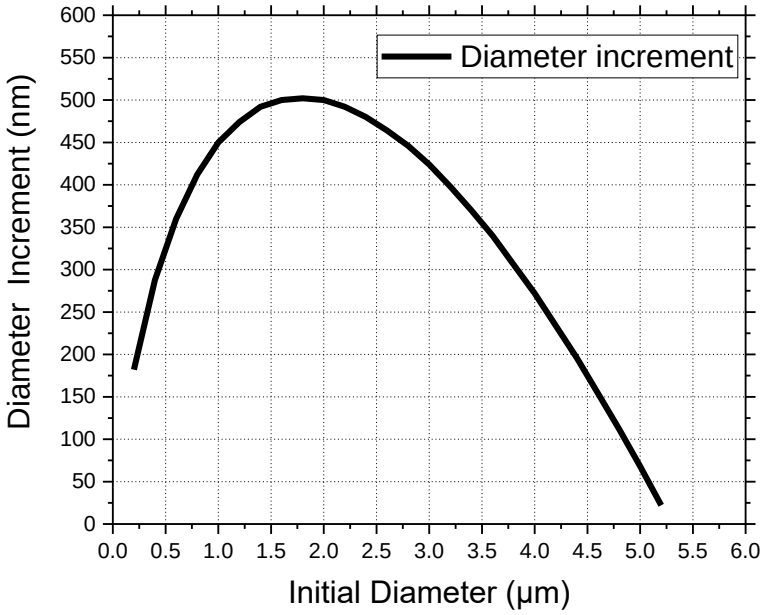

Fig. 7: Maximum diameter increment as a function of the initial diameter of the electrically charged droplet

The maximum diameter increment, resulted in an initial diameter of the electrically charged droplet of approximately 2 μm. A suitable diameter range to have a diameter increment for the prescribed conditions was between 200 nm up to about 5 μm.

As it will be shown later, the maximum diameter increment did not coincide with the maximum water vapor mass depletion per droplet, which was the real quantity to maximize for an improved dehumidification. This was related to the fact that the equation (13) for the evaluation of the vapor mass depletion was not linear in the diameter.

3.2.2 Maximum Vapor Mass Depletion Potential

In order to achieve a higher dehumidification rate, the critical parameter to maximize was the water vapor effectively wiped out from the humid air that condensed on the charged droplet surface, and not the maximum achievable diameter increment. Indeed, the optimal diameter for the maximum vapor

mass depletion did not coincided with the optimal one for the maximum diameter increment. The water vapor wiped out from the humid air, or simply the vapor mass depletion, was evaluated by equation (13) and Fig. 8 shows its trend as function of the initial droplet diameter.

$$Vapor\ Mass\ Depletion = \frac{4}{3}\pi\rho\left(\left(\frac{D}{2}\right)^3_{@\frac{p}{p_{sat}}=0.995} - \left(\frac{D}{2}\right)^3\right)\ [mg] \tag{13}$$

With equation (13), the maximum water vapor depletion that a charged droplet could collect was evaluated, considering the droplet's increase in volume due to vapor condensation and the density of the water.

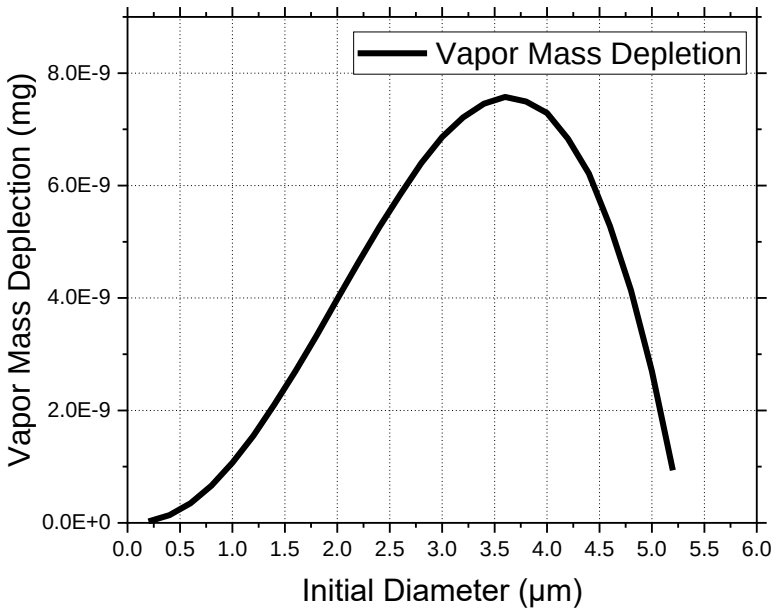

Fig. 8: Maximum water vapor mass depletion per droplet as a function of the initial diameter of the electrically charged droplet

The initial diameter D that maximized the vapor mass depletion was approximately equal to 3.6 μm and the suitable diameter range was comparable to the one for the maximum diameter increment. However, under the same operating conditions, smaller droplets were less effective in dehumidifying the air.

As a rule of thumb, droplets of a few microns or lower were required for diffusional growth and, if different operating conditions were chosen, the suitable range could only translate towards smaller diameters. In fact, larger droplets could theoretically hold more electric charge than smaller ones but they did not seem to be ideal for dehumidification processes, because the evaluated difference between the saturated vapor pressure over the charged droplet surface and the bulk air vapor pressure was minimal. A sensitivity analysis, in particular referred to the size and charge of the droplets, will be provided in a later section.

In these optimal operating conditions, assuming that all the electrosprayed droplets had the same initial diameter, it was also possible to evaluate the number of droplets per second required to achieve a specified dehumidification rate. Knowing the airflow rate to dehumidify, as well as the initial ω_{in} and target absolute humidity ω_{out}, the number of droplets might be evaluated with equation (14). All the droplets were assumed to have the same initial size.

$$n^{\circ}_{droplets} = \frac{\left((\omega_{in} - \omega_{out}) * \dot{m}_{dryair}\right)}{Vapor\ Mass\ \ Deplection} \left[\frac{droplet}{s}\right] \tag{14}$$

Fig. 9 shows the number of droplets required as function of the initial diameter, if the airflow rate was equal to 5 cfm and the target dehumidification rate was equal to 5 % in terms of relative humidity and constant dry bulb temperature. As a reminder, a target dehumidification rate of 5 % with an air flow rate of 5 cfm was indeed the goal of the experimental work of this thesis. The initial conditions were again

$RH = 100\%$ and $T = 22°C$, which was assumed constant throughout all the dehumidification process even if, in case of condensation, a slight increase should be detected.

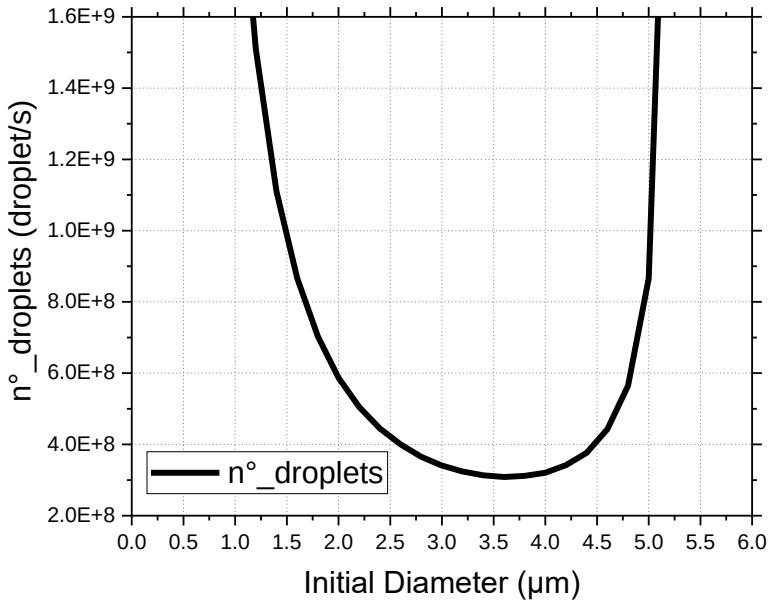

Fig. 9: $n°_{droplets}$ as a function of the initial diameter of the electrically charged droplet

The number of droplets required was in the range of hundreds of millions per second, with a minimum for a diameter approximately equal to 3.6 μm, as already shown with the maximum vapor mass depletion analysis.

Knowing the number of droplets required, additional considerations were made. In particular, it was possible to evaluate which technology was the most suitable for the droplets' production. The electrospray technology appeared the most appropriate, as it will be further explained, with however some challenges associated with the number of electrospray heads required to generate the desired number of droplets. The number of necessary electrospray heads was evaluated using equation (15).

$$n^{\circ}_{electrosprays} = \frac{n^{\circ}_{droplets}}{\frac{\dot{Q}_{electrospray}}{\frac{4}{3}\pi R^3}} \quad (15)$$

where $\dot{Q}_{electrospray}$ is the volume flow rate injected by a single electrospray head. The electrosprayed droplets' properties depended mainly on the fluid characteristics, the fluid flow rate, and the voltage applied to the needle. When the spayed fluid was chosen, i.e. water in this application, the droplet size depended mainly on the flow rate of the liquid for single electrospray. For this reason, knowing the optimal droplet size, the volume flow rate could be estimated thanks to the data available in the open literature. Electrosprayed droplets whose size was in the range predicted by the dehumidification model were produced [25, 26]. This work was one of the few where a stable electrospray of water was achieved for relatively small flow rates. However, the use of a CO_2 sheath flow was required for the stability and monodispersity of the spray, which may complicate the future overall design of the electrospray. According to this work, droplets with a diameter of 3.6 μm may be achieved with a water flow rate slightly higher than 10 $\mu l/min$. Under the assumption of spherical droplets of the same size and a target dehumidification of 5 % for an air flow rate of 5 cfm, this led to more than 300 electrospray heads.

It must also be considered that the droplets should have enough time to grow until the oversaturation ratio reaches the arbitrary chosen value of 0.995, i.e. critical assumption of the model, which may or may not be the case. In case the droplets did not have enough time to grow until this threshold, the model would overestimate the actual dehumidification rate.

Any deviation from these ideal or optimal conditions led to a decrement of the potential. For this reason, a sensitivity analysis on the main operating parameters will be later performed to estimate their effect on the maximum dehumidification potential.

3.3 Droplet Growth Rate

In order for the droplets to collect all vapor predicted by the vapor mass depletion potential, sufficient time had to be given for the droplets to grow. As an analogy, the chemical equilibrium of a chemical reaction is as important as the kinetics of the reaction itself.

It was important to estimate, together with the maximum potential, the droplet growth rate. In other words, information on how fast the droplets grow at predetermined conditions was essential. This rate would be dependent on the time of flight of the droplets and their trajectory and relative velocity with respect to the humid airflow. Applying an energy balance and the heat and mass transfer analogy, the vapor mass condensation rate was estimated. With the mass condensation rate, the droplet radius growth rate was evaluated, as shown in equation (16).

$$\frac{dr}{dt} = \frac{h_m}{R_v T \rho}(p_{bulk} - p) \tag{16}$$

where ρ is the density of the water, p_{bulk} is the vapor pressure far away from the droplet and p is vapor pressure on the surface of the charged droplet. h_m is instead the mass transfer coefficient, which was the most critical parameter to estimate. In fact, due to the very small length scale of the problem, it was not possible to correctly estimate it by means of the widely accepted heat and mass transfer correlations over a sphere. In general, the mass transfer coefficient was always overestimated by several orders of magnitude.

Equation (16), as also equation (10), stated that, in order for the droplet to continue to grow, the vapor partial pressure in the bulk air must be higher than the partial pressure of vapor near the droplet surface, which may be evaluated thanks to the MKT oversaturation ratio. This requirement must be met at all the time in order for the droplets to grow.

3.4 Sensitivity Analysis

The thermodynamics model developed so far considered only ideal conditions and the dehumidification potential predicted was relatively limited. As an additional concern, any deviations from these conditions may compromise the already limited dehumidification potential and their influence should be properly assessed. As an example, the influence of different environmental factors were investigated. In particular, the impact of a variation of the droplet charge on the minimum relative humidity of the air stream that can be dehumidified was considered. During the ideal analysis, it was already shown that a suitable range for the diameter was comprised between 200 nm and 5 μm. When the electrical charge was reduced, the suitable range shifted towards smaller diameters and the minimum relative humidity increased, as shown in Table 2.

Table 2: Minimum relative humidity (RH) of the air stream that can be dehumidified as a function of the electrical charge set on the droplets

***Droplet Initial Diameter* [μm]**	RH @ $q = q_{Rayleigh}$	RH @ $q = 0.8\, q_{Rayleigh}$	RH @ $q = 0.6\, q_{Rayleigh}$	RH @ $q = 0.4\, q_{Rayleigh}$
0.02	> 33%	> 49%	> 69%	> 89%
0.2	> 87%	> 92%	> 96%	> 99%
1	> 97%	> 98%	> 99%	-
2	> 98%	> 99%	-	-
3	> 99%	-	-	-
4	> 99%	-	-	-
5	> 99%	-	-	-

Table 2 reports the minimal relative humidity of the bulk air that can be dehumidified for different droplet charge conditions and diameter if only growth by diffusion was considered. With the reduction of the

charge, the minimum relative humidity of the bulk air that can be dehumidified at a fixed initial diameter was increased. As the charge was reduced, the suitable diameter range shifted towards much smaller diameter values. For instance, with droplets charged to 40 % of the Rayleigh limit, droplets smaller than 200 nm were required. At a constant charge, smaller droplets can dehumidify a bulk air whose relative humidity was lower.

This sensitivity analysis was important because, in practice, it is hard to charge the droplets to their maximum limit due to droplet surface instabilities, and, more likely, the air stream to be dehumidified has a relative humidity lower than 100%. For this reason, sub micron meter droplets may be required and the electrospray technology appeared the only technology with the flexibility to produce droplets of this size. This was an addition reason why the electrospray technology was chosen.

Comparing the conclusions of this thermodynamics model with some experimental results available in the open literature [13, 14, 15], some inconsistencies appeared. Droplets growth beyond 100 μm was observed in experimental investigations even if this theoretical model predicted a potential to grow for much smaller droplet sizes. Due to the apparent inconsistency, experimental data should be collected to better estimate the dehumidification potential, validate the model and for comparison with the data available in the literature. The experimental investigation of the electrostatically enhanced condensation process will be the focus of the next sections of this thesis.

3.5 Considerations for the experimental investigation

Following the development of this model, some expectations for the experimental tests were drawn. In particular, the exact number of electrospray heads required to reach the target dehumidification of 5 % with an air flow rate of 5 cfm was reported in Table 3. Additional air flow rates, such as the ones actually tested in the experimental facility or considered in the open literature, were also reported.

Table 3: $n°_{electrosprays}$ required for different air flow rate and 5 % dehumidification rate

Air flow rate **[cfm]**	$\boldsymbol{n°_{electrosprays}}$ ***required*** **[-]**
5	362
2	145
0.5	37
0.04	3

This estimation was performed assuming that droplets with a diameter of 3.6 μm, i.e. the optimal predicted for dehumidification, may be achieved with a water flow rate slightly higher than 10 $\mu l/min$ [25, 26]. Smaller or larger water flow rates would lead to different droplet sizes.

If a more practical number of electrospray heads were simulated, i.e. up to six (6) as during the experimental campaigns, a dehumidification rate in terms of relative humidity equal or lower than 1 % were predicted, for all the air flow rates considered expect 0.04 cfm.

If, hypothetically, droplets with a diameter of 3.6 μm could be achieved with a water flow rate of 100 $\mu l/min$, as opposed to 10 $\mu l/min$ evaluated in [25, 26], the droplet production frequency considerably increased and a higher dehumidification rate was evaluated . In particular, with six (6) electrospray heads a dehumidification rate above 5 % was predicted, in the case of 0.5 cfm. Dehumidification rates lower than 5 % were predicted for all the other cases.

Chapter 4: Experimental Methodology

4.1 Introduction

The goal of the experimental campaign of this thesis was to prove the potential of electrostatically enhanced condensation and to validate the thermodynamics model previously developed. For this purpose, an assembly of electrospray heads were designed and tested. The electrospray heads generated the small and highly charged droplets to attract and condense the water vapor out of the air and to dehumidify the air stream. In general, the charged droplets were injected perpendicular with respect to the humid air stream and they were collected in a counter count electrode. No centrifugal forces were employed for an enhanced removal of the droplets out of the air stream. In an upgrade version, water absorbing materials were also placed on the counter count electrode to facilitate the collection of water and avoid the evaporation of the collected water. The section of the experimental facility dedicated to the investigation of the enhanced condensation process with the electrospray head assembly will be referred as test apparatus.

The experimental setup was indeed constituted by the test apparatus and by a larger experimental facility. The experimental facility had the role of housing the test apparatus, providing a controlled environment for the experiment to be conducted in, and facilitating the collection of data from various sensor equipment. The test apparatus, instead, allowed for the operation of the electrospray technology, where all the working parameters can be precisely controlled. No thermal power, in particular cooling, was provided in the test apparatus.

4.2 Experimental Facility

The experimental facility was characterized by a subsonic, closed return, climate controlled wind tunnel with a flow path square cross section of 2 ft. x 2 ft. as shown in Fig. 10. Additional details of the piece of equipment are also provided in Fig. 10, except for the low temperature refrigeration system and the pump module, which were installed in a dedicated equipment room. More details can be found in [32, 33], as the overall experimental facility and some components in the test apparatus were previously designed and assembled for the investigation of frost formation on horizontal flat plates.

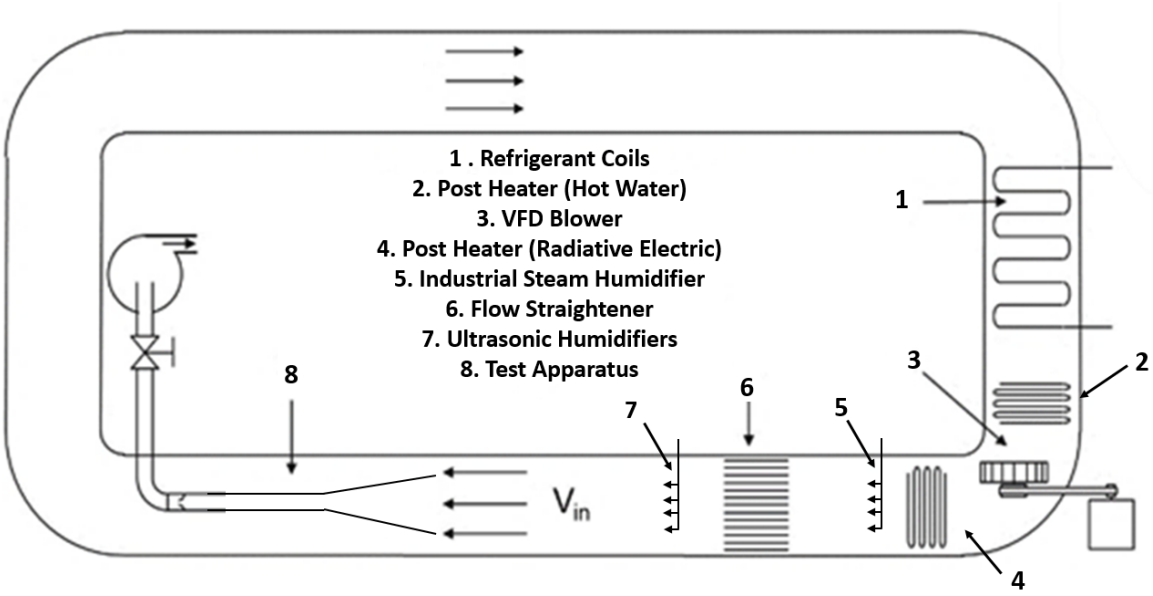

Fig. 10: Schematic of the experimental facility characterized by a wind tunnel with a flow path square cross section of 2 ft. x 2 ft.

The main components in the closed return airflow wind tunnel were refrigerant coils, radiative heaters, flow straighteners, humidifiers, a VFD blower and the test apparatus, which will be analyzed in more details in the next section. The experimental facility precisely controlled the air temperature, humidity, and air flow rate and velocity. It was of paramount importance to keep these parameters

constant throughout the experimental tests, reason why PID controllers were developed in the data acquisition (DAQ) and control system (NI).

In the refrigeration coils, a stream of chilled ethylene glycol and water mixture (EGW) flowed to facilitate the heat removal from the wind tunnel and help to regulate the humidity of the wind tunnel by condensing moisture out of the air. The temperature and flow rate of the EGW stream to the coils were monitored and controlled by a pump module and a low temperature refrigeration system (chiller), installed in a dedicated room. The pump module consisted of a Mydax PM 180 shown in Fig. 11, which contained three pumps, in line and immersion heaters and a 180 gallon storage tank for EGW, which acted as a large thermal mass allowing for a relatively constant EGW temperature. The low temperature refrigeration system, shown in Fig. 11, consisted of a CryoDax 25 water-cooled chiller, again from Mydax, working with refrigerant R507. It was used to cool a Syltherm™ low temperature heat exchange secondary fluid. On the hot side of the chiller, heat was extracted by chilled water sourced from the building facility, while, on the cold side, the chilled Syltherm™ was cooled down to provide cooling to the EGW through a brazed plate heat exchanger, installed in the pump module. The CryoDax 25 was capable of providing chilled fluid at a temperature range of -70°C to +80°C and it was able to provide up to 25 kW of cooling power.

A radiative air heater fine-tuned the air temperature after the refrigeration coils to bring the air temperature back up to desired conditions. Higher air temperatures may be reached with a hot water post-heater operated by an external heat pump system. In this thesis, the radiative air heater was sufficient to reach the desired conditions and the heat pump system was not used.

Fig. 11: Chiller with up to 25 kW of cooling power (left) and pump module with three dedicated pumps and in line and immersion heaters (right)

A variable speed fan moved the airflow through the large wind tunnel and a flow straightener helped to ensure a homogeneous flow up to the test apparatus. An air filter of MERV 9 was installed before the test section, in proximity of the variable speed fan, to filter the incoming air.

Two humidifiers were implemented after the radiative air heater and just before the inlet of the test apparatus to control the humidity level of the experiments. Indeed, the humidifiers were essential to increase the humidity to levels close to saturation or to precisely tune the humidity if its reduction after the cooling coils resulted to be excessive. Fig. 10 clearly shows the positions of the two humidifiers with respect to the whole wind tunnel.

An industrial steam HumidiClean Series HC-6100 Humidifier was the first one to encounter in the direction of the flow and it was used to increase the relative humidity of the air up to about 90/95%. Indeed, when the relative humidity exceeded the 90/95% level, a safety switch cut the power input to the

humidifier to prevent floating the wind tunnel. The HumidiClean converted ordinary tap water, internally purified, to steam by means of heating elements, for distribution inside the wind tunnel to raise the relative humidity level. The demand for humidity, which could be set manually by the operator through the control system, was sensed by a humidistat or sensor that sent a control signal to the HumidiClean.

Two smaller residential Pureguardian H7550 90-Hour Smart Mist Ultrasonic Humidifier was placed in parallel very close to the test apparatus, to finely control the relative humidity level at the inlet of the test apparatus. The working principle of this device was different with respect to the previous one. It consisted of a reservoir of tap water and a diaphragm or other type of vibrating element, which vibrated at an extremely high frequency. The vibrations propelled microscopic water droplets into the air, which evaporated in the air adding humidity. In contrast to evaporative humidifiers, no heating of water was used. The generated steam, or mist, traveled through plastic tubes, through the wall of the large wind tunnel, to a steam wand/nozzle. The steam wand/nozzle evenly distributed the vapor across the section of the wind tunnel. This ultrasonic humidifier had a maximum capacity of 1.3 gallon and it was able to generate mist for up to 90 hours. The mist could be generated as warm or cold mist. The use of two identical ultrasonic humidifiers installed in parallel enhanced the flexibility and allowed for a better control of the relative humidity. Indeed, more than once, at specific operating conditions, only one ultrasonic humidifier was not able to provide the desired levels of humidity of about 90% or higher.

Fig. 12 and Fig. 13 shows respectively the industrial and the residential humidifiers.

Fig. 12: HumidiClean Series HC-6100 industrial steam humidifier up to 15 kW

Fig. 13: Residential ultrasonic humidifier with a maximum capacity of 1.3 gallon

4.3 Test Apparatus

The experimental facility allowed for a precise control of the all the working air conditions, while the test apparatus was the actual section of the wind tunnel where all the experimental tests were

conducted. The spray injection tests were indeed carried out in this section in two different configurations (first and second experimental campaign), as it will be detailed later. The test apparatus was a subsonic open return wind tunnel and Fig. 14 shows a detailed representation of it. More details on the sensors of this section and relevant dimensions will be later provided. The test apparatus was placed within the larger climate controlled wind tunnel with the main advantage to minimize the thermal losses. In fact, the stable air conditions inside the test apparatus were approximately the same as the ones in the larger wind tunnel, all around it. With balanced temperatures on both sides of the test apparatus walls, there would be no heat transfer.

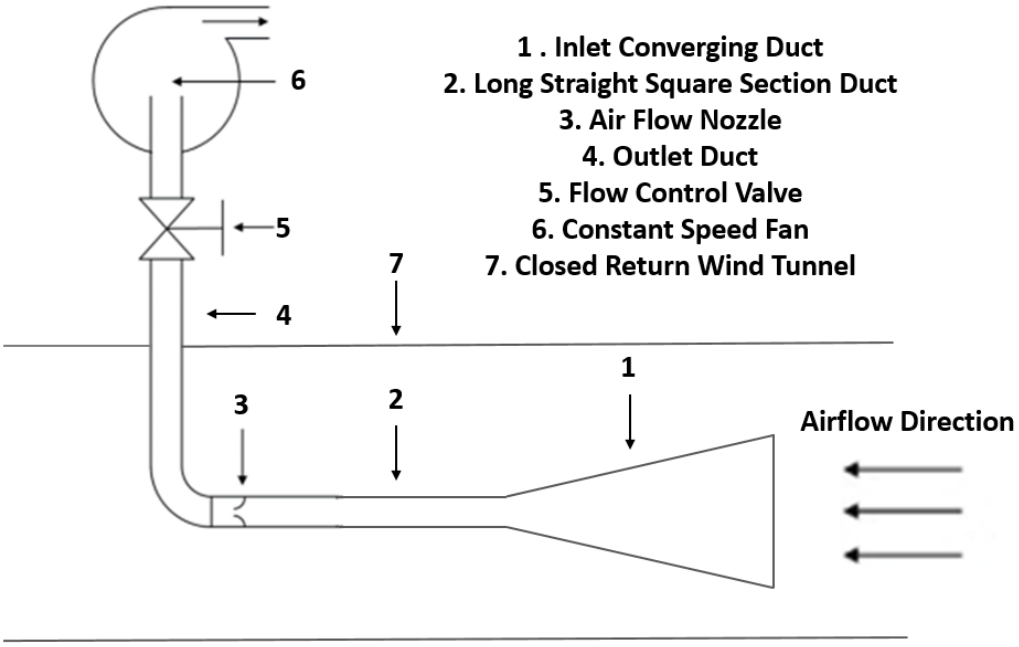

Fig. 14: Schematic of the main test apparatus placed within the larger climate controlled wind tunnel to minimize the thermal losses

The test apparatus consisted of an inlet converging duct, a long straight square section duct, and an outlet duct.

The inlet converging duct, which directed the air flow to the subsequent sections of the test apparatus while maintaining a smooth flow, is represented in Fig. 15. It was constructed from dielectric acrylic sheets with a wall angle of 7° and reinforced with aluminum angle. Silicone caulk was used to seal the corners and walls. A PTFE coated fiberglass fabric sheet with a 7 in. gap attached both portions of the inlet duct and it was installed for practical purposes, i.e. slide the downstream portion back and forth on a set of stainless steel guide rails to facilitate the installation of the long straight square section duct and to provide easy access in case modifications were required. Considering the downstream portion, it was 45 in. long, and it had an approximately 13 in. x 14 in. and 2.5 in. x 7.5 in. inlet and outlet cross section respectively. It also housed thermocouples and RTD temperature probes for air temperature measurements, air sampling probes to measure the dew point temperatures, and the electrospray assembly for the first experimental campaign. The layout of these sensors and more details on the electrospray assembly test section will be shown later.

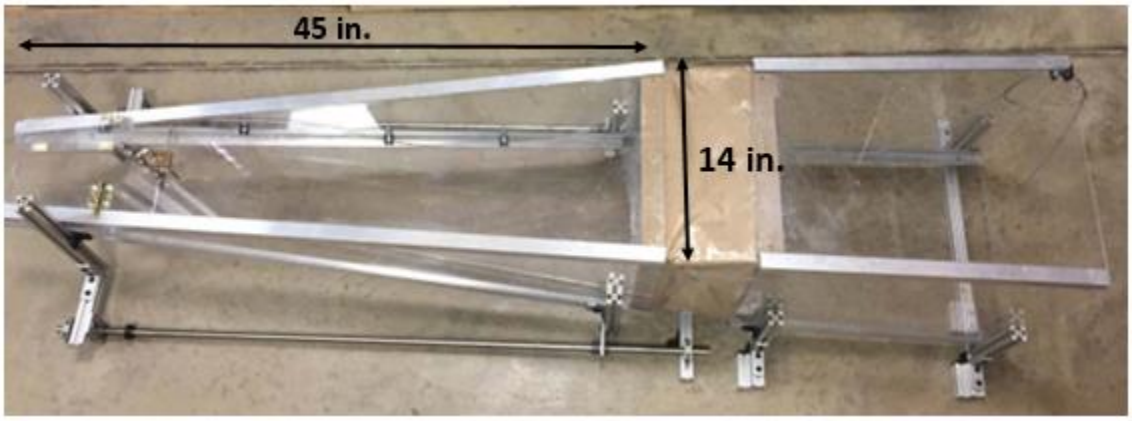

Fig. 15: Inlet converging duct construction

The long straight square section duct, 2 in. x 2 in., was approximately 20 in. long. In the first experimental campaign, when the electrospray assembly was installed in the inlet converging duct, it was simply used to connect the inlet converging duct to the outlet one. In the second experimental campaign, instead, it was used as the actual test section, where four (4) electrospray heads were installed. The two experimental campaigns differed for different aspects but, in particular, for the number of electrospray heads employed and their position in the test apparatus. Due to the different positions along the test apparatus, the cross section area where the droplets were injected differed. Fig. 16 shows a 3D rendering of the overall test apparatus where the three different sections were connected by means of 3D printed couplings, while Fig. 17 shows the details on the positions of the electrospray heads in the two different experimental campaigns, together with some position of the sensors used.

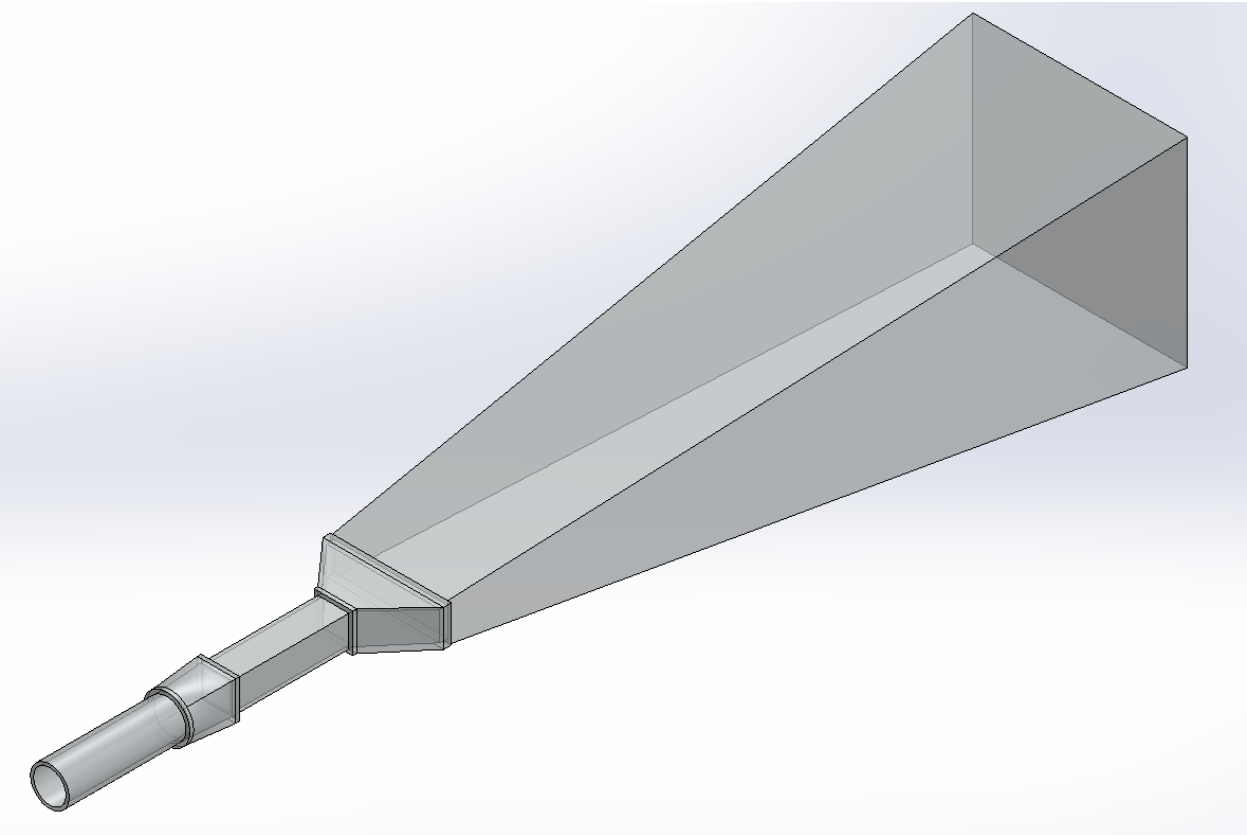

Fig. 16: 3D rendering of the overall test apparatus

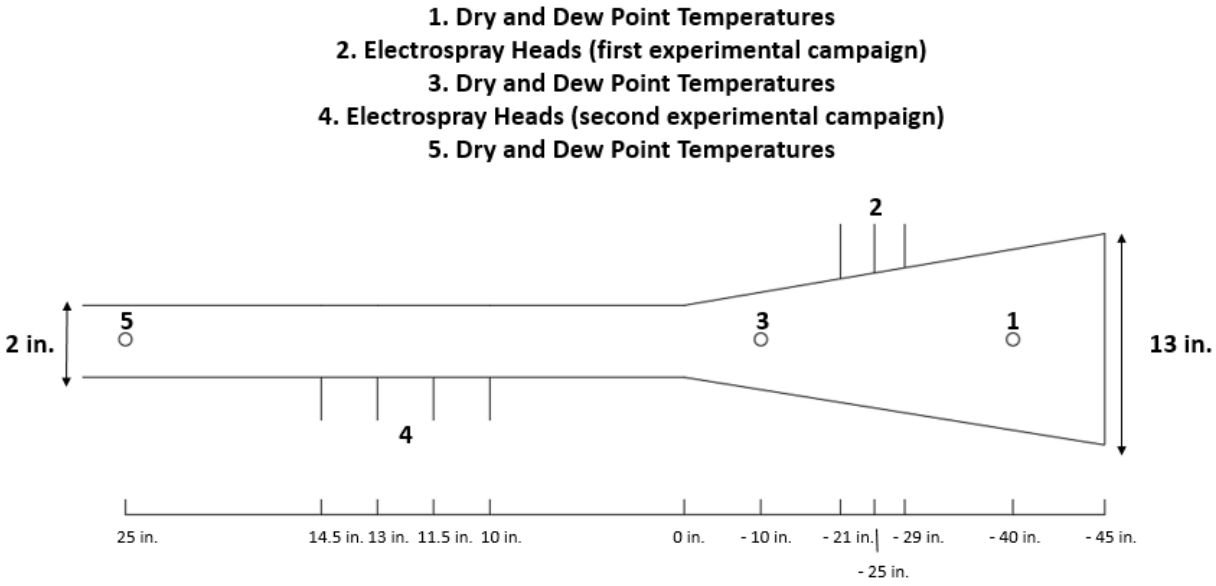

Fig. 17: Details on the positions of the electrospray heads in the two different experimental campaigns (figure not to scale)

For the first experimental campaign, up to six (6) electrospray heads were installed in the downstream portion of the inlet converging duct. The heads were installed on the top surface of the converging duct, while up to three (3) counter count electrodes, one for each row, were installed on the bottom surface, about 2 in. apart from the heads. The six (6) electrospray heads were installed in three (3) subsequent rows, in a slightly staggered configuration so that the flow would be less affected by the previous row. The two (2) electrospray heads in each row were 4 in. apart, about 4 in. away from the edges of the inlet converging duct. They were installed in such a way the electrospray plumes spread throughout the cross section area, which was equal to 12 in. x 7 in, in proximity of the second row. When only one electrospray head was tested, only the second row was used.

Instead, for the second experimental campaign, four (4) electrospray heads were installed towards the end of the straight square section duct. The heads were installed on the bottom surface of the straight duct, while a single counter count electrode was installed on the top surface. The different

positions along the test apparatus were important to investigate the effect of a different air velocities to the growth of the droplets. In addition, the electrospray plume could cover more evenly the entire cross sectional area, when the area was reduced.

Depending on the configuration tested, dry bulb and dew point temperatures were measured in different location, as shown in Fig. 17. In particular, the sensors in position 1 and 3 were used in the first experimental campaign, while the sensors in position 3 and 5 were used in the second experimental campaign. Up to three thermocouples, an RTD probe and the air sampling inlet for the measurement of the dew point temperature were installed in these positions. The additional thermocouple meshes, the flow nozzle and RH sensors were installed outside the portion of the test apparatus represented.

Finally, the outlet duct was employed to recirculate back the air into the large wind tunnel and to precisely control the air flow rate through the test apparatus. This section also housed sensors, control valves and fans, as detailed in Fig. 14. The pressure differential across the flow nozzle was measured to estimate the air flow rate. In proximity of the flow nozzle, also the static pressure was measured to estimate the air density.

To control the flow rate a flow metering valve and two (2) centrifugal blowers in series were installed after the flow nozzle. The exhaust air was then recirculated back by means of semi-flexible tubing and injected back in the wind tunnel, just before the variable speed fan. This position, characterized by the lowest air pressure in the wind tunnel, was strategically chosen to allow a very limited air flow rate throughout the test apparatus, even when the two (2) centrifugal blowers were off. The air flow rates that could be accurately measured ranged from 0.5 cfm to 5 cfm. Smaller flow rates could not be measured because of the relatively large flow nozzle adopted, while larger flow rates were not achievable with the centrifugal blowers.

4.3.2 Electrospray Assembly

The electrospray assembly was the key component of the overall spray injection experiments. The electrospray technology itself was extensively studied in the literature [34, 35, 36, 37, 38, 39], giving several inputs for an optimal design and operation in this thesis. It was mainly selected because of its ease to generate small and highly charged droplets, as required by the thermodynamics model for an enhanced dehumidification process. In addition, its flexibility of operation and low energy consumption were great advantages compared to other similar technologies.

The electrospray assembly consists in an apparatus, which employs electricity to disperse a liquid towards a counter count electrode. High voltage is applied to a liquid supplied through an emitter, such as a needle or a metallic tube, and, when the liquid reaches the emitter tip, it forms a Taylor cone, which emits a liquid jet through its apex. Varicose waves on the surface of the jet lead to the formation of small and highly charged liquid droplets, which are radially dispersed due to Coulomb repulsion. A key advantage of the electrospray is that the application of an electrostatic field to liquid emerging from a capillary tube provides a means for generating small droplets without the need for high pressure, reducing the amount of energy required for the droplets' production.

The main components of the electrospray were indeed the emitter and the counter count electrode. As emitter, stainless steel needles with different gauges and tip length were used, as shown in Fig. 18. In particular, 21, 27, 31, 33 and 34 gauge 2 inches long stainless steel needles, as well as 30, 32 and 34 gauge 0.5 inch long stainless steel needles were considered**.** Fig. 18 shows only some of the needle gauges but both the needle tip lengths adopted. The shorter needle length allowed for an easier distribution of the flow, due to the lower internal resistance to the flow. The longer needles were mainly used during the first experimental campaign, where it was realized that the water flow was sometime interrupted due to the clogging of the long needles. For this reason, in the second experimental campaign, it was preferred to use shorter needles.

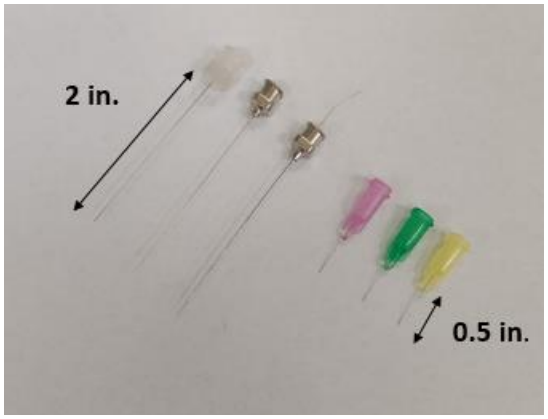

Fig. 18: Stainless steel needle emitters with different gauges and tip lengths

The counter count electrode was instead a simple brass rectangular plate 9.5 in. x 2.5 in., placed perpendicularly below the needle tip. The distance between the needle tip and electrode was kept at about 2 in., throughout all the thesis. This distance was indeed suggested in the open literature for a stable electrospray.

The needles were connected to a syringe pump by means of dielectric PVC tubes with an internal diameter of 0.25 in., connectors and valves. Luer lock fittings were used to connect the needles to the rest of the system. Depending on the number of electrospray heads tested, a programmable single syringe pump (New Era, NE-1000) or a six channel programmable syringe pump (New Era, NE-1600) were used. The pumps were able to provide a maximum water flow rate of 2100 $\frac{\mu l}{min}$ per channel, producing roughly 30 psi at slow speed. However, with these small needle tips, 30 psi was, in general, not enough to push more than 100 $\frac{\mu l}{min}$ due to high internal resistance to the flow. When more than one electrospray heads were tested, each head was served by a single 60 ml syringe and line in order to guarantee the same flow in all the heads. A representation of the water injection lines, together with the programmable single syringe pump employed, is provided in Fig. 19. Both the needles with the two different tip lengths could be connected to the water injection lines.

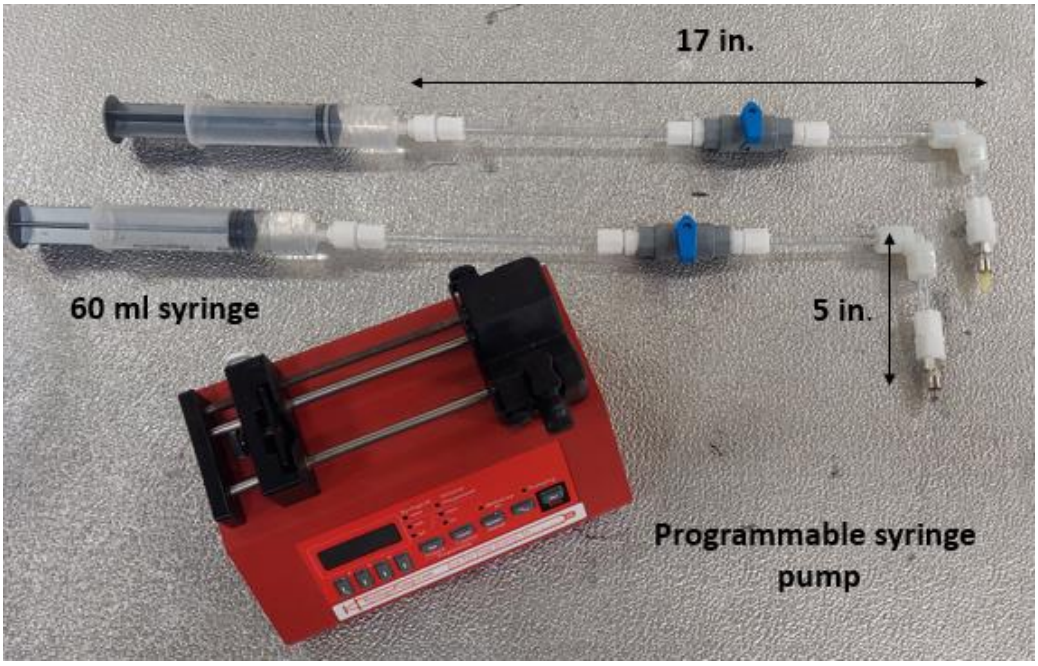

Fig. 19: Representation of the water injection lines and of the programmable single syringe pump

The last key component was the high voltage (HV) power supply to electrify the liquid water. Power supplies of different polarity (HV350REG (+) and HV350REG (-)) were used in this thesis. They were able to provide an adjustable output up to 30 kV at 1 mA and 35 kV at 700 μA. The high voltage power supply was either connected to the needles or to the plate electrode. When the high voltage is applied to the needles, droplets with the same polarity of the power supply are generated. Instead, when the high voltage is applied to the plate electrode, droplets of opposite polarity with respect to the power supply are generated. Both these configuration were tested throughout this thesis.

According to the open literature, liquids characterized by high surface tension, such as water, required very high voltages for the establishment of the electrospray, and the appearance of corona dischargeS limited the maximum applicable electric field. For water, since the necessary voltage was usually higher than the surrounding air's electric breakdown threshold, corona discharges occurred from time to time. Their presence destabilized the electrospray and, in particular, its monodispersity. To

address this challenge, in the present set-up, an additional sheath gas flow of CO_2 characterized by a higher electric breakdown threshold than air may be added to prevent or delay the onset of the corona discharges. The CO_2 was injected in proximity of the needle tip and its flow was controlled by a flow gauge, connected to an industrial grade CO_2 tank. The implementation of the CO_2 flow was then important to avoid the onset of corona discharge and the destabilization of the electrospray. However, as it will be seen later, in some of the spray injection tests the CO_2 flow was not implemented, but it was verified that no corona discharge occurred during the experimental tests. In general, it was not noted any electrical discharges or any bluish glow in the air adjacent to the pointed electrospray head during the spray injection tests. In the very first tests, some electrical discharges occurred towards metal objects within the test apparatus, and, for this reason, all not necessary metals were eliminated from the test apparatus in order to avoid corona discharge.

Additional components, which may be added, consisted of water absorbing materials such as molecular sieves and silica gel polymer sheet, placed on top of the plate electrode to promote the collection of water and avoid its re evaporation, and electrical resistors to limit the electrospray current.

Fig. 20 shows the electrospray head set up when the aforementioned components were integrated together. In particular, Fig. 20 referred to the case when only one electrospray head was used, the negative or positive high voltage power supply was connected to the needle and the plate electrode was grounded. No resistors were connected in series in the high voltage line to limit the current. Fig. 20 includes also the multimeter for current measurements, which it will be described later.

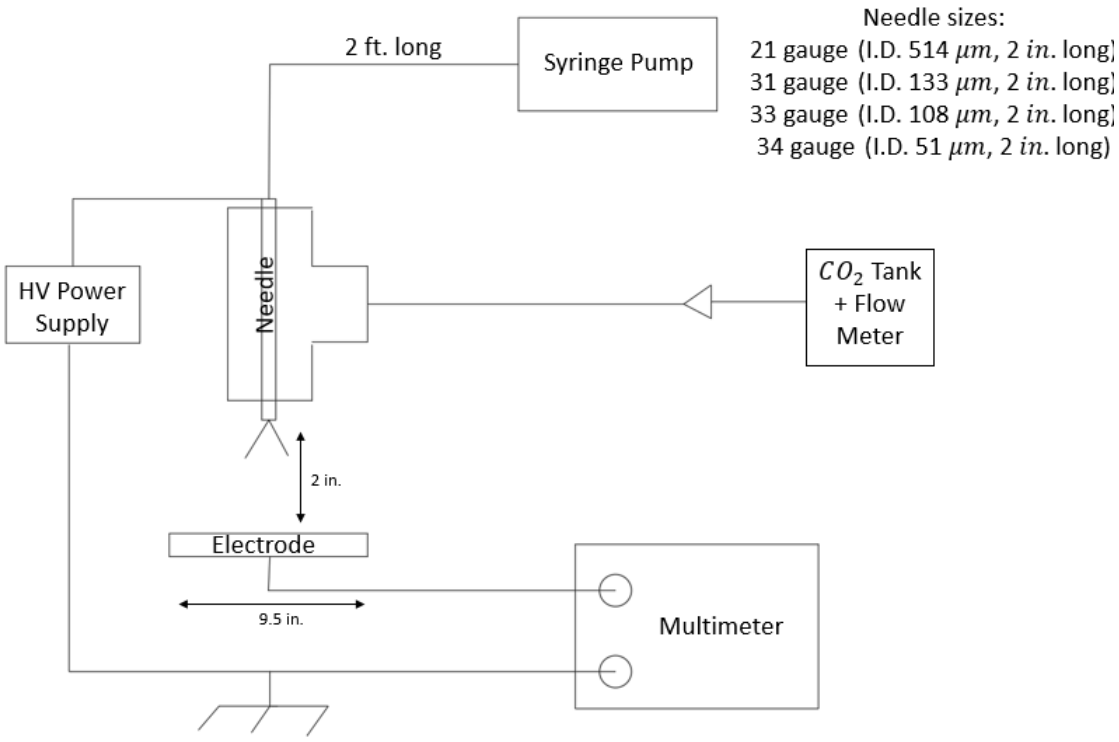

Fig. 20: Schematic of the electrospray set-up (HV supply applied to the needle, electrode grounded) (figure not to scale)

Fig. 20 represents only an example of how the different components can be combined together. This particular set up was used both in the tests in still air as well as in the spray injection tests, when only one electrospray head was used. In the still air tests, all the needles were tested to find the more suitable for stability, which appeared to be the 33 and 34 gauge ones. Among the two, the 33 gauge needle was the easiest to assemble, especially when multiple heads were used due to the connectors required for a leak tight connection, and it was then mainly used during the subsequent spray injection tests. More details will be presented later.

Different modifications were possible and they were investigated throughout all the spray injection tests, in the two different experimental campaigns. Some key differences existed comparing the six (6) and four (4) needle configurations to the single head set up shown in Fig. 20.

For the six (6) needle configuration, each of the six needles had a dedicated water injection line and syringe, connected to the six channel programmable syringe pump. Again, the needle mainly used was the 33 gauge one. The negative or positive high voltage power supply was connected in parallel to the needles and the plate electrodes were grounded. Three (3) 9.5 in. x 2.5 in. rectangular electrodes, one for each electrospray row, were used. The CO_2 sheath was not always employed because it did not provided any benefits in the dehumidification rate and it further complicated the overall system. When two (2) high voltage power supplies were used, they electrified three (3) electrospray heads. When three (3) high voltage power supplies were used, they electrified two (2) electrospray heads. In this configuration, the high voltage power supply was also applied to the plate electrodes, while the needles were grounded, to investigate the change of polarity of the droplets.

For the four (4) needle configuration, each of the four needles had again a dedicated water injection line and syringe, connected to the six channel programmable syringe pump. The needle mainly used in this case was the 32 gauge 0.5 in. long one, while the 30 and 34 gauge ones may be used in the future work. Only the positive high voltage power supply was tested and connected to the plate electrode and the needles were grounded. Only one (1) 9 in. x 2.5 in. rectangular electrode was shared by all the four (4) needles. The CO_2 sheath was not employed because it did not provided any benefits in terms of the dehumidification rate and it further complicated the overall system. Only one power supply was tested in this case. As additional features for this configuration, two (2) electrical resistors and water absorbing materials were added. A 10 $M\Omega$ resistor was connected in series between the power supply and the plate electrode, and 10 $k\Omega$ one was connected between the needles and the return wire to the power supply. The absorbing materials were placed on top of the plate electrode.

As an example, a representation of the overall system with the four (4) electrospray heads in place for the second experimental campaign, when the resistors were used, is provided in Fig. 21.

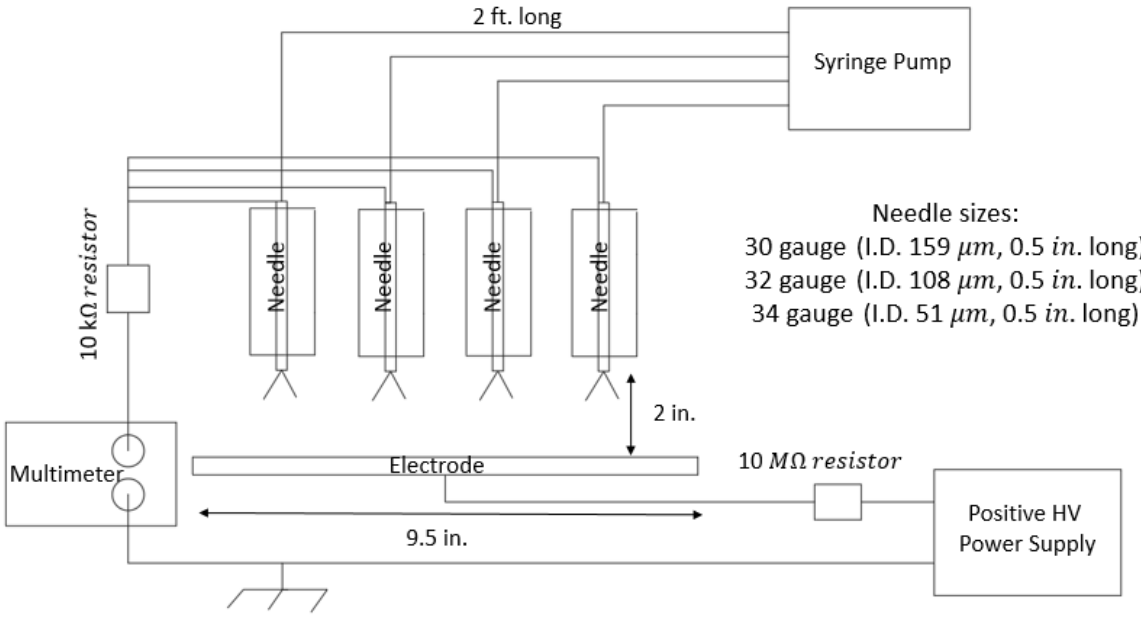

Fig. 21: Schematic of the electrospray set-up (positive HV supply applied to the electrode, needles grounded) (figure not to scale)

With this configuration, both the cases with and without resistors may be tested to investigate the influence of the electrospray current.

4.4 Sensor instrumentation

Many sensors were used to observe and measure the different operating parameters of the experiments in real time. Some of the parameters included temperatures, pressures, flow rates and velocities. All the measurements were processed using a National Instruments™ data logging acquisition system (DAQ) and an in-house developed LabView™ program, which sampled the data every 2 seconds. The program was able to manipulate the acquired data to calculate derived quantities, plot the operating parameters, and store the data in appropriate CSV files. Control and safety routines were also embedded in the program to control the entire experimental facility, for instance, to regulate the power input to

heaters when a desired target temperature was entered in the program or to shut down the entire system if dangerous conditions were reached.

The sensors were installed throughout the experimental facility and the test apparatus, but only the latter will be analyzed in detail. Fig. 22 shows the position of sensors installed and used, limitedly in the test apparatus. More details on the sensors in the overall experimental facility can be found in [38, 39].

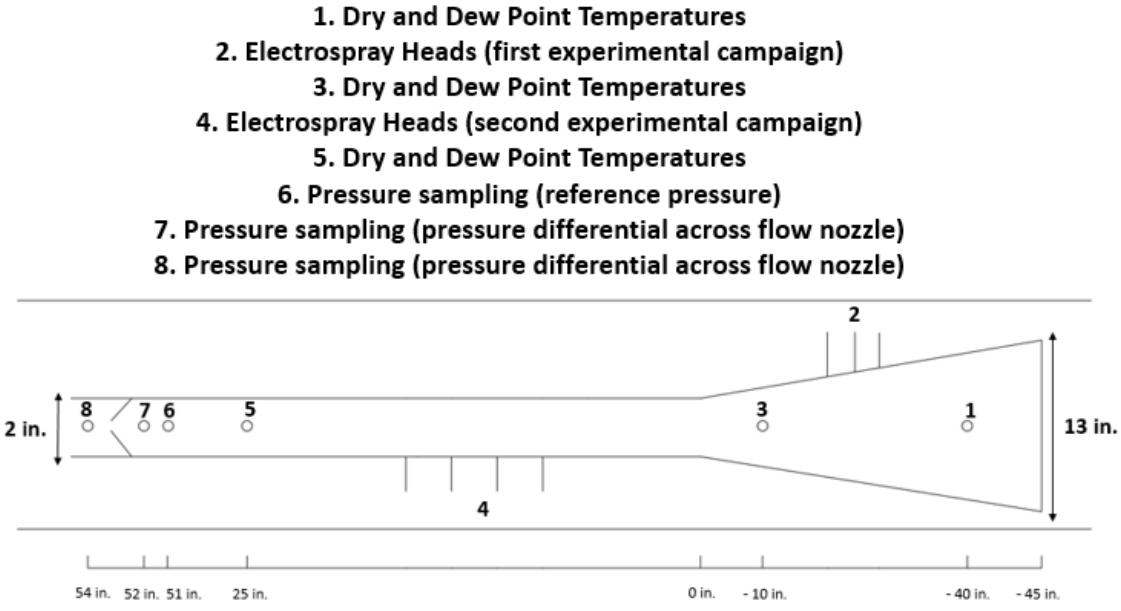

Fig. 22: Position of the sensors positions and their distance to the outlet section of the inlet converging duct (figure not to scale)

T-type thermocouples, RTD temperature probes, chilled mirror dew point meters, flow nozzles, and pressure transducers measured the operating parameters of interest. Many of these sensors were installed in two different positions, usually before and after the test section, to fully characterize both the inlet and outlet conditions and have an understanding on how the phenomenon occurring in the test

section modified the operating conditions. Additional sensors, not represented in Fig. 22, were also used. In particular, upstream and downstream of the portion of the test apparatus represented in Fig. 22, additional thermocouple meshes and RH probes were installed to have redundant measurements of the more relevant operating parameters, i.e. humidity.

A $6\frac{1}{2}$ digit graphical touchscreen digital multimeter was adopted to measure the electrospray current, while a high resolution charged couple device (HR CCD) and a high speed camera were used to visually verified the presence of the electrospray plume. These sensors were not integrated in the LabView™ program.

Table 4 represents important details for the calibration procedure, the operating range and the accuracy of the main sensors employed.

Table 4: Measurement devices, set points, range and accuracies of the sensors employed

Parameter measured	Measuring device	Calibration	Range	Accuracy
Air Temp. (dry bulb)	Thermocouple (grid/mesh)	In situ *	48 to 88 °F	$\pm$ 0.1 °F
Air Temp. (dew point)	Chilled Mirror Dew Point Meter	Manufacturer	33 to 83 °F	$\pm$ 0.5 °F
Relative Humiditity	RH Probe	Manufacturer	0 to 100 %	$\pm$ 1.5 %
Air Pressure Drop	Pressure Transducer	Manufacturer	0 to 3" H_2O	$\pm$ 0.25 %
Water Volume Flow Rate	Programmable Syringe Pump	Manufacturer	0.001 to 3470 $\frac{ml}{hr}$	$\pm$ 1 %
Air Volume Flow Rate	Flow Nozzle	Manufacturer/In Situ	0 to 5 cfm	$\pm$ 0.05 cfm

Note: *Tempearture bath and temperature sensor with accuracy of +/-0.1 F were used for on-site calibration

4.4.1 Temperature probes

Temperatures were measured by two different kind of temperature sensors, i.e. T-type thermocouples and RTD temperature probes. T-type thermocouples were selected for their stability and

excellent repeatability of the measurements. They had a suitable temperature range for the application and, if compared to all the base metal thermocouples (in particular K-type, which is the most popularly used), they had the tightest accuracy. The thermocouples were welded and calibrated in house and the temperature range and accuracy strictly depended on the number of calibration points considered during the calibration procedure. The RTD temperature probes were instead directly provided and calibrated by the dew point sensors' manufacturer. They were installed in the specific location where the two dew point sensors sampled the air, before and after the test section. Both the thermocouples and the RTD temperature probes measured the dry bulb temperature of the air in different locations within the wind tunnel. To enhance accuracy, the thermocouples were usually organized in mesh configurations, with up to nine thermocouple wires per mesh. For instance, a 3x3 mesh configuration with nine thermocouples were used to measure the air temperature after the flow straightener, upwind and downwind to the cooling coils of the large wind tunnel. The accuracy for the thermocouples reported in Table 4 considered the mesh configuration with multiple thermocouples measuring the same quantity.

Always T-type thermocouple probes, but manufactured by Omega, measured the temperature in the pressurized cooling tubing. They were calibrated and verified by the manufacturer.

4.4.2 Dew Point Sensors and RH sensors

Two chilled mirror dew point sensors sampled air upstream and downstream to the test section to measure the dew point temperatures. The dew point measurement was based on the proven, fundamental optical chilled mirror measurement principle. At the sensor, the temperature of a chilled gold plated mirror was decreased until water condensed on the surface as sampled air passed over the mirror. An optical light source and sensor above the mirror measured the light reflected off the mirror to determine when condensation occurred. A sensor control unit modulated the chilled mirror temperature and measured the exact temperature, i.e. the dew point temperature, at which condensation occurred. The Michell Instruments S8000 Remote Chilled Mirror Hygrometer was selected for these measurements

due to its high accuracy and its long term drift free humidity measurement over the entire operating range.

The dry bulb temperatures were also measured by RTD probes and thermocouples in the location of the air sampling and, together with the dew point temperatures, allowed for the calculation of the humidity both upstream and downstream of the test section. In particular, both the relative humidity and the air water content of the sampled air were calculated by means of EES thanks to these measurements.

The dew point sensors were crucial for the characterization of the electrostatically enhanced condensation process, occurring in the test section. Indeed, thanks to the humidity readings, it was possible to estimate the amount of vapor wiped out from the humid air and condensed on the plate electrode. If the sensor downstream to the test section detected a lower value of humidity, dehumidification occurred.

To function, a sample of air from the area of interest needed to be extracted and pumped across the chilled mirror sensors, located outside the wind tunnel. Custom made sampling wands and stainless steel tubing, to avoid moisture retention, were utilized to direct the air towards the mirrors. The sampling procedure occurred evenly throughout all the width of the test section duct. For a correct operation of the sensors, at least 2 $scfh$ of air must be guaranteed and flow across the chilled mirrors. After the mirrors, the sampled air travelled across air pumps and it was pumped back into the wind tunnel. To guarantee the mass conservation, the air sampled from the outlet must be pumped back before the flow nozzle for a correct air flow rate measurement.

The S800 sensor has an uncertainty of ± 0.5 $^{\circ}\mathrm{F}$ for the dew point temperatures, which is a quite tight uncertainty considering the difficulty of the measurement.

Throughout the experiments, the correct operation of the dew point sensors were verified either by comparison with each other, in the so called iso-ω tests as detailed later, or by comparison with different sensors. In particular humidity and temperature probes (Vaisala HMP110) were selected for this

purpose. They were installed upstream and downstream to the test section as well and they were characterized by high accuracy, i.e. ± 1.5 % RH, and good stability.

If the correct operation of the dew point sensors was not verified, the sensors were cleaned per the manufacturer's instructions.

4.4.3 Pressure Transducers

The air flow rate across the test section was evaluated by means of air pressure measurements. For more details on the locations of the pressure sampling and of the flow nozzle used to measure the air flow rate, refer to Fig. 22.

As detailed in Fig. 22, all the air pressure measurements occurred after the test section. The first measurement provided a reference pressure, while the measurements across the flow nozzle provided a pressure differential for the estimation of the air flow rate. ANSI/ASHRAE Standard 41.2-2018, Standard Methods for Air Velocity and Airflow Measurements detailed the design of the airflow nozzle. Across the airflow nozzle, the static pressure from four points (top, bottom, left and right) were sampled and averaged by directly connecting all four points together into one pressure tube, as represented in Fig. 23 Throughout the test apparatus, no pressure losses measurements were carried out.

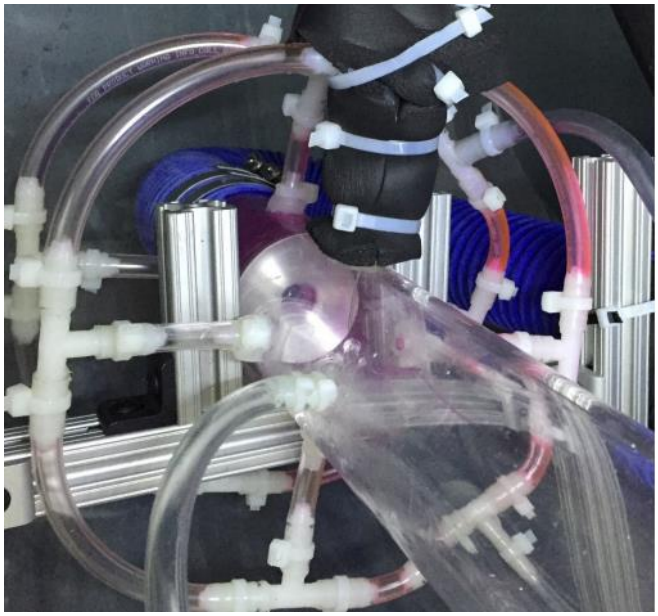

Fig. 23: Outlet nozzle and pressure sampling configuration

Pressure transducers (Setra Systems), which communicated with LabView, with different pressure ranges were used. The air flow rate across the test section was varied between 0.5 and 5 cfm. In particular, up to about 2 cfm, a 0 – 0.5 inches water column transducer was used, while, up to 5 cfm, a 0 – 3 inches water column transducer was used. This choices improved the accuracy of the measurement. An air flow rate of about 0.04 cfm was tried to measure, but the current airflow nozzle resulted too big for this measurement. Indeed, for flow rates lower than 0.5 cfm, the readings resulted to be fluctuating either due to the large size of the flow nozzle or due to the intermittency of the flow across the test apparatus.

4.4.4 Multimeter

As detailed in the open literature, the electrospray current transferred by the charged droplets between the emitter and the collecting electrode was a good parameter to estimate the charge of the droplet. In accordance to the thermodynamics model, a high electrical charge would correspond to a high dehumidification potential. In addition, if a current, higher than the current detected when no

electrospray was present, was measured, it was a further verification of the presence of the electrospray. Currents in the $nA - \mu A$ range were usually measured and an instrument able to detect these extremely low current needed to be selected. A DMM6500 $6\frac{1}{2}$ Digit Graphical Touchscreen Digital Multimeter (Tektronix) was chosen for this purpose. It was particularly suitable to make low current and low resistance measurements on low power devices and to capture transient signals with the built in digitizer. It was connected in series between the grounded electrode and the return wire to the power supply and it was mainly used to evaluate the average electrospray current during each spray injection test. In general, the electrospray current was not constant but fluctuating at high frequency, especially when the electrospray operational mode was not stable. For this reason, the ability of the instrument to capture transient and automatically provide averages, maximum and minimum values was extremely useful. Details of the electrical connection of this device were provided in Fig. 20 and 21. In case of the six (6) electrospray head configuration, the device usually measured simultaneously the current delivered by the two heads in the middle row. In case of the four (4) electrospray head configuration, the device, connected in series between the grounded needles and the return wire to the power supply, measured simultaneously the current delivered by the all four heads.

4.4.5 Video scope and High Speed Camera

The electrospray plume, characterized by transparent sub micro meter droplets, was observed by a video scope and a high speed camera. The main goals of this observation were the verification of the presence of the plume and the Taylor cone and the measurement of the droplet size and velocity, between the needle and the plate electrode.

A High Resolution Charged Couple Device (HR CCD) video scope (Olympus IPLEX NX IV9000N) and a Photron Mini AX100 540k Color 16 GB high speed camera were located nearby the electrospray plume. Due to the nature of the fluid injected (water), the observation was not always successful and, in general,

low quality images were captured. It was still possible to verify the presence of the electrospray mainly by checking the deposition of tiny droplets on the counter count electrode, but the size and the velocity of the droplets were not measurable with this implementation.

4.5 Calibration and Verification of the Test Setup

Data acquisition was highly automated and LabView was used to acquire, visualize and control different quantities. Prior to testing, in order to calibrate and verify the sensors, various procedures were conducted, in particular to check the correct operation of the thermocouples, RTD temperature probes, dew point sensors, flow meters and electrospray heads. The electrical components, such as the high voltage (HV) power supplies and the multi-meter, were calibrated by the manufacturer and no verification procedures were carried out.

During the calibration process, the sensor to be calibrated was compared to a more accurate sensor. The verification was instead accomplished by measuring again some points in the calibration range and comparing them to the calibration curve or by comparing multiple sensors, calibrated independently, to check that they were all in agreement. For instance, the flow meters, in particular the ones embedded in the syringe pumps, were directly calibrated by the manufacturer and the verification was simply performed by collecting the water in a beaker for a specific amount of time (30 min) and making sure that it was in agreement with the flow rate, which could be read on the pump, in the same amount of time. Thermocouples, RTD temperature probes and the dew point sensors were instead calibrated and/or verified in-situ. The electrospray operational modes were investigated and verified before installing the heads in the test section for the spray injection tests. The cone jet operational mode was the one to achieve for monodispersity and specific ranges in terms of high voltage potential were identified for its establishment.

4.5.1 Temperatures

Temperatures were measured throughout the wind tunnel with thermocouples and RTD temperatures probes. Usually thermocouples were organized in meshes, up to nine (9) thermocouples per mesh, to improve the accuracy of the temperature reading in the specific location but also to verify their correct operation by comparison. Each of the thermocouples were calibrated and verified in-situ prior to the installation. Using the National Instruments Measurement & Automation Explorer (NI MAX) program, the thermocouples were calibrated in reference to a VWR® Traceable® platinum ultra-accurate thermometer which had an uncertainty of ±0.0234°F, and is represented in Fig. 24. A Cole-Parmer Polystat® cooling/heating circulating bath was used to maintain a mixture of ethylene and water at a constant temperature and allow an optimal calibration and verification of the thermocouples. The circulating bath is shown in Fig. 25.

Fig. 24: Ultra accurate thermometer

Fig. 25: Circulating temperature bath

The circulating bath was set at different constant temperatures within the calibration range. For each temperature, about a half of hour was allowed for the bath to reach a fully steady temperature, which was confirmed by the ultra accurate thermometer. When steady state was reached, the temperature was measured and recorded in the NI MAX program by both the ultra-accurate thermometer and all of the thermocouples to be calibrated, which were together submerged in the bath. This process was repeated for all the temperature points across the desired range of calibration. Using the routine of the NI MAX program, a line-fit interpolation for all the measured temperature values was generated, and the thermocouples were then calibrated. The calibration was finally verified by repeating the

measurement process at a few different temperature points and in a different order than the calibration was made. It was done to ensure that there was no hysteresis effect during the initial calibration.

The RTD temperatures probes were instead calibrated by the manufacturer and the verification was performed in-situ by comparing their readings against the thermocouple readings in different locations within the wind tunnel, before their installation.

In addition, before each spray injection experimental test, the proper operation of all the temperature sensors were frequently verified by means of a so-called iso-T test, which was a kind of test where the dry bulb temperature was kept constant throughout the test apparatus and it was measured in different locations. More details will be provided later.

4.5.2 Air Water Content (ω) and Relative Humidity

The measurements of omega and relative humidity were particular critical for this project. For humid air, to fully determine a thermodynamics point, at least three properties, such as dry and dew point temperatures and pressure, must be known. Once these properties were known, the others could be indirectly determined by means of psychrometric property tables or EES. Water content in the air was only indirectly measured by relative humidity (RH) sensors and dew point sensors, while relative humidity was either directly or indirectly measured by relative humidity (RH) sensors or dew point sensors. If compared to each other, the RH sensors were less accurate than the dew point sensors, especially at measuring the air water content, but they were still useful to collect additional readings and verify the proper operation of the dew point sensors. Both these sensors were calibrated by the manufacturer and verified in-situ.

The simple verification tests consisted of measuring the air water content or specific humidity (ω) in different positions within the wind tunnel, making sure that all the readings were in agreement. In these tests no water was injected in or removed from the system. Verification tests on the relative humidity were a little bit trickier because, to have agreement in the readings, the dry bulb temperatures

needed to be the same throughout the wind tunnel. It was indeed extremely important, in order to have correct measurements, that the dry bulb temperatures were measured in the same exact sampling location of either the RH sensors or dew point sensors.

Temperature, humidity, and flow rate were kept at a constant level for approximately thirty minutes and all the data from the sensors were measured and recorded. From these data, water content in the air at each point was calculated using EES. Always with EES, an uncertainty analysis was conducted to confirm that the measured differences or error between the sensors fell between the sensor's tolerance levels. These verification tests, as the iso-T tests, were also performed before each spray injection experimental test. They were named iso-ω tests and more details will be again provided later.

4.5.3 Electrospray

The operational modes of the electrospray were also investigated and verified. The electrospray assembly was similar to one previously described and represented in Fig. 19. Dielectric PVC tubes were used to connect the syringes to the needles. Needles with different size and length could be connected to the rest of the assembly by means of luer lock connectors. Fig. 26 shows instead an enlargement of the electrospray head, where it is possible to see the needle, the high voltage connection and the CO_2 intake duct. The plate electrode was placed perpendicularly below the needle tip, maximum 2 in. apart.

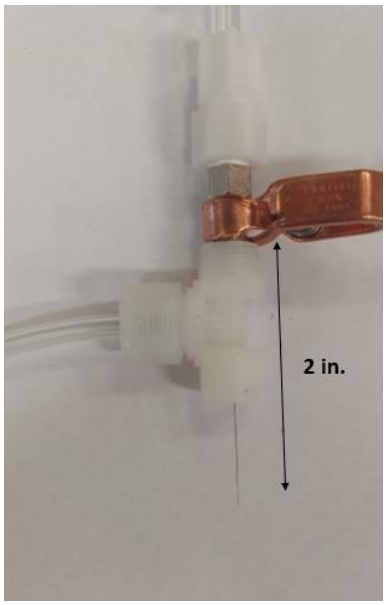

Fig. 26: Enlargement of the electrospray head

As described in the literature, the electrospray can be operated in different operational modes, each of them characterized by their own particular features. In particular, in the absence of an electric field, i.e. high voltage potential difference, the water flowed drop by drop at the outlet of the needle, but when a direct current voltage was applied between the needle and the electrode, the droplet emission frequency increased, and a reduction of the droplet size was promoted. Varying the voltage applied, different electrospray modes would ensue, as detailed and summarized in [22].

Among all the operational modes, the cone jet mode was identified as the most adequate for the monodispersity of the droplets and the most suitable for the dehumidification processes. The monodispersity was indeed important to have all the droplets within the suitable range predicted by the model and to facilitate a further theoretical investigation on the droplets growth.

For this reason, a set of experimental tests were conducted before the actual spray injection tests to identify the high voltage operational range for this particular mode. The experiments were conducted at atmospheric air pressure and room temperature of about 68 °F (20 ℃). The water flow rate was varied

in the range from 5 to 40 $\frac{\mu l}{min}$, while the CO_2 flow rate was kept fixed at about 1.5 $\frac{l}{min}$. 21, 27, 30, 31, 32, 33 and 34 gauge needles were tested. In the ambient air, the continuous electrospraying process was observed when a potential difference of several thousand volts was applied between the electrode and the needle emitter.

The cone jet operational mode was based on the formation of a sharp liquid cone, i.e. the Taylor cone, whose apex region was characterized by mass and charge ejection. The influence of the needle emitter size was not always explicitly addressed in the open literature, but, for a given flow rate, the maximum droplet emission frequency should increase and the minimum droplet size should instead decrease, if the needle diameter was reduced.

It was also observed that the needle size had a significant influence on the stability of the electrospray in the experiments conducted and, in general, smaller needles facilitated the stability of the cone jet mode. With the larger needles tested in these preliminary tests, it was never possible to observe a clear voltage range where the jet was stable for all the liquid flow rates considered. The jet was emitted only intermittently or characterized by several emitting sites, i.e. a multicone jet. Instead, when a positive (+) or negative (-) HV potential was applied to the 33 and 34 gauge needles, a stable jet was observed within a precise voltage range. The Taylor cone and the plume were observable and reasonably stable. Fig. 27 and Fig. 28 show the voltage stability domain, respectively for the 33 and 34 gauge needles.

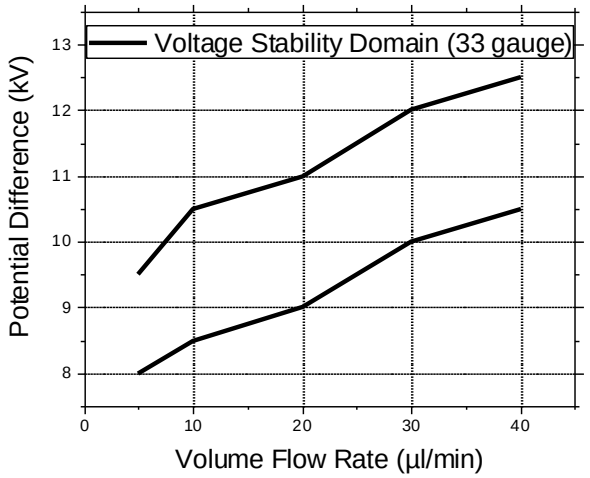

Fig. 27: Voltage stability domain for the 33 gauge needle with a water flow rate between 5 and 40 $\frac{\mu l}{min}$

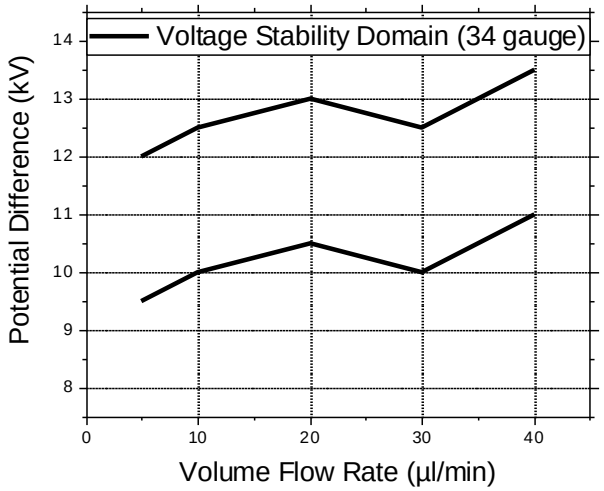

Fig. 28: Voltage stability domain for the 34 gauge needle with a water flow rate between 5 and 40 $\frac{\mu l}{min}$

The set up used for these tests was exactly the same as reported in Fig. 20, with the only difference that the electrospray current was not measured in the tests in still air. A sheath CO_2 flow was essential for the stability of the electrospray and to avoid disrupting corona discharge phenomena. The stability was again defined as the condition required to achieve droplets monodisperse in size. In these particular

tests, only when the Taylor cone and the plume were consistent and not intermittent, the electrospray operational mode was considered stable.

The smallest needle required a slightly higher voltage potential difference to achieve a stable cone jet mode. These two domains resembled the stability domain observed by [25] and referred to as the “low voltage stability domain”. The same authors also observed a different stability domain referred to as the “high voltage stability domain”, with a similar electrospray configuration adopted in this analysis. However, this high voltage domain, i.e.14 – 18 kV, was not observable in these tests.

In the “low voltage stability domain”, the admissible flow rate range was wider (0.2 – 60 μl/min), and the droplet sizes were slightly smaller than in the “high voltage stability domain”. A wider flow rate range allowed for a broader droplet size distribution because droplet size and flow rate are directly proportional. The flow rate may be further increased or decreased with respect to the range considered in these tests to achieve the most suitable droplet size for the dehumidification processes.

A stable electrospray operation in the cone-jet mode was not a strict requirement of the dehumidification processes. Indeed, a relative humidity reduction of approximately 5% with an air flow rate of 0.04 cfm was shown when the electrospray jet was unstable, characterized by the formation and subsequent disruption of the Taylor cone [16]. However, the electrospray's stability and its monodispersity might facilitate a subsequent theoretical investigation of the droplet growth and analysis of the dehumidification processes' experimental results. Starting from droplets all of the same size, a prediction of their growth could be indeed easier.

In the actual spray injection tests, a stable electrospray was first implemented and tested but, due to the difficulty in his implementation and poor dehumidification rates, an electrospray operated in the same voltage range but without CO_2 flow was preferred for its easier implementation. Tests with 20 kV high voltage potential were also carried out to maximize the electrospray current and then the droplet charge. Higher water flow rates with respect to the one tested in still air were also considered.

Additional tests were conducted with this same set-up to investigate also the influence of the electrode needle distance. In general, when the distance between the needle tip and plate electrode was increased, it was possible to identify a voltage stability domain that resulted similar but slightly (1 – 2 kV) translated towards higher voltage potentials. With a distance way higher than 2 in., it was more difficult to identify a clear voltage stability domain.

Additional investigations were also conducted when HV potentials were applied to the plate electrode. The main advantage of this last set-up was the possibility of electrifying only the electrode and not all the supply lines due to water's conductive nature. In these cases, the jet was no more as stable as the cases when the HV was applied to the 33 or 34 gauge needles. It was slightly intermittent or characterized by multiple emissions sites. This configuration will be adopted in the second experimental campaign, with the goal to replicate the experimental tests in [16].

As an example, Fig. 29 shows a digital image of the electrospray in the cone-jet operational mode, where the Taylor cone and plume were visible and have been highlighted using the yellow dashed lines.

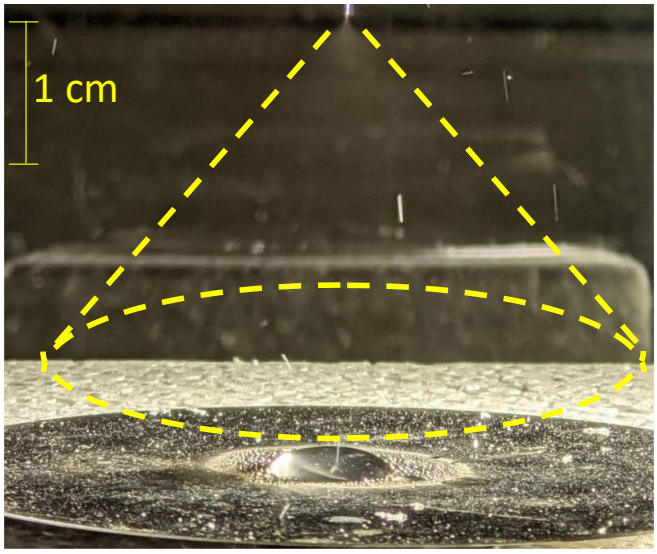

Fig. 29: Image of the electrospray in the cone-jet operational mode (34 gauge needle, 10 μl/min, 11 kV)

Fig. 29 shows the relative low quality of the images it was possible to collect with the instruments and the set up employed. It was then difficult to use these images to estimate the droplet size and charge.

In the absence of direct measurements of these quantities, scaling laws, only developed for the cone jet mode and available in the open literature, were used to evaluate the net current carried by the electrospray and the mean diameter of the associated droplets. Examples of these scaling laws were reported in the literature review. In particular, Equation (3) and Equation (5) were applied to estimate the net spray current and droplet size only when, with the 33 and 34 gauge needles, the electrospray was operated in the stable cone jet mode. The constants $f(\varepsilon_l)$ and $G(\varepsilon_l)$ in the equations were a function of the dielectric constant of the liquid, and they were considered equal to 18 and 0.648 respectively for water. No clear distinctions were made on the particular kind of water, i.e. deionized, distilled or tap water.

Fig. 30 shows the trend of the current as a function of the water volume flow rate, while Fig. 31 shows the trend of the mean droplet diameter. Two electric conductivities were considered, i.e. 1.02 and 0.056 $\frac{\mu S}{cm}$.

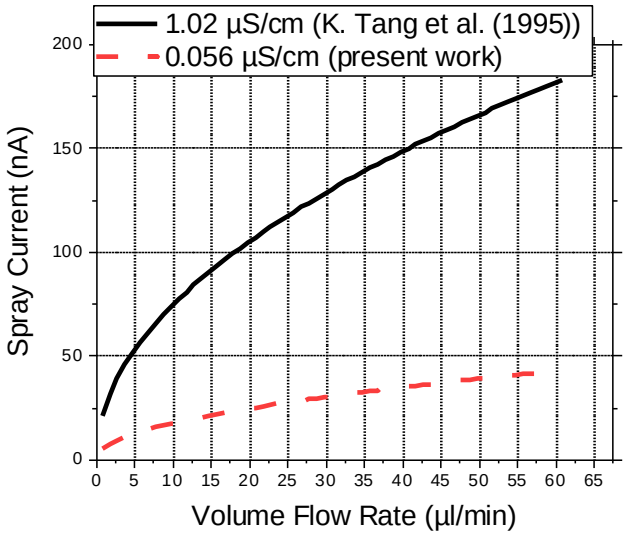

Fig. 30: Net spray current as a function of the volume flow rate (cone-jet mode)

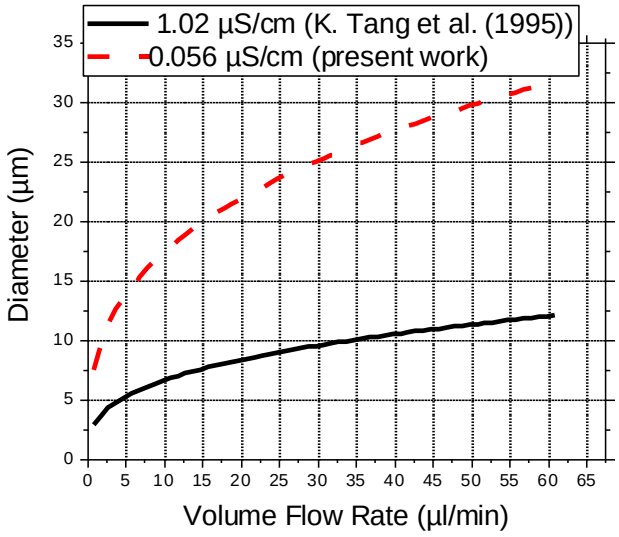

Fig. 31: Droplet diameter as a function of the volume flow rate (cone-jet mode)

The impact of the electric conductivity on both net spray current and the droplet diameter was evident. The current increased as the volume flow rate increased, and a higher electric conductivity

resulted in a higher net spray dispersion current. The droplet diameter increased as the flow rate increased as well, and a higher liquid electric conductivity promoted the formation of smaller droplets. For these reasons, different kind of waters, i.e. deionized type I, type II, and type IV were investigated in the spray injection tests.

Chapter 5: Experimental Test Procedure

A detailed description of the experimental test procedure was presented. Before the actual spray injection tests, a series of preliminary verification tests were performed. In particular, temperatures, air water content and heat balance tests were carried out to verify the correct operation of the facility and its sensors. Once the correct operation was verified, the actual tests, i.e. the spray injection tests, were performed with the scope of investigating the electrostatically enhanced condensation process. The main goal was the evaluation of the air water content difference between the inlet and the outlet of test section in order to estimate the dehumidification potential of the proposed process. In the actual tests, different operating parameters, such as flow rates and high voltage potentials, were varied to estimate their impact on the overall process. The actual tests were carried out in two different locations of the test apparatus, characterized by different geometry and cross sectional areas. The testing schedule on both these two locations shared many similarities, as described in the last paragraph of this chapter.

5.1 Temperature and Air Water Content Verification Tests

Dry bulb temperatures and dew point temperatures were measured at different locations along the test apparatus, as represented in Fig. 22. These temperatures were jointly used to derived, through EES, the relative humidity and air water content, i.e. ω. In this way, the time variation of temperatures, together with the time variation of relative and specific humidity was known throughout the apparatus.

The humidity in the wind tunnel was controlled by means of an industrial steam humidifier and/or by means of two ultrasonic humidifiers, connected in parallel. Both these devices were controlled manually in order to reach a steady state humidity, usually of about 90%, at the inlet of the test section, throughout all the duration of the tests.

When the aforementioned steady state humidity was reached, after about an hour, the temperature and air water content verification tests, also called iso – T and iso – ω tests respectively, were performed. These tests were usually carried out simultaneously, provided that the temperatures at the inlet and at the outlet of the test section were the same. They were performed at least once during each testing day, when no spray injection was occurring.

Fig. 32 and Fig. 33 represent the trends of the temperatures and of the specific humidity as function of time respectively, measured at three (3) and/or four (4) different locations along the test apparatus. For more details on the measurement locations, refer to Fig. 22**.** The average temperature of the inlet mesh represented the temperature measured upstream with respect to the portion of the test apparatus shown in Fig. 22. Again, the specific humidity inlet and outlet (yellow and black line in Fig. 33) represented the specific humidity measured upstream and downstream with respect to the portion of the test apparatus shown in Fig. 22.

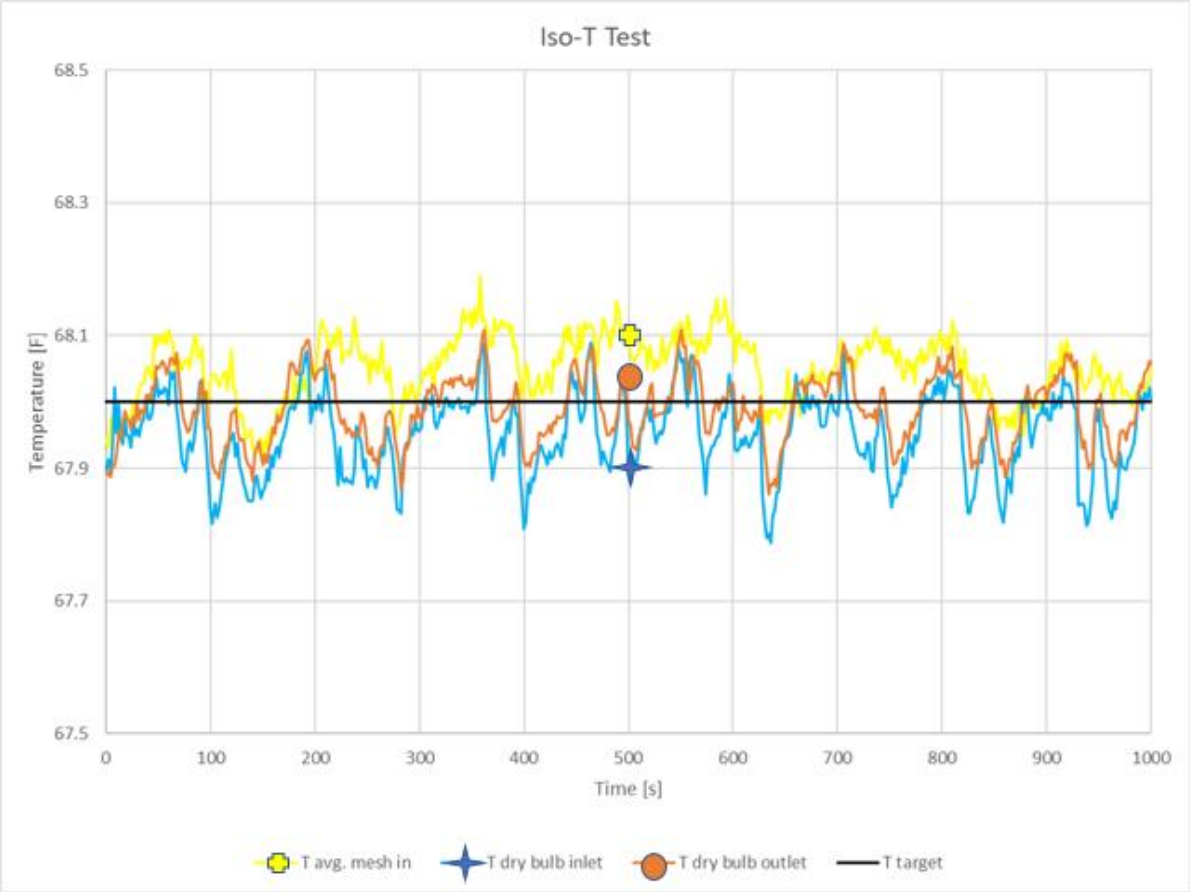

Fig. 32: Example of temperature verification tests at different locations along the test apparatus

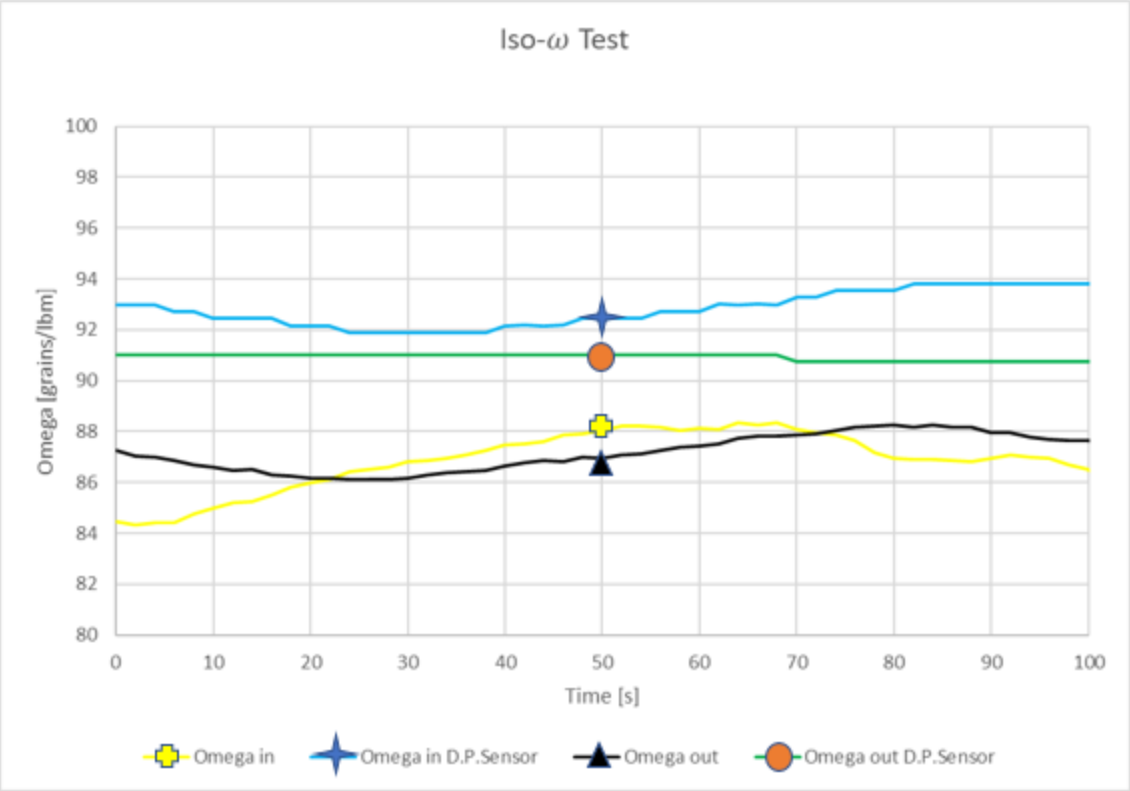

Fig. 33: Example of air water content verification tests at different locations along the test apparatus

The constant temperature line in Fig. 32 represented the target temperature to reach. The temperatures measured with the thermocouples were in agreement with the target temperature with an uncertainty of about $\pm$ 0.1 °F (0.056 °C), as predicted by the Taylor series uncertainty propagation method. The temperatures in some of these locations were also measured by RTD probes and they were in agreement with the thermocouple readings, with a higher uncertainty.

The air water content or specific humidity was instead derived by the dry bulb and dew point temperatures or by the dry bulb temperature and relative humidity. Using the dew point temperatures, the specific humidity derived were in good agreement, within the uncertainty predicted by the Taylor series propagation method. A larger offset existed if the relative humidity was instead used, reason why the specific humidity derived in this way was just used as an additional verification and not to actually evaluate the performance of the electrostatically enhanced dehumidification process.

During these tests a representation of the trend of the relative humidity would have had the same meaning, considering the equality of the dry bulb temperatures. However, in case of not constant dry bulb temperatures along the wind tunnel, just the relative humidity would not have been enough to verify the air was holding the same amount of water vapor. For this reason, in this thesis, the variation of humidity was provided only in terms of the specific humidity.

5.2 Heat Balance Tests

The heat balance tests were additional tests performed to verify the correct operation of the measuring sensors and of the data acquisition system. In particular, these kind of tests were performed solely at the beginning of different experimental campaigns, where the test apparatus configuration, together with connections and fittings, was changed or modified. For instance, these kind of tests were performed at the beginning of the second experimental campaign, where major geometry and connection changes were made. The main goal was the verification of the correct operation of the air flow rate measuring system, inherited by a prior research setup and briefly described in the previous chapter. As a consequence, with a successful verification, it was also possible to guarantee that the new connections were totally leak tight.

The tests were carried out by placing a 10 Ω resistor (HS100-10RF ARCOL), able to provide up to 100 W, in the air stream. The heater was powered by a DC power supply (PS-A305D DAZHENG), which allowed for a precise estimation of the power input into the heater. Once the heater temperature reached a steady state or constant value, an approximately 30 minutes recording was initiated to acquire the temperature at the inlet and the outlet of the heater position. The air flow rate was then verified by means of an energy balance on the heater, as represented by Equation (17).

$$\dot{Q}_{el} = \dot{m} c_p \Delta T \tag{17}$$

Knowing the heater electric power and the temperature difference, the air mass flow rate was evaluated by both the energy balance, Equation (17), and the air flow rate measuring system, constituted by the flow nozzle and a pressure transducer. If the two measuring procedures gave, within the uncertainties of the sensors, the same result, the heat balance tests were considered successful.

5.2 Air Water Content and Relative Humidity Variation Analysis

As an additional procedure to verify the meaningfulness of the spray injection tests, the maximum air water content and relative humidity increase was evaluated, with the assumption that all the water injected into the system evaporated. This evaluation was performed with 5, 10, 15 and 100 $\mu l/min$ of water injected and with 0.5, 2 and 5 cfm of air flow rate. The water injected referred to the water injected per electrospray head, and the cases with one (1), four (4) and six (6) heads were considered. The air flow rate of 0.04 cfm, as investigated in [16], was not tested because it was not possible to measure it precisely with the current setup. An inlet relative humidity of 90 % and a dry bulb temperature of 68 °F (20 °C) were assumed.

When no high voltage potential was applied, the highest humidification rate should be experienced. In fact, all the tiny droplets injected were neutral and their evaporation should be favored, as predicted by the Kelvin model. In all other tests, when the HV was applied, a lower humidification rate or, for successful electrostatically enhanced condensation process, a dehumidification rate should be instead experienced. With this analysis, it was possible to verify that the humidity increase in all the spray injection tests were lower than the maximum humidity increase here evaluated. In fact, as it can be seen in chapter 7, in many spray injection tests a humidification of the air stream was measured and, for this reason, it was important to verify and estimate the physical limit of this process.

The following equations (18, 19, 20) were used to predict the maximum humidification, when all the water injected evaporated.

$$\dot{m}_{a1} = \dot{m}_{a2} = \dot{m}_a \tag{18}$$

$$\dot{m}_a \omega_1 + \dot{m}_{water} = \dot{m}_a \omega_2 \tag{19}$$

$$\dot{m}_a h_1 + \dot{m}_{water} h_{water} = \dot{m}_a h_2 \tag{20}$$

Knowing the steady state inlet conditions, the air flow rate and the water flow rate injected, it was possible to evaluate the outlet absolute humidity and enthalpy. All the other outlet conditions, in particular the outlet relative humidity, were derived through EES. If the temperature of the water injected is similar to the air temperature, this evaluation can be also made assuming a constant wet bulb temperature.

Table 5 provides the variation of relative and absolute humidity of the air for 0.5 cfm and 5 cfm when 5, 10, 15 and 100 $\mu l/min$ of water was injected. One (1) electrospray head was considered. In the table, the delta symbol corresponds to the difference between the inlet, i.e. point 1, and the outlet, i.e. point 2, quantities. The ratio $\frac{\Delta\omega}{\omega_1}$ instead, as it will be seen later, was a key parameter to evaluate the electrostatically enhanced dehumidification processes.

Table 5: Variation of relative and absolute humidity of the air for 0.5 cfm and 5 cfm when 5, 10, 15 and 100 $\mu l/min$ of water was injected (one electrospray head).

Water flow rates (1 head)	***0.5 cfm air flow rate***				***5 cfm air flow rate***			
	$\Delta \boldsymbol{RH}$ [%]	$\frac{\Delta \boldsymbol{RH}}{\boldsymbol{RH_1}}$ [%]	$\Delta \boldsymbol{\omega}[\frac{\boldsymbol{gr}}{\boldsymbol{lbm}}]$	$\frac{\Delta \boldsymbol{\omega}}{\boldsymbol{\omega_1}}$ [%]	$\Delta \boldsymbol{RH}$ [%]	$\frac{\Delta \boldsymbol{RH}}{\boldsymbol{RH_1}}$ [%]	$\Delta \boldsymbol{\omega}[\frac{\boldsymbol{gr}}{\boldsymbol{lbm}}]$	$\frac{\Delta \boldsymbol{\omega}}{\boldsymbol{\omega_1}}$ [%]
5 $\frac{\boldsymbol{\mu l}}{\boldsymbol{min}}$	-6.16	-6.644	-2.093	-2.266	-0.5999	-0.666	-0.2093	-0.2266
10 $\frac{\boldsymbol{\mu l}}{\boldsymbol{min}}$	-10	-11.11	-3.767	-4.078	-1.2002	-1.335	-0.4100	-0.4531
15 $\frac{\boldsymbol{\mu l}}{\boldsymbol{min}}$	-10	-11.11	-3.767	-4.078	-1.1808	-2.009	-0.6278	-0.6797
100 $\frac{\boldsymbol{\mu l}}{\boldsymbol{min}}$	-10	-11.11	-3.767	-4.078	-10	-11.11	-3.767	-4.078

When ΔRH of 10 % was provided, saturation conditions ($RH > 100\%$) were achieved. For saturation conditions, the $\frac{\Delta \omega}{\omega_1}$ ratio corresponded to about - 4 %. This corresponded to the condition when the constant wet bulb temperature line, originating from the initial conditions here considered, intercepted the saturation line in the phychrometric chart. During the complete evaporation processes, a decrease of the dry bulb temperature was predicted. The highest decrement was equal to about 2 °F (1.1 ℃), when saturation conditions were achieved.

The same analysis was performed also when four (4) and six (6) electrospray heads were considered. In other words, when more water was injected in the air stream. The results are provided in Table 6 and in Table 7 respectively. As opposed to the case with only one electrospray head, the air flow rate of 2 cfm was reported. In fact, with 0.5 cfm all the cases were saturated.

Table 6: Variation of relative and absolute humidity of the air for 2 cfm and 5 cfm when 5, 10, 15 and 100 $\mu l/min$ of water was injected (four electrospray heads).

Water flow rates (4 heads)	***2 cfm air flow rate***				***5 cfm air flow rate***			
	$\Delta \boldsymbol{RH}$ [%]	$\frac{\Delta \boldsymbol{RH}}{\boldsymbol{RH_1}}$[%]	$\Delta \boldsymbol{\omega}[\frac{\boldsymbol{gr}}{\boldsymbol{lbm}}]$	$\frac{\Delta \boldsymbol{\omega}}{\boldsymbol{\omega_1}}$[%]	$\Delta \boldsymbol{RH}$ [%]	$\frac{\Delta \boldsymbol{RH}}{\boldsymbol{RH_1}}$[%]	$\Delta \boldsymbol{\omega}[\frac{\boldsymbol{gr}}{\boldsymbol{lbm}}]$	$\frac{\Delta \boldsymbol{\omega}}{\boldsymbol{\omega_1}}$[%]
5 $\frac{\boldsymbol{\mu l}}{\boldsymbol{min}}$	-6.16	-6.844	-2.093	-2.266	-2.418	-2.687	-0.8371	-0.9063
10 $\frac{\boldsymbol{\mu l}}{\boldsymbol{min}}$	-10	-11.11	-3.767	-4.078	-4.897	-5.441	-1.674	-1.813
15 $\frac{\boldsymbol{\mu l}}{\boldsymbol{min}}$	-10	-11.11	-3.767	-4.078	-7.438	-8.264	-2.511	-2.719
100 $\frac{\boldsymbol{\mu l}}{\boldsymbol{min}}$	-10	-11.11	-3.767	-4.078	-10	-11.11	-3.767	-4.078

Table 7: Variation of relative and absolute humidity of the air for 2 cfm and 5 cfm when 5, 10, 15 and 100 $\mu l/min$ of water was injected (six electrospray heads).

Water flow rates (6 heads)	***2 cfm air flow rate***				***5 cfm air flow rate***			
	$\Delta \boldsymbol{RH}$ [%]	$\frac{\Delta \boldsymbol{RH}}{\boldsymbol{RH_1}}$[%]	$\Delta \boldsymbol{\omega}[\frac{\boldsymbol{gr}}{\boldsymbol{lbm}}]$	$\frac{\Delta \boldsymbol{\omega}}{\boldsymbol{\omega_1}}$[%]	$\Delta \boldsymbol{RH}$ [%]	$\frac{\Delta \boldsymbol{RH}}{\boldsymbol{RH_1}}$[%]	$\Delta \boldsymbol{\omega}[\frac{\boldsymbol{gr}}{\boldsymbol{lbm}}]$	$\frac{\Delta \boldsymbol{\omega}}{\boldsymbol{\omega_1}}$[%]
5 $\frac{\boldsymbol{\mu l}}{\boldsymbol{min}}$	-9.385	-10.43	-3.139	-3.399	-3.65	-4.056	-1.256	-1.359
10 $\frac{\boldsymbol{\mu l}}{\boldsymbol{min}}$	-10	-11.11	-3.767	-4.078	-7.484	-8.264	-2.511	-2.719
15 $\frac{\boldsymbol{\mu l}}{\boldsymbol{min}}$	-10	-11.11	-3.767	-4.078	-10	-11.11	-3.767	-4.078
100 $\frac{\boldsymbol{\mu l}}{\boldsymbol{min}}$	-10	-11.11	-3.767	-4.078	-10	-11.11	-3.767	-4.078

As already mentioned, in all the spray injection tests with HV applied, the humidity increase must be always lower than these values, because of the new equilibrium condition dictated by the charge of the droplets. This kind of verification was performed while analyzing the experimental results.

As an additional preliminary verification, it was important to provide a sort of estimation of the maximum amount of water it was expected to collect, according to the open literature. According to [16],

a relative humidity decrement of the air of about 5 % was experienced after the onset of corona discharge, regardless of the humidity fed into the system. The humidity fed was 70, 80 and 90 %, the air flow rate was equal to about 0.04 cfm, and four (4) electrospray heads were used, which injected a flow rate comprised between 5 and 10 $\mu l/min$. The dry bulb temperature evaluated in these tests was constant and equal to 75.2 F. The net amount of moisture to collect in a thirty minutes test for all the three different cases of relative humidity is summarized in Table 8. Table 8 also summarizes the moisture collection rate, again for all the three cases.

Table 8: Water collection amount and rate for a target dehumidification rate of 5 % at constant temperature and 0.04 cfm

Water collection parameters	$\boldsymbol{RH = 70}$ %	$\boldsymbol{RH = 80}$ %	$\boldsymbol{RH = 90}$ %
Net amount of water collected $[\boldsymbol{mg}]$	37.71	37.82	37.93
Net water collection rate $[\frac{\boldsymbol{mg}}{\boldsymbol{min}}]$	1.257	1.261	1.264

The net amount of water considered only the water to collect to reach a relative humidity decrement of 5 % and it appeared fairly similar for all the fed humidity considered. It did not consider any other phenomenon, such as the water collected due to the use of water absorbing materials, reason why it differs from the values reported in [16]. About 1 mg every minute needed to be effectively wiped out from the air stream to reach the target dehumidification rate.

Assuming that the net amount of water collected remained the same regardless of the air flow rate, a new dehumidification rate may be estimated for all the new air flow rates. Of course, the dehumidification rate decreased while the air flow rate was increased, when the same amount of water collected for 0.04 cfm was considered. This assumption was particularly coarse, but it still provided an idea of the dehumidification rate to expect. The estimation was carried out for 0.5, 2 and 5 cfm, when

constant 37.93 mg of water was collected with an inlet relative humidity of 90 %. Table 9 shows the new expected dehumidification rate, under these assumptions.

Table 9: Expected new dehumidification rate with different air flow rates, when the same amount of water collected for 0.04 cfm was considered

Air flow rates	$\Delta \boldsymbol{RH}$ [%]	$\frac{\Delta \boldsymbol{RH}}{\boldsymbol{RH_1}}$ [%]	$\Delta \boldsymbol{\omega}[\frac{\boldsymbol{gr}}{\boldsymbol{lbm}}]$	$\frac{\Delta \boldsymbol{\omega}}{\boldsymbol{\omega_1}}$ [%]
0.04 $\boldsymbol{cfm}$	5	5.555	6.757	5.698
0.5 $\boldsymbol{cfm}$	0.3994	0.4438	0.5405	0.4558
2 $\boldsymbol{cfm}$	0.09984	0.1109	0.1351	0.114
5 $\boldsymbol{cfm}$	0.03994	0.04437	0.05405	0.04558

It was clear that, with a constant collection rate, the humidity differential deceased as the air flow rate increased. Extremely limited dehumidification rates were predicted for air flow rates higher than 0.04 cfm. The scalability of the process appeared then one of the biggest challenge of this research project.

If instead, as also defined by the preliminary target of the research project for 5 cfm, a dehumidification rate in terms of relative humidity of about 5 % must be achieved, the net amount of water to collect changed with the air flow rates. In particular, at fixed inlet relative humidity of 90 % and constant dry bulb temperature, the water to collect increased as the air flow rate increased. Table 10 reports the new water collection rates to meet the target dehumidification requirements. Again, a 90 % inlet relative humidity was considered.

Table 10: New water collection amount and rate to reach the target 5 % dehumidification rate in terms of relative humidity with different air flow rates

Air flow rates	***Net amount of water collected*** $[\boldsymbol{mg}]$	***Net water collection rate*** $[\frac{\boldsymbol{mg}}{\boldsymbol{min}}]$	$\Delta\boldsymbol{\omega}[\frac{\boldsymbol{gr}}{\boldsymbol{lbm}}]$	$\frac{\Delta\boldsymbol{\omega}}{\boldsymbol{\omega_1}}[\%]$
0.04 $\boldsymbol{cfm}$	37.93	1.264	6.757	5.698
0.5 $\boldsymbol{cfm}$	472.2	15.81	6.757	5.698
2 $\boldsymbol{cfm}$	1897	63.22	6.757	5.698
5 $\boldsymbol{cfm}$	4742	158.1	6.757	5.698

In this table, the $\frac{\Delta\omega}{\omega_1}$ ratio remained constant since the target 5 % dehumidification rate was considered for all cases. The net amount of water to collect and the net water collection rate drastically changed with air flow rates higher than 0.04 cfm.

In order to compare the net water collection rate to the actual water injection rate, Table 11 and Table 12 are also provided, considering as example the configuration with four electrospray heads. The water injection rates were first converted to $\frac{mg}{min}$ and later compared to the water collection rates, estimated in Table 10. Note that the total water injection rate represents the water injected by the single electrospray head multiplied by the four electrospray heads here considered.

Table 11: Comparison between the total water injection rates and the water collection rates for different air flow rates (0.04 and 0.5 cfm)

Water flow rates	***0.04 cfm air flow rate***			***0.5 cfm air flow rate***		
	Total water Injection Rate $[\frac{mg}{min}]$	***Water Collection Rate*** $[\frac{mg}{min}]$	***Percentage*** [%]	***Water Injection Rate*** $[\frac{mg}{min}]$	***Water Collection Rate*** $[\frac{mg}{min}]$	***Percentage*** [%]
5 $\frac{\mu l}{min}$	19.96	1.264	6	19.96	15.81	79
10 $\frac{\mu l}{min}$	39.93	1.264	3	39.93	15.81	40
15 $\frac{\mu l}{min}$	59.89	1.264	2	59.89	15.81	26
100 $\frac{\mu l}{min}$	399.3	1.264	0	399.3	15.81	4

Table 12: Comparison between the total water injection rates and the water collection rates for different air flow rates (2 and 5 cfm)

Water flow rates	***2 cfm air flow rate***			***5 cfm air flow rate***		
	Total water Injection Rate $[\frac{mg}{min}]$	***Water Collection Rate*** $[\frac{mg}{min}]$	***Percentage*** [%]	***Water Injection Rate*** $[\frac{mg}{min}]$	***Water Collection Rate*** $[\frac{mg}{min}]$	***Percentage*** [%]
5 $\frac{\mu l}{min}$	19.96	63.22	317	19.96	158.1	792
10 $\frac{\mu l}{min}$	39.93	63.22	158	39.93	158.1	396
15 $\frac{\mu l}{min}$	59.89	63.22	106	59.89	158.1	264
100 $\frac{\mu l}{min}$	399.3	63.22	16	399.3	158.1	40

With the higher air flow rates, the water collection rates resulted mainly higher than the actual total injection rates. According to the thermodynamics model, the potential of charged droplets to grow was relatively limited, and it appeared unrealistic that several times the water injected could be effectively

wiped out from the air stream. More electrospray heads may be required to achieve this target dehumidification rate.

All these preliminary analyses were fundamental for a better interpretation of the experimental data. In fact, they provided a benchmark to compare the actual data and assess their validity.

5.3 Spray Injection Test Procedure

The spray injection tests were carried out in the test apparatus. Before starting the tests, the humidity was varied either by the industrial steam humidifier or by two ultrasonic humidifiers to reach a relative humidity equal to approximately 90 % at the inlet of the test section. When the humidity, together with all the other parameters of interest, reached a steady state condition, the actual tests were initiated through LabView. In the first five minutes, the steady state conditions were recorded. At the beginning of the sixth minute instead, the syringe pump, the high voltage power supply and the CO_2 flow (if used) were started. Only when the CO_2 flow was used, an additional five minutes recording was added, where the CO_2 flow was on and both the syringe pump and the high voltage power supply were off. The overall duration of the spray injection tests were then 35 minutes, when no CO_2 flow was used, and 40 minutes when it was used. These recordings were useful for a real estimation of the humidity difference across the test section, as it will be detailed in a later section. Either the single syringe pump or the multi-syringes pump were used, according to the number of electrospray heads tested. The water injection flow rate was set manually on the syringe pump control panel and it was verified periodically considering the piston displacement. Up to 3 high voltage power supplies were connected to electrify the droplets. In particular, when multiple power supplies were tested, each of them electrified an even number of heads. In the first experimental campaign with one or six electrospray heads, the high voltage power supply/s were mainly connected to the needle/s and the plate electrode was grounded. Some tests with a reversed electrical configuration were run as well. In the four electrospray heads tests, during the second experimental campaign, the positive high voltage power supply was always connected to the plate electrode and the

needles were grounded. Regardless of the polarity of the high voltage power supply, the potential was set manually on the control panel of the instrument. The correct operation of the instrument was verified by means of the multimeter, making sure that the current readings during the spray injection tests were higher than when no high voltage potential was applied. The CO_2 flow rate was manually controlled by a dedicated flow gauge. The target flow rate was kept between 1.5 $\frac{l}{min}$ to 0.0048 $\frac{l}{min}$ [25], with the goal to keep it as low as possible to limit the impact of the CO_2 on the overall process. The LabView recording continued after all this setting procedure was completed, for about thirty minutes. Temperatures, i.e. dry bulb and dew point ones, were recorded in all the different positions along the test apparatus. The relative humidity measurements were also acquired and recorded as an additional verification to the information already provided by the dew point temperatures. The air flow rate, which could be controlled by the regulating valve install in the test apparatus, was recorded as well through LabView. The only parameters that were acquired and recorded manually were the water injection flow rate, the high voltage potential and polarity, the CO_2 flow rate (if used), the average electrospray electrical current and the overall water mass collected during the complete tests. The container where the electrode was placed or the water absorbing material was measured before and after the tests, and the difference between these two values corresponded to the water collected during the tests. Due to the very small amount of water injected and collected by condensation of the vapor molecules on the charged droplets, these measurements were affected by large uncertainty.

At the end of the tests, all the data were exported to Excel and analyzed. The main quantities of interest were the humidity before and after the test section, where the electrospray heads were installed. Knowing the dry bulb and dew point temperatures, the relative and specific humidity, i.e. the air water content, were evaluated indirectly through EES. When also the relative humidity measurements were available, the specific humidity were also evaluated with the relative humidity as an input for further verifications.

The estimation of the humidity difference before and after the test section was essential for the evaluation of the electrostatically enhanced condensation process. If a reduction of humidity was detected passing through the test section, the overall process was considered successful, i.e. dehumidification occurred. The humidity difference could have been computed either in terms of relative humidity and specific humidity. However, if the relative humidity was used, the estimation was meaningful only if the dry bulb temperature was constant throughout the test apparatus. In fact, if the dry bulb temperature was not constant, this difference did not provide the real vapor amount wiped out from the air. For simplicity, throughout this thesis, only the specific humidity was used. The difference was reported as a ratio in percentage terms, as represented by Equation (21).

$$\frac{\Delta\omega}{\omega_1} = \frac{\omega_1 - \omega_2}{\omega_1} \, [\%] \tag{21}$$

where 1 and 2 represented the conditions before and after the test section, respectively. Once again, when Equation (21) was positive, dehumidification occurred.

5.3.1 Parameters Actively Controlled during the Experiments

The thermodynamics model highlighted some of the parameters, such as the droplet size, droplet charge and the inlet relative humidity, which can considerably affect the electrostatically enhanced condensation process. Other parameters, such as the cross sectional area, the distance between the capillary (needle) tip and the electrode, air flow rate regimes and velocities were instead not taken into consideration in the model. Indeed, the model was not able to characterize and predict the best geometrical and fluid dynamics features for the test section and further investigations were carried out experimentally. Particular care was first directed towards those parameters already treated in the thermodynamics model with the goal to validate the trends and behaviors predicted by the model. As additional goal, it was important to have a first understanding of the impact of all those parameters not

actively considered in the model. For instance, the geometry and air flow rates were varied in the experimental tests to test different fluid dynamics features.

According to the thermodynamics model developed, smaller droplet sizes enhanced the overall dehumidification process and, according to the open literature, droplet size can be reduced keeping the water injection flow rate as low as possible. For this reason, the water injection flow rate was varied to control the size of the droplets as well as to change the overall amount of water injected in the air stream. In the stability region of the cone-jet operational mode, correlations indeed suggested that the size of the droplets was directly proportional to the water injection rate. 5, 10, 15 and 100 $\frac{\mu l}{min}$ were actively tested as constant water flow rates for each electrospray head. The actual size of the droplets, however, were not verified by imaging techniques, but it was indirectly estimated by the correlations available in the open literature for the cone-jet operational mode. In addition, in this particular mode, the droplet size distribution should be fairly monodisperse.

Higher droplet charge enhanced the overall dehumidification process and, according to the open literature, droplet charge can be increased augmenting the electrical conductivity of the electrosprayed liquid or increasing the high voltage potential, provided that the operational mode remained in the stability region. The electrical conductivity of the injected liquid was varied changing the liquid electrosprayed. Deionized water of type I, type II and type IV were used for this purpose. These kinds of water were characterized by different conductivities due to a different purity. According to the water parameters for ASTM types, type I is characterized by an electrical conductivity of 0.056 $\mu S/cm$, type II of 1.0 $\mu S/cm$ and type IV of 5.0 $\mu S/cm$, at 25 ℃. The electrical conductivity had also a minor influence of the droplet size, according to the open literature. The high voltage was increased up to 20 kV and the voltage potentials mainly tested were 5, 10, and 20 kV. The high voltage potential was applied either to the needle/s or to the plate electrode, knowing that, according to the open literature, droplets negatively

charged provided a better dehumidification potential. Indeed, the choice of the power supply and its application affect the polarity of the charged droplets.

The inlet relative humidity was kept mainly at 90 %, knowing that the best dehumidification performance was predicted for saturated air. 90 % was selected instead of saturation conditions because the safety switch was set to this value to avoid flooding the wind tunnel. Either the only industrial steam humidifier or the steam humidifier and the ultrasonic humidifiers were used for this purpose. A brief attempt to test at lower humidity was carried out, showing a consistent decrement in performance of the overall system.

Moving now towards those parameters not actively analyzed in the thermodynamics model, the following variations were carried out.

The geometry and the number of electrospray heads were changed passing from the first experimental campaign to the second. During the first one, the cross sectional area in proximity of the electrospray heads was larger and one (1) and six (6) electrospray heads were testes, while, in the second campaign, four (4) electrospray heads were tested in a square duct with a smaller cross sectional area. Additional details on the geometry and the associated dimensions are provided in the previous chapter. The geometry mainly affected the pressure drops across the test section and the velocity of the air in proximity of the injection of the charged droplets at a fixed air flow rate and, consequently, the heat and mass transfer between the air and the droplets. For instance, in case of the second experimental campaign, the air velocity varied between 0.125 and 1.25 ft/min (0.00064 and 0.0064 m/s).

The geometry of the injection water cone, i.e. the electrospray plume, was instead not actively controlled. It was a complex function of different operating parameters, in particular of the distance between the needle and the electrode, which was not changed in this thesis.

The geometry of the injection water cone as well as the size and charge of the droplets may be also affected by the internal diameter of the needles. For this reason, different needle gauges were used during the experiments. 30, 32, 33 and 34 gauge needles were considered.

The air flow rate tested were 0.5, 2 and 5 cfm. Increasing the air flow rate, the absolute amount of water to remove to reach a target dehumidification rate increased, suggesting that more electrospray heads may be required. A higher air flow rate corresponded also to a higher air velocity and pressure losses across a fixed test section, which can affect the fluid dynamic regime and enhance the heat and mass transfer. An attempt to test flow rate lower than 0.5 cfm, in particular 0.04 cfm as tested in [16], was carried out, but the flow nozzle sensor did not provide an accurate measurement for this extremely low rate.

The overall electrical connections were again changed, passing from the first experimental campaign to the second. In particular, resistors were added or removed with an attempt to vary the electrospray current. During the first experimental campaign, no resistors were installed in the circuit in order to deliver the maximum current possible. In order to further increase the electrical current, up to three (3) HV power supplies in parallel were installed with the six (6) electrospray heads configuration. When three (3) power supplies were used, each of them power two (2) electrospray heads. Instead, in the second experimental campaign, an electrical configuration with resistors was also considered. In this configuration, a 10 $M\Omega$ resistor was installed in series between the output of the power supply and the plate electrode and a 10 $k\Omega$ was installed in series between the four (4) needles and the return wire to the power supply. As additional difference, in the first campaign the needles were mainly at high negative potential while, in the second campaign, the plate electrode was at high positive potential.

As a further modification for the second experimental campaign, water absorbing materials were used to promote the collection of water and prevent its evaporation. The water absorbing materials were installed on top of the plate electrode. In other words, the usage of water absorbing materials was not to

increase the dehumidification rate, but to avoid the evaporation of the already collected and condensed vapor. The absorbing materials were indeed placed only on top of the electrode and any advantage on the dehumidification rate due to the presence of these water absorbing materials was taken into consideration, i.e. subtracted from the dehumidification rates of the actual spray injection tests, during the correction on the air water content procedure.

A CO2 flow rate was used only during the first experimental campaign, when the single electrospray head was tested. The CO2 flow guaranteed the monodispersity of the electrospray but it did not provided any advantages in terms of dehumidification rate. For this reason, its use was discarded in the remaining tests, but advanced imaging techniques may be employed to characterize the electrosprayed droplets. Indeed, outside the stability region for the cone jet operational mode, correlations for the droplet size and charge were not easily available in the open literature.

5.3.2 Test Schedule

According to the previous paragraph, many variations may be done in order to verify the trends predicted by the model or to investigate other operating parameters not considered in the model. Table 13 summarizes of all the experimental tests and parameters actually investigated in this thesis, whose dehumidification results are provided in a later chapter.

Table 13: Summary of all the experimental tests and parameters investigated in the experimental campaigns

Parameters actively controlled	***First Experimental Campaign***		***Second Experimental Campaign***
	1 Electrospray Head	***6 Electrospray Heads***	***4 Electrospray Heads***
Water Injection Flow Rate $[\frac{\mu l}{min}]$	5, 10, 15 and 100	5, 10, 15 and 100	5, 10, 15 and 100
Deionized Water Type (electrical conductivity)	Type I, II and IV	Type I, II and IV	Type II
High Voltage Potential	5, 10 and 20	10 and 20	10
High voltage power supply (droplets' polarity)	HV (-/+) to the needle or to the electrode	HV (-/+) to the needle or to the electrode	HV (+) to the electrode
Inlet Relative Humidity	90 % (steam humidifier)	90 % (steam humidifier)	90 % (steam + ultrasonic humidifiers)
Cross Sectional Area	12 in. x 7 in.	12 in. x 7 in.	2 in. x 2 in.
Emitter/Electrode Distance	2 in.	2 in.	2 in.
Needle Gauge	33 gauge	33 gauge	30, 32 and 34 gauge
Air Flow Rate	0.5 and 5 cfm	0.5 and 5 cfm	0.5, 2 and 5 cfm
Electrical Configuration	No resistors	No resistors	10 $M\Omega$ + 10 $k\Omega$ resistors
Number of Power Supply	1	1, 2 and 3	1
Water Absorbing Materials	No	No	Yes
CO_2 Flow	Yes	Yes	No

The majority of the tests here reported were carried out in the actual experimental campaigns. A few of the parameters, such as the different kind of needles, were not fully investigated in this thesis, and they should be considered in the future work.

Different variables were considered and the criteria of the variable selection was to test all the possible variables that may affect the main operating parameters described in the model, in particular the

droplet size and charge. A direct measurement of the droplet size and charge was not possible in this thesis and a way to assess the influence of the charge and size of the droplets on the dehumidification rate was to vary experimentally as many variables as possible, one at a time.

In order to build confidence on the particularly limited dehumidification results, some of the tests were repeated up to three times. In those cases, appropriate error bars were shown in the presentation of the results. In particular, average values over all the repeated tests performed were provided, together with error bars highlighting the distribution of the data reached throughout the tests, for that specific condition.

Chapter 6: Data Analysis

Once the raw data was acquired through the data acquisition system (DAQ), it was processed and analyzed. In general, all data was exported to an appropriate Excel file, where the analyses and subsequent representations of the data were performed. Additional software used for this purpose were Python, C++, and EES. In the case of the video scope and high speed camera, some footage were also analyzed and shown in the thesis by means of jpeg images. However, as already mentioned, it was not possible to use this footage to estimate the droplet size and velocity. Successful estimations of these quantities may be a great upgrade for a future work. As a reference, in a previous work carried out in the same research group [38, 39], the smallest droplets that could be individually distinguished from each other had diameter of 110 to 120 μm. Possible challenges may arise if the droplets to measure are smaller than this threshold, as in the case of electrosprayed droplets.

Relative humidity and air water content were key parameters for the evaluation of the electrostatically enhanced condensation process and its dehumidification potential. A reduction of humidity across the test section would confirm a successful removal of vapor, i.e. dehumidification, from the humid air. The vapor removed and condensed may be indeed estimated thanks to the air water content different across the test section. An uncertainty analysis and correction procedure, when needed, were performed on these parameters.

6.1 Relative Humidity and Air Water Content Uncertainty Analysis

The relative humidity and the air water content were measured throughout the test apparatus, in particular before and after the test section. They were evaluated by means of direct readings from

sensors and/or derived quantities. For example, the air water content could be calculated knowing the dry bulb and dew point temperatures, together with the air pressure.

An uncertainty analysis was then conducted to determine the uncertainty of calculated variables based on individual sensor uncertainties. The uncertainties of individual sensors were provided by the manufacturer, and they were summarized in Table 4**,** in a previous chapter. The instruments considered for the evaluation of relative humidity and air water content were thermocouples, RH sensors and dew point meters. EES, which implements a Taylor series uncertainty propagation method, was used to carry out the uncertainty analysis of these variables. This method was based on Equation (22) to calculate the uncertainty of the calculated variable.

$$U_Y = \sqrt{\sum_{i=1}^{n} \left(\frac{\partial Y}{\partial X_i}\right)^2 U_{X_i}^2} \tag{22}$$

where U_Y is the uncertainty of the calculated variable, U_{X_i} is the uncertainty of the individual sensor and n is the number of sensors.

When multiple sensors were used to measure a single variable in the exact same location along the wind tunnel, the uncertainty to consider was not the one of the single sensor itself, but it should be computed according to the bias uncertainty analysis method. In particular, in this thesis, this applied to thermocouples arrays, measuring air average temperatures in a common location. This method was based on Equations (23, 24, 25) to calculate the bias uncertainty of the calculated variable.

$$B_{T,distribution} = \frac{T_{max} - T_{min}}{n} \tag{23}$$

$$B_{T,uniform} = \Delta T_{\frac{uniform}{n}} \geq U_T \tag{24}$$

$$B_T = \sqrt{B_{T,uniform}^2 + B_{Tdistribution}^2} \tag{25}$$

where B_T is the bias uncertainty of the calculated average temperature, $B_{T,distribution}$ is the uncertainty based on the thermocouple array configurations and $B_{T,uniform}$ was assumed equal to the uncertainty of the single sensor.

The bias uncertainty for all air average temperatures depended on the actual number of thermocouples used in the array and it was always less than 0.1 °F (0.056 °C), according to bias uncertainty analysis method. However, a more conservative thermocouple temperature uncertainty of ± 0.1 °F (0.056 °C) was considered for the following analyses.

Going back to the Taylor series uncertainty propagation method on the relative humidity and air water content, the uncertainties of the calculated quantities are reported in Table 14. Different combinations of measured quantities were considered.

Table 14: Uncertainties of relative humidity and air water content evaluated with the Taylor series uncertainty propagation method

Calculated quantities	***Measured quantities***	$\boldsymbol{U_{calculated\ quantities}}$
$\boldsymbol{\omega}\ [\frac{\boldsymbol{grains}}{\boldsymbol{lbm}}]$	$RH\ and\ T_{dry\ bulb}\ (P_{atm})$	$\pm\ 1.45\ (\pm 1.6\ \%)$
$\boldsymbol{\omega}\ [\frac{\boldsymbol{grains}}{\boldsymbol{lbm}}]$	$T_{dry\ bulb}\ and\ T_{dew\ point}\ (P_{atm})$	$\pm\ 0.45\ (\pm 0.5\ \%)$
$\boldsymbol{RH}\ [\%]$	$T_{dry\ bulb}\ and\ T_{dew\ point}\ (P_{atm})$	$\pm\ 0.53\ (\pm 0.6\ \%)$

Table 14 shows how the Taylor uncertainty on the air water content, when relative humidity and dry bulb temperature were considered as measured quantities, was particularly high. For this reason, the air water content was always derived from the dry bulb and the dew point temperatures.

In the worst case scenario, in the evaluation of the air water content different across the test section during an iso – ω test, when the air water content should remain constant, the difference would be equal to ± 2.9 $\frac{grains}{lbm}$ when relative humidity and dry bulb temperature were used and it would be equal

to ± 0.9 $\frac{grains}{lbm}$ when dry bulb and dew point temperatures were used. In terms of the ratio $\frac{\Delta\omega}{\omega_1}$, it would be equal to ± 3.14 % and ± 0.97 % respectively, with a dry bulb temperature of 68 °F and a relative humidity of 90 %.

6.2 Air Water Content Correction

As previously evaluated, in the worst case scenario, a relative high air water content offset between the inlet and the outlet of the test section during iso – ω tests was predicted. In the actual tests, other factors may arise such that this offset could be higher or lower with respect to the one predicted by the uncertainty analysis.

For this reason, in the attempt to provide a better estimation than the worst case scenario approach, multiple iso – ω tests were performed every day in between different spray injection tests. The average air water content difference, among all these tests, was evaluated. When this average value was consistently, i.e. for multiple consecutive days, higher than the worst case scenario offset predicted by the uncertainty analysis, the dew point meters were cleaned per manufacturer's instructions.

In general, the measured offset was lower than the worst case one scenario and it could be either positive, i.e. dehumidification, or negative, i.e. humidification. In order to have a better estimation of the performance of the electrostatically enhanced condensation process, the average offset of the day was always subtracted from the air water content difference of all the spray injection tests, carried out during the same day. With this procedure, it was tried to limit the negative impact associated with the uncertainties of the sensors and possible experimental errors. The resulting air water content difference, was in general very limited and frequently negative, but it should represent the best estimation of the performance of the process under analysis.

A similar approach was also applied when the CO_2 flow was employed in the very first spray injection tests. The iso – ω tests were carried out without spray injection, but when the CO_2 flow was

present as well. The offset recorded during these tests were subtracted from the air water content different measured during the actual spray injection tests.

The use the air water content, instead of relative humidity, was advantageous for an easier estimation of the vapor mass condensation, as detailed in the following paragraph.

6.3 Vapor Mass Condensation Calculation

During the spray injection tests, the key parameter for the performance of the electrostatically enhanced condensation process was the ratio $\frac{\Delta\omega}{\omega_1}$, evaluated for each spray injection test. Knowing this ratio for each test, the vapor mass that condensed was easily estimated with Equation (26).

$$m_{condensed} = \dot{m}_{air}\omega_1\frac{\Delta\omega}{\omega_1}t_{test} \tag{26}$$

Taylor series uncertainty propagation analysis could also be performed on the condensed vapor mass, including the uncertainty of the flow nozzle for the estimation of the air volume flow rate. However, the evaluation of the condensed vapor mass was rarely carried out due to the very limited ratio $\frac{\Delta\omega}{\omega_1}$.

In general, as further verification, the water collected in the container housing the plate electrode or absorbed by the water absorbing materials may be evaluated for each test. Subtracting the water injected by the electrosprays, the condensed water may be evaluated.

Chapter 7: Results and Discussion

A summary of the experimental expectations was considered in order to facilitate the discussion on the results. In particular, the dehumidification performance predicted by the previously developed thermodynamics model and extrapolated from relevant literature was provided.

The results collected during the first experimental campaign, with one (1) and six (6) electrospray heads, and the second experimental campaign, with four (4) electrospray heads, were presented and discussed. All the dehumidification results were presented in terms of the $\frac{\Delta\omega}{\omega_1}$ ratio, and the dew point sensors were used for the evaluation of the air water content. The dehumidification performance appeared particularly limited, and often negative, suggesting that not an effective dehumidification was obtained for the conditions considered. The number of electrospray heads were increased with the goal to increase the dehumidification rate and to obtain results outside the uncertainty of the dew point sensors used to measure the air water content, before and after the test section. However, even after augmenting the number of electrospray heads and then the water injected in the air stream, the results obtained were still within the uncertainty of the instrumentation. In general, this made the analysis of the results more difficult.

Solutions to increase the dehumidification rates need to be found in order to proceed with the commercial development of the electrostatic dehumidifier prototype.

7.1 Experimental Expectations

The initial and overall goal of this research project was to achieve a dehumidification rate of 5 % for an air flow rate of 5 cfm, at constant dry bulb air temperature. In order to have a better estimation of the amount of water effectively wiped out from the air stream, the overall goal was translated in terms

of the air water content, which is independent of the variations of the dry bulb temperature. It corresponded to a $\frac{\Delta\omega}{\omega_1}$ ratio equal to 5.7 %, when the inlet temperature and relative humidity were equal to 68 °F and 90 % respectively. It was important to note that, as the air flow rate increased, the amount of vapor to effectively wipe out from the air increased, with a constant target $\frac{\Delta\omega}{\omega_1}$ ratio. For this reason, the achievement of this goal was more challenging at higher air flow rates, as shown later.

According to the thermodynamics model, the dehumidification rate increased as function of the number of charged droplets with the correct size and charge effectively injected in the air stream. The number of droplets injected could be increased augmenting the electrospray heads used.

Table 15 summarizes the dehumidification rates predicted in terms of the air water content for six (6) electrospray heads, assuming that 3.6 μm droplets in diameter can be produced by a water flow rate of 10 $\mu l/min$ [25, 26], but also by 100 $\mu l/min$, per single electrospray head. The number of 3.6 μm droplets in diameter that could be produced by a single head were estimated as well.

Table 15 also reports the dehumidification rates assuming that the same amount of water collected for an air flow rate of 0.04 cfm [16], which corresponded exactly to a 5 % reduction in relative humidity, could be collected also for all the other air flow rates considered. The fact that only 0.04 cfm was tested in [16] was found out very late in the course of this thesis, and this extrapolation was then required and necessary.

The main reason why a maximum of six (6) electrospray heads were considered in the following experimental campaigns was mainly practical. In particular, only a six (6) syringes pump with the desired capacity was readily available in the market and higher number of electrospray heads would have also further complicated the high voltage electrical configuration for this initial experimental investigation.

Table 15: Predicted dehumidification rates in terms of the air water content for different air flow rates

Dehumidification rate	$\mathbf{0.5\ cfm}$	$\mathbf{2\ cfm}$	$\mathbf{5\ cfm}$
$\frac{\Delta\boldsymbol{\omega}}{\boldsymbol{\omega_1}}$ [%] ($\mathbf{6\ needles}, \boldsymbol{D = 3.6\ \mu m}$, $\mathbf{10}\frac{\boldsymbol{\mu l}}{\boldsymbol{min}}$, $\mathbf{8.5\ 10^5\ droplets}$)	0.85	0.22	0.08
$\frac{\Delta\boldsymbol{\omega}}{\boldsymbol{\omega_1}}$ [%] ($\mathbf{6\ needles}, \boldsymbol{D = 3.6\ \mu m}$ $\mathbf{100}\frac{\boldsymbol{\mu l}}{\boldsymbol{min}}$, $\mathbf{8.5\ 10^6\ droplets}$)	8.48	2.08	0.85
$\frac{\Delta\boldsymbol{\omega}}{\boldsymbol{\omega_1}}$ [%] ($\boldsymbol{same\ water\ collected\ for\ a}\ \mathbf{5}$ % $\boldsymbol{dehumidification\ at}\ \mathbf{0.04\ cfm}$ [16])	0.45	0.11	0.04

For any of the water flow rates considered and six (6) electrospray heads, the dehumidification rate was at least one order of magnitude lower than the target one, for 5 cfm. The dehumidification rates predicted were indeed very low in all the cases, except the case where it was assumed that 3.6 μm droplets in diameter could be produced with a water injection flow rate of 100 $\mu l/min$ per electrospray head. In this case, a dehumidification rate higher than 5 % in terms of relative humidity was predicted only for an air flow rate of 0.5 cfm. A dehumidification rate of about 1 % in terms of relative humidity was instead predicted for an air flow rate of 5 cfm. This assumption was, however, quite unrealistic, considering that with this water flow rate droplets with a diameter way larger than 10 μm, and then outside the suitable range predicted by the model, were expected. To verify it experimentally, a water injection rate of 100 $\mu l/min$ was tested in both the experimental campaigns. When the number of droplets injected was decreased, the predicted dehumidification rate decreased as well.

As an additional consideration, all the predicted dehumidification rates, except the cases with 100 $\mu l/min$, were within the uncertainty for the air water content differential evaluated in the worst case

scenario, i.e. $\frac{\Delta\omega}{\omega_1} = 0.97\ \%$., with the dew point sensors. The correction on the air water content, thanks to multiple iso – ω tests performed in between the spray injection tests, was then adopted to mitigate this fact and for a better representation of the dehumidification performance, as previously described. However, a level of uncertainty still remained in the corrected results, making their interpretation sometimes tricky. As a clarification, if also the corrected results were consistently outside the evaluated uncertainty, conclusions could have been drawn with more confidence.

Due to these limited dehumidification rates predicted and the uncertainty of the dew point sensors, it would have been best to test a sufficient number of electrospray heads to have a dehumidification rate outside this $\frac{\Delta\omega}{\omega_1} = 0.97\ \%$ threshold, drastically complicating the set up. However, in the open literature related to this new field of study, apparent inconsistencies existed on the droplets' optimal size for maximum dehumidification [12, 13, 14, 15] and on the expected dehumidification rates [16] (once again the fact that only 0.04 cfm was tested in [16] was found out only later in this research). For this reason, in this initial investigation, it was decided to conduct an extensive experimental investigation with up to six (6) electrospray heads. The experimental data was then collected to validate the model and to understand if the considerable improvements in the dehumidification rate obtained in the literature could be obtained, in particular for higher flow rates, i.e. 5 cfm. Two different experimental campaigns were conducted, as described in the next sections.

7.2 First Experimental Campaign

During the first experimental campaign, one (1) and six (6) electrospray heads were tested in the same location along the test apparatus. A negative or positive high voltage potential was applied to the 33 gauge heads and the counter count plate electrode, about 2 in. apart, was grounded. A different configuration was also briefly tested, as described later. Different deionized water kinds, with different electrical conductivities, and water flow rates were tested. No resistors were used with the goal to

maximize the current and then the charge of the droplets, and the electrical configuration is already shown in Fig. 20. Only the industrial steam humidifier was used to raise the relative humidity to about 90 %, with a dry bulb temperature of 68 °F in this campaign.

The first tests with only one electrospray head were carried out with and without the sheath CO_2 flow, when the high voltage potential was kept within the stability domain for the cone jet operational mode previously determined, at about 10 kV. Fig. 34, 35 and 36 represent the results for deionized water type I, type II and type IV respectively. The average offset on the air water content during the multiple iso – ω tests, when also CO_2 was employed, was subtracted from the actual result of each test.

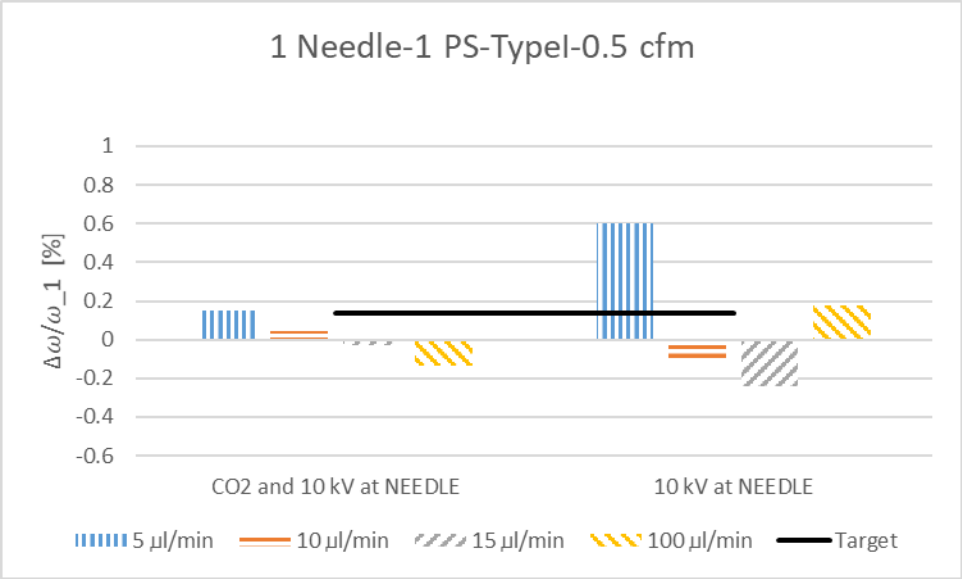

Fig. 34: Dehumidification results first experimental campaign (1 Needle – 1 PS (-) at needle – Type I – 0.5 cfm)

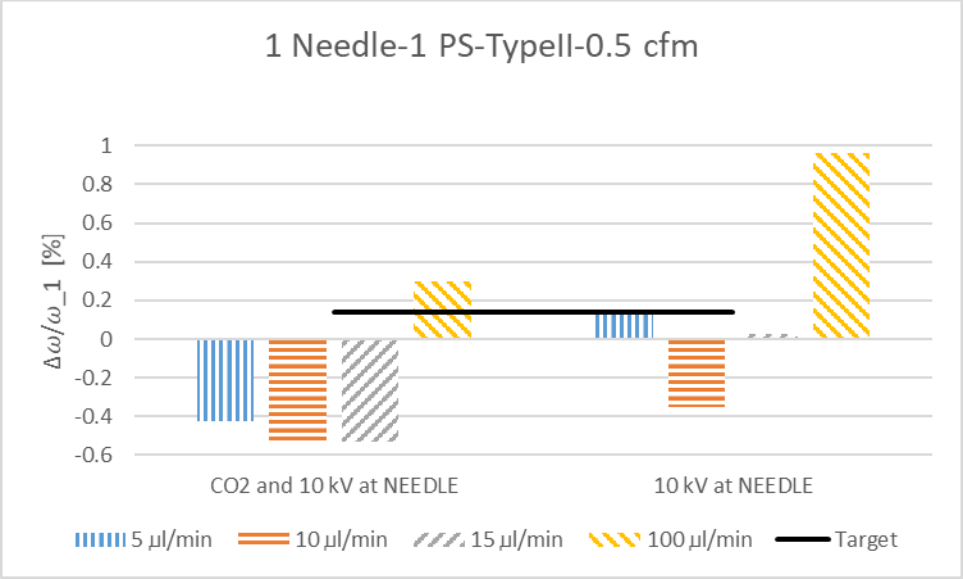

Fig. 35: Dehumidification results first experimental campaign (1 Needle – 1 PS (-) at needle – Type II – 0.5 cfm)

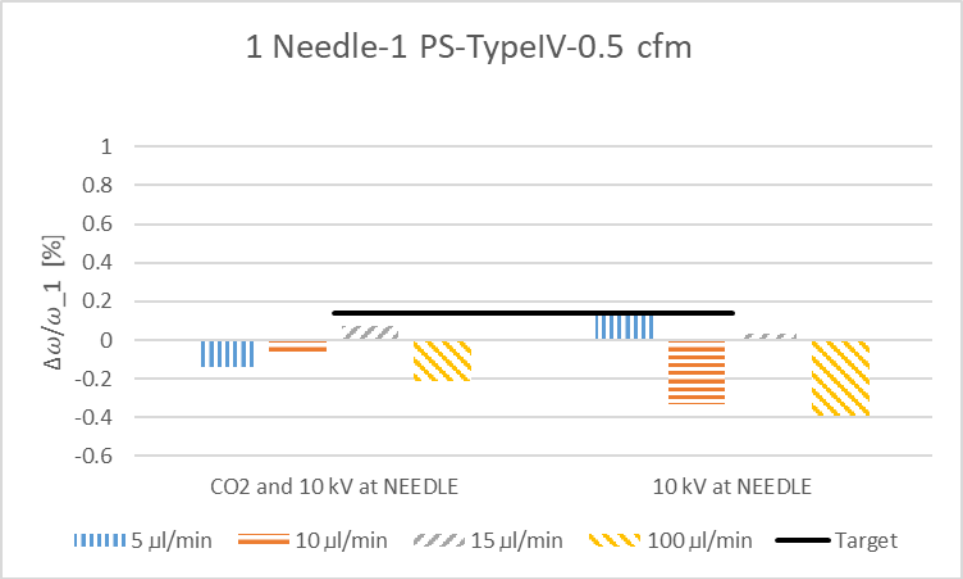

Fig. 36: Dehumidification results first experimental campaign (1 Needle – 1 PS (-) at needle – Type IV – 0.5 cfm)

For each deionized water kind, four different water injection rates were tested with and without the sheath CO_2 flow. A water flow rate of 100 $\mu l/min$ was tested to assess if higher dehumidification rates could be obtained, even if droplets larger than 10 μm were expected with this water flow rate.

The black straight target lines in the figures above represent the dehumidification rate predicted by the model, when droplets emitted by a single electrospray head were considered. This predicted dehumidification rate was lower than the one reported in Table 15 because less droplets, i.e. droplets produced by only one head and a water flow rate of 10 $\mu l/min$, had the potential to grow. The maximum humidification rate, in case of all the water evaporated, was equal or lower than -2.3 % as reported in Table 9, and this limit was not shown in the figures for a better readability of the bar chart.

Results similar or higher to the ones predicted by the thermodynamic model, when only the droplets emitted by one head were considered, were sometimes obtained, such as with water type I and 5 $\mu l/min$ and with water type II and 100 $\mu l/min$, when no CO_2 flow was used. The other results were in general very limited and sometimes negative, i.e. signifying humidification.

All the results, which were presented following the air water content correction previously described, resulted all within the uncertainty for the air water content ratio, evaluated as $\frac{\Delta\omega}{\omega_1}$ ratio equal to $\pm$ 0.97 %. Again, if evaporation of all the water injected was assumed, a $\frac{\Delta\omega}{\omega_1}$ ratio equal to - 2.266 % or lower was expected. All the results were far away from this limit, and, in particular, always higher than -0.6 %. None of these first tests were repeated, and no experimental error bars were provided.

According to these results, it was not clearly possible to assess which water kind and which water injection rate were the most suitable for an improved dehumidification. No water flow rate and no water kind provided consistently positive dehumidification rates. In addition, the stable electrospray operational mode achievable with the CO_2 flow did not provide any competitive advantage in terms on dehumidification rate.

For this reasons, additional tests were carried out to explore the influence of other operational conditions, such as different air flow rates, and different magnitudes and locations of the high voltage potential applied. The air flow rates considered were 0.5 cfm and 5 cfm, while the high voltage potentials considered were 5, 10 and 20 kV, applied either to the needle or to the plate electrode. A higher flow rate

was tested mainly to increase the velocity of the air around the charged droplets, while a higher potential to increase the electrospray current. Applying the negative high voltage potential either to the needle or to the plate electrode allowed also to change the polarity, i.e. the charge sign, of the electrosprayed droplets.

With these new conditions, one electrospray head was again tested at the same location with only deionized water type II, which had an intermediate electrical conductivity between the water kinds considered. The CO_2 flow was not used.

Fig. 37 and 38 represent the results for deionized water type II for 0.5 and 5 cfm respectively. Three (3) high voltage potentials, i.e. 5, 10 and 20 kV, were applied to the needle and tested.

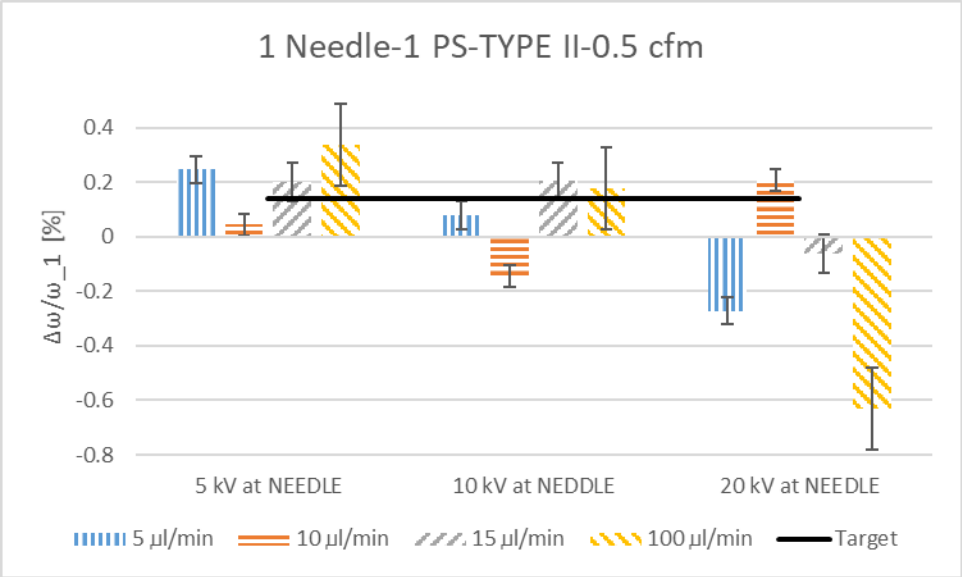

Fig. 37: Dehumidification results first experimental campaign (1 Needle – 1 PS (-) at needle – Type II – 0.5 cfm) and three different high voltage potentials to the needles (5, 10, 20 kV)

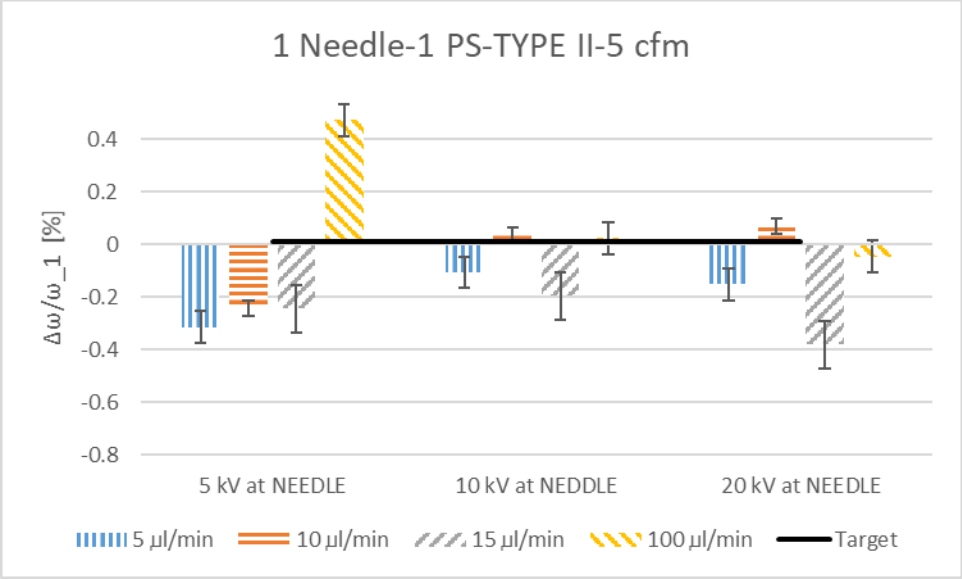

Fig. 38: Dehumidification results first experimental campaign (1 Needle – 1 PS (-) at needle – Type II – 5 cfm) and three different high voltage potentials to the needles (5, 10, 20 kV)

The black straight lines represent the dehumidification rate predicted by the model, when droplets emitted by a single electrospray head were considered. The dehumidification rate predicted by the model decreased as the air flow rate increased. More positive dehumidification results were experienced with 0.5 cfm rather than with 5 cfm, where more bars exceeded the predictions of the model. An outlier existed for the 5 cfm case with a $\frac{\Delta\omega}{\omega_1}$ ratio approximately equal to 0.4 %, higher than the prediction of the model.

The results were again within the evaluated uncertainty for the air water content ratio. These tests were repeated up to three times and appropriate error bars were reported in the figures.

As an additional modification, the negative high voltage potential was also applied to the plate electrode, to investigate also the effect of the polarity of the droplets. Fig. 39 represents the results for deionized water type II and 0.5 cfm. Only two (2) high voltage potentials, i.e. 10 and 20 kV, were applied to the electrode and tested.

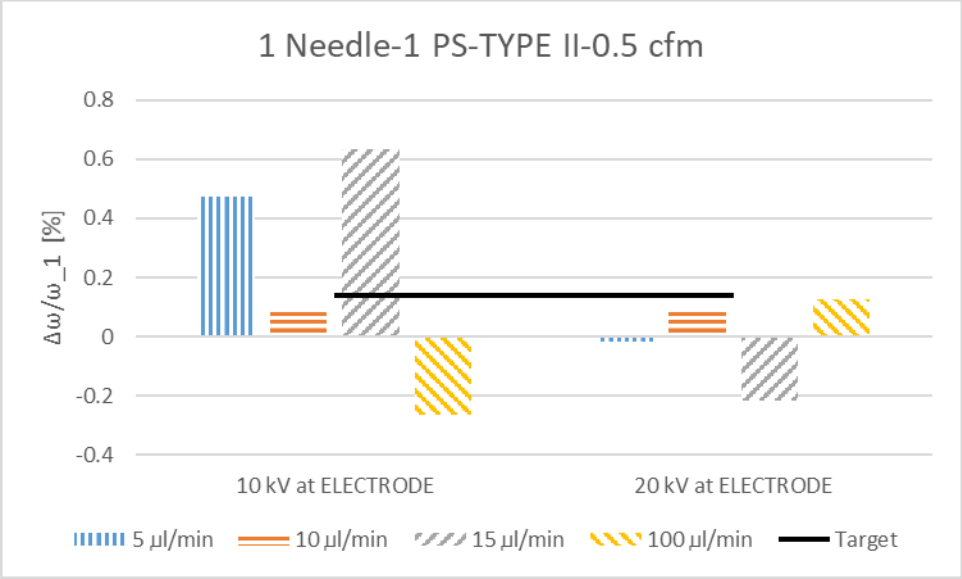

Fig. 39: Dehumidification results first experimental campaign (1 Needle – 1 PS (-) at electrode – Type II – 0.5 cfm) and two different high voltage potentials to the electrode (10, 20 kV)

A more consistent and higher dehumidification was experienced in this case, even if positively charged droplets were expected to have a lower dehumidification potential. The results were mainly higher than the predictions of the model for 0.5 cfm, i.e. the straight black target line in the figure, when a lower high voltage potential was applied.

According to the literature, the droplet charge was directly proportional to the electrospray current, if no discharge phenomena occurred, and droplets with more charge were expected to have a higher dehumidification potential. Once again, key parameters affecting the electrospray current were the electrical conductivity of the liquid, the high voltage potential applied and, possibly, the location of the high voltage application.

The current was then also measured for deionized water type II to estimate the droplet charge. Fig 40, 41 and 42 represent the results of the average current for deionized water type II.

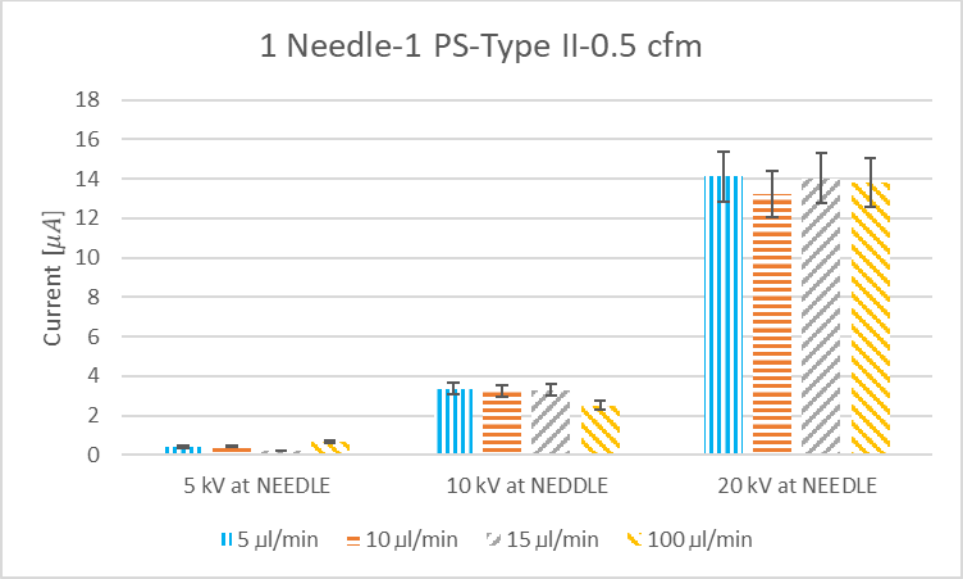

Fig. 40: Electrospray current first experimental campaign (1 Needle – 1 PS (-) at needle – Type II – 0.5 cfm) and three different high voltage potentials to the needles (5, 10, 20 kV)

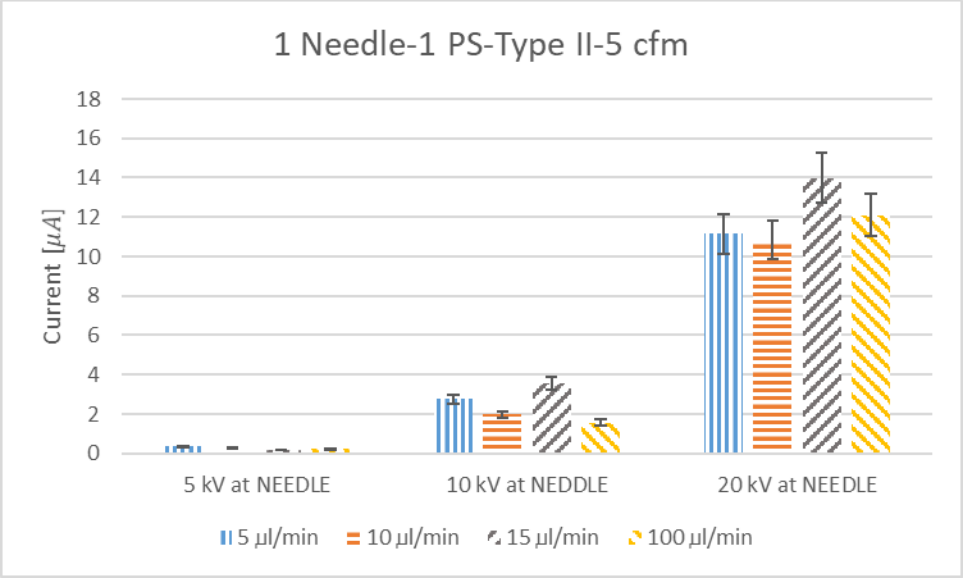

Fig. 41: Electrospray current first experimental campaign (1 Needle – 1 PS (-) at needle – Type II – 5 cfm) and three different high voltage potentials to the needles (5, 10, 20 kV)

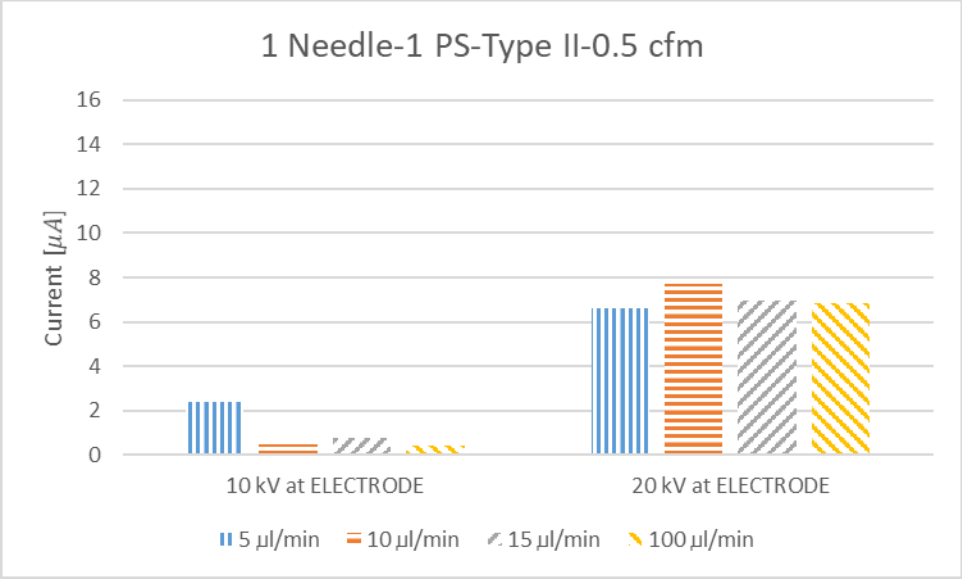

Fig. 42: Electrospray current first experimental campaign (1 Needle – 1 PS (-) at electrode – Type II – 0.5 cfm) and two different high voltage potentials to the electrode (10, 20 kV)

Increasing the voltage, the current increased and the charge density of the electrosprayed droplets should then augment. Applying the same high voltage potentials at the plate electrode, instead to the needles, a current about 50 % lower was measured. It appeared that the dehumidification rate was better in this case of limited current. A direct measurement of the size and charge of the droplets could have helped with a better explanation of the results. The experimental error bars were reported only when repeated tests were carried out.

The dehumidification results obtained with only one electrospray head were promising, with several bars higher than the predictions of the thermodynamic model. However, considering the limited performance obtained with only one electrospray head, six (6) electrospray heads were also tested at the same location in the test apparatus to augment the dehumidification rate. The goal was to obtain a dehumidification rate about six times higher than in the case with only one (1) electrospray head, considering that six times the droplets previously injected had the potential to grow. The water flow rates reported were indeed always referred to the water flow rate fed to the single electrospray head. Two (2)

high voltage potentials and two (2) different air flow rates were tested. In some cases, the influence of both positive and negative potentials applied to the needles were investigated, without providing any considerable difference. For only the tests with type I, also the CO_2 flow was considered, with the same conclusions drawn with the case with only one electrospray head. For type I, the results with a positive potential to the needles were reported in Fig. 43 and 44 for 0.5 and 5 cfm. One power supply electrified all the electrospray heads in parallel. The current was not measured in this case.

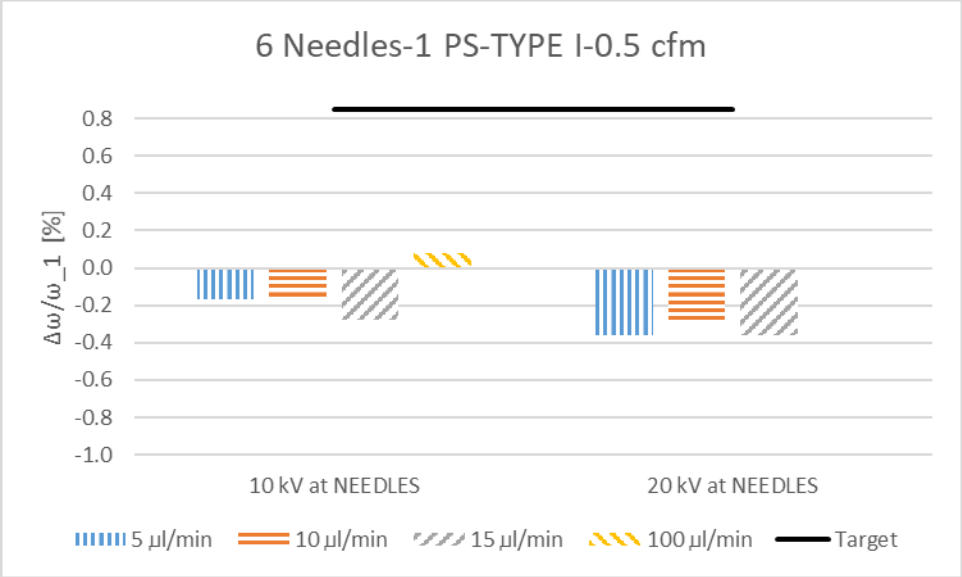

Fig. 43: Dehumidification results first experimental campaign (6 Needle – 1 PS (+) at needles – Type I – 0.5 cfm) and two different high voltage potentials to the needles (10, 20 kV)

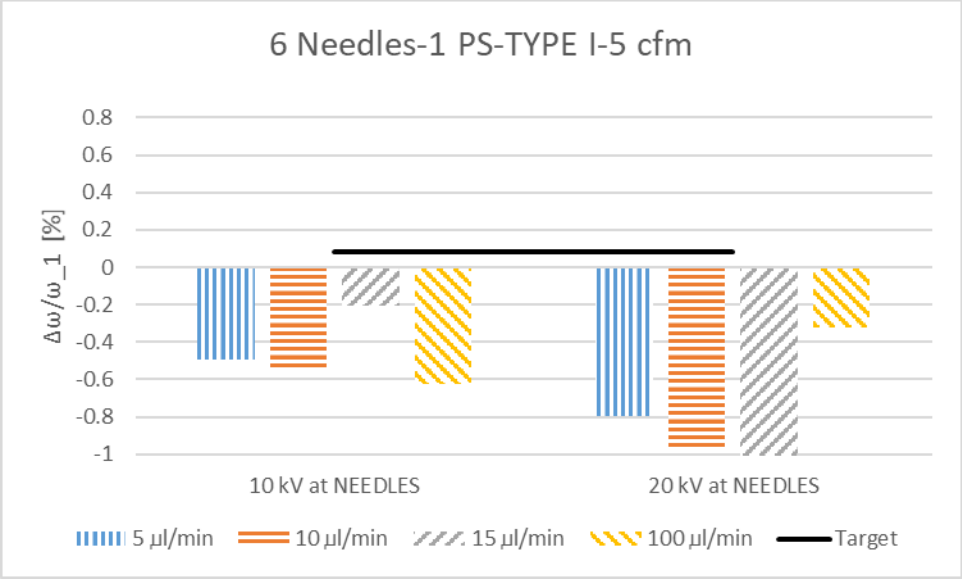

Fig. 44: Dehumidification results first experimental campaign (6 Needle – 1 PS (+) at needles – Type I – 5 cfm) and two different high voltage potentials to the needles (10, 20 kV)

The tests were the first ones with the six (6) electrospray heads configuration. As opposed to the expectations, the dehumidification rates were consistently negative, i.e. humidification, except for a water flow rate of 100 $\mu l/min$ with 10 kV and 0.5 cfm. The results were lower than the predictions of the model, represented by the straight black lines in the figures, with numerical values equal to the ones reported in the first line of Table 15 for different air flow rates. Promising was the fact that all the results were way far away from the case where all the water injected was assumed to evaporate. A more detailed analysis, highlighting the maximum dehumidification and humidification limits, will be presented in Fig. 51 and Fig. 52.

There are several reasons for these unexpected results, as it will explain after all the results with the six (6) electrospray heads configuration are presented in the next sections.

In order to make sure that these poor results were not related to the low conductivity of the deionized water type I or to the low current that a single power supply could supply simultaneously to the six (6) electrospray heads, similar tests were carried out also with water type II and type IV, the ones with

the higher electrical conductivity. Up to three (3) power supplies were tested: when two (2) power supplies were used, they electrified three (3) needles each, when three (3) power supplies were used, they electrified two (2) needles each. The cases with type II explored the effect of only negative power supplies connected to the heads, while the cases with type IV explored again the effect of both negative and positive power supplies, applied to the heads. As a reminder, the open literature predicted an improved dehumidification performance when the droplets were negatively charged, and configurations to produce droplets with negative polarity were preferred in this investigation. The current was measured to explore the effect of multiple power supplies connected in parallel.

Fig. 45 and 46 represent the results for deionized water type II for 0.5 cfm and 5 cfm respectively. Two (2) high voltage potentials, i.e. 10 and 20 kV, were applied to the needles when only one (1) power supply was used.

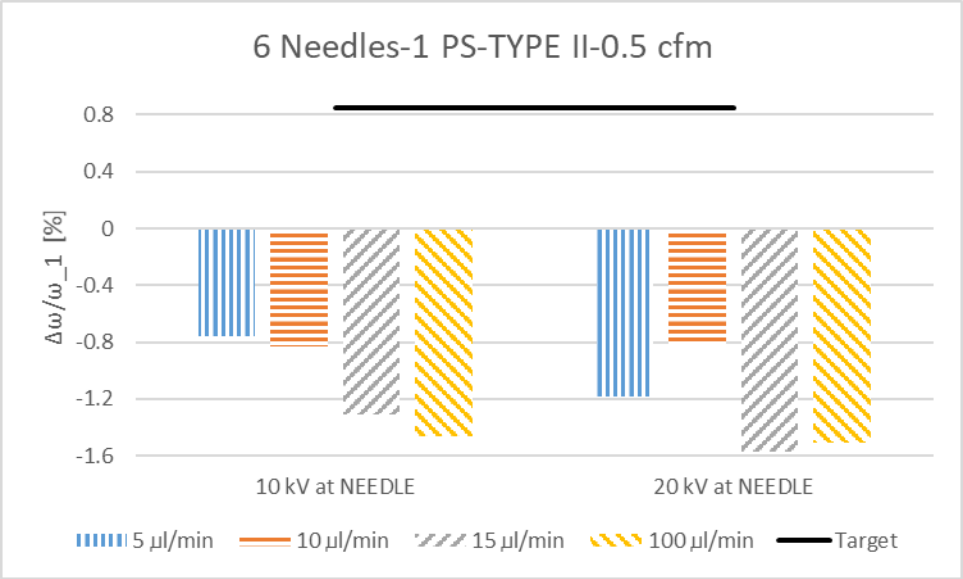

Fig. 45: Dehumidification result first experimental campaign (6 Needle – 1 PS (-) at needles – Type II – 0.5 cfm) and two different high voltage potentials to the electrode (10, 20 kV)

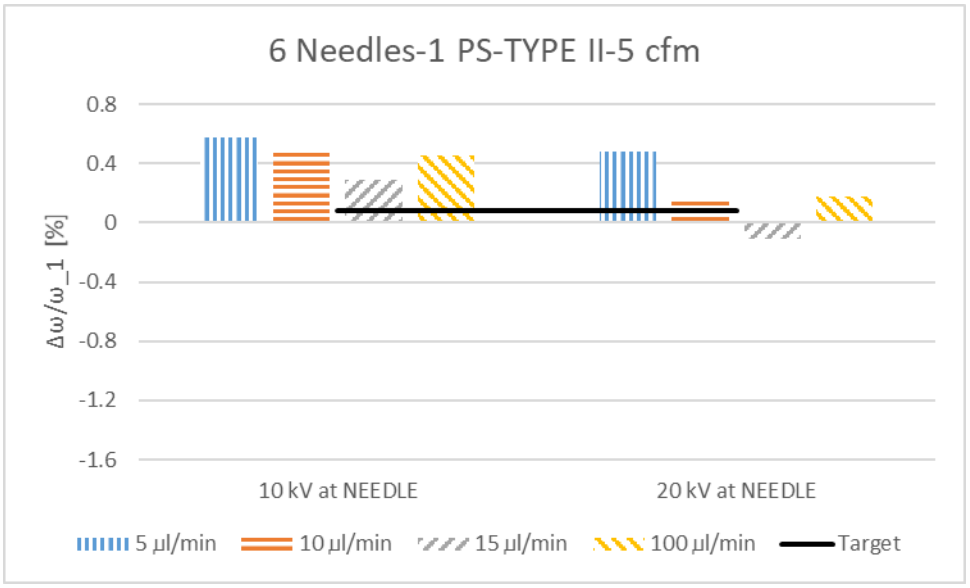

Fig. 46: Dehumidification results first experimental campaign (6 Needle – 1 PS (-) at needles – Type II – 5 cfm) and two different high voltage potentials to the needles (10, 20 kV)

The tests with only one power supply were not repeated, and the experimental error bars were not provided. Particularly interesting was the fact that dehumidification rates higher than the predictions of the model were obtained only for 5 cfm. The cases with 0.5 cfm provided instead humidification under the same conditions, even if, as already pointed out, cases with lower air flow rates should be easier to dehumidify.

With the goal to increase the electrospray current, Fig. 47 and 48 represent the results for deionized water type II for 0.5 cfm and 5 cfm respectively. Two (2) high voltage potentials, i.e. 10 and 20 kV, were applied to the needles when three (3) power supplies were used.

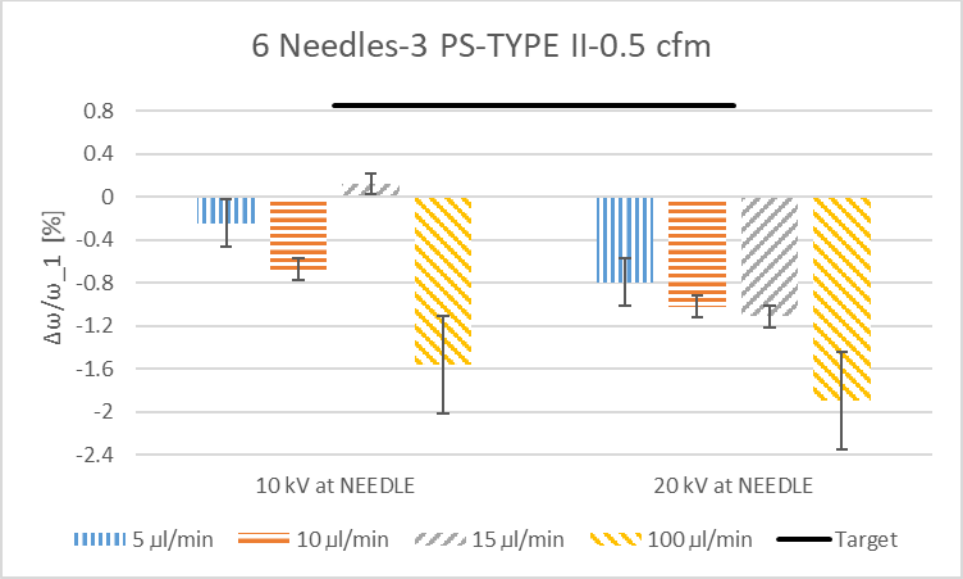

Fig. 47: Dehumidification results first experimental campaign (6 Needle – 3 PS (-) at needles – Type II – 0.5 cfm) and two different high voltage potentials to the needles (10, 20 kV)

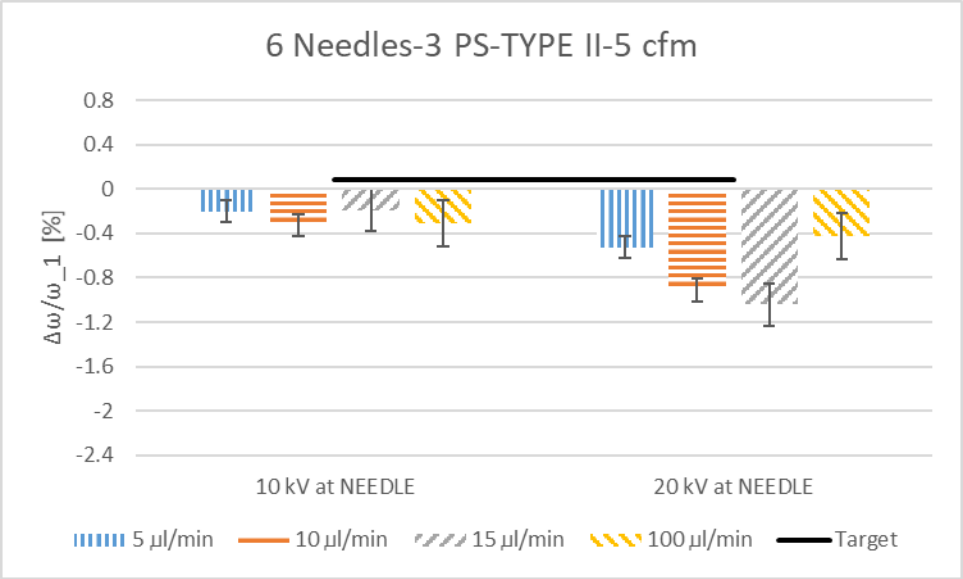

Fig. 48: Dehumidification results for the first experimental campaign (6 Needle – 3 PS (-) at needles – Type II – 5 cfm) and two different high voltage potentials to the needles (10, 20 kV)

The results with three (3) power supplies were again negative for the most. More consistent repeated tests were carried out when three (3) power supplies were utilized and the error bars for the

repeated tests are shown in the figures. The results were always smaller than the target black lines, and again consistently within the evaluated uncertainty for the dew point sensors.

In order to better assess the effect of multiple power supplies and try to explain the positive results with only one (1) power supply and 5 cfm, the electrospray current was measured for these cases. When only one power supply was used, the single multimeter measured the current delivered simultaneously by all the six (6) electrospray heads. When three power supply were used, the single multimeter measured the current delivered simultaneously by only two (2) electrospray heads.

Fig. 49 and 50 shows the current measurements for deionized water type II for 0.5 and 5 cfm respectively.

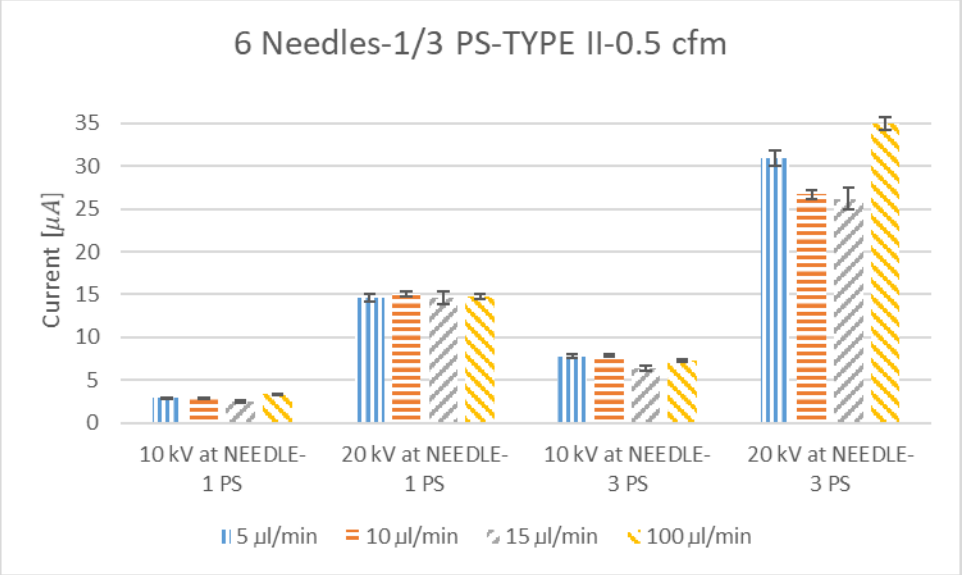

Fig. 49: Electrospray current for the first experimental campaign (6 Needles – 1/3 PS – Type II – 0.5 cfm) and two different high voltage potentials to the needles (10, 20 kV)

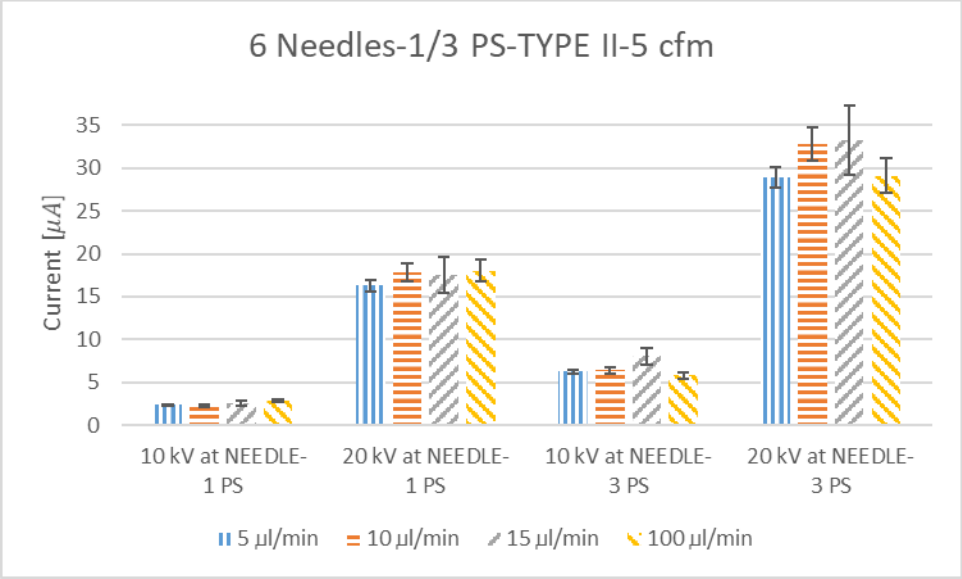

Fig. 50: Electrospray current for the first experimental campaign (6 Needles – 1/3 PS – Type II – 5 cfm) and two different high voltage potentials to the needles (10, 20 kV)

The measured current increased with the high voltage potential and with the number of power supplies simultaneously used. Comparing the current measurements between 0.5 and 5 cfm cases, no significant differences were noticed for all the conditions considered. For instance, the currents delivered by three (3) power supplies at 10 kV were essentially comparable between the 0.5 and 5 cfm cases. This made particularly tricky the explanation of the results obtained with 5 cfm, considering also that, to have the same dehumidification rate at a higher air flow rate, the vapor to effectively wipe out from the air increased. A direct measurement of the charge and size of the droplets could have helped with a better explanation of these unexpected results.

When three power supplies were tested in parallel, the highest electrospray current per electrospray head was registered, i.e. a current equal to about 35 μA. With this current, the maximum power consumption per head could be estimated, and it resulted equal to 0.7 W, when 20 kV was applied. A more detailed analysis on the power consumption and the potential savings with compared to conventional dehumidification processes was not performed because, even if the electrical charge

prevented the complete evaporation of the droplets, it was not enough to allow for a consistent dehumidification. For instance, with six (6) electrospray heads the results indicated humidification for the most, while, to save energy, dehumidification must be achieved instead. However, if the electrostatically enhanced condensation system could reduce the latent load of the conventional A/C system, the energy efficiency of the overall A/C system would be improved due to a reduction of the temperature lift in the A/C system and an improvement of the Energy Efficiency Ratio (EER).

The same experimental procedure was adopted to test also deionized water type IV, which had the highest electrical conductivity. Both positive and negative high voltage potentials were applied to the heads, at 10 and 20 kV, when up to three (3) power supplies were connected in parallel. All the four (4) water flow rates were tested both at 0.5 and 5 cfm. The results are not shown considering that also with type IV the dehumidification rates were in general negative, with similar considerations to the cases previously discussed.

To summarize, the dehumidification rate expressed in terms of $\frac{\Delta\omega}{\omega_1}$ ratio was estimated for three (3) different water kinds, when mainly 33 gauge needles were used. Up to six (6) electrospray heads were tested with up to three (3) power supplies. This exploratory experimental investigation was carried out with the main goal to explore if a considerable, i.e. about 5 % in terms of relative humidity, dehumidification rate could be achieved. This dehumidification rate, which was higher than the predictions of the thermodynamics model, was recorded in a few works available in the open literature.

In general, under the conditions investigated, the dehumidification rate was very limited, and only in a few cases, when only one electrospray head was used, it reached or exceeded the values predicted by the thermodynamic model. More often the dehumidification rates were negative, suggesting that humidification instead of dehumidification was occurring. However, the obtained humidification rates were higher than the maximum humidification predicted if all the water was assumed to evaporate, as it is possible to see in Fig. 51 for 0.5 cfm and Fig. 52 for 5 cfm.

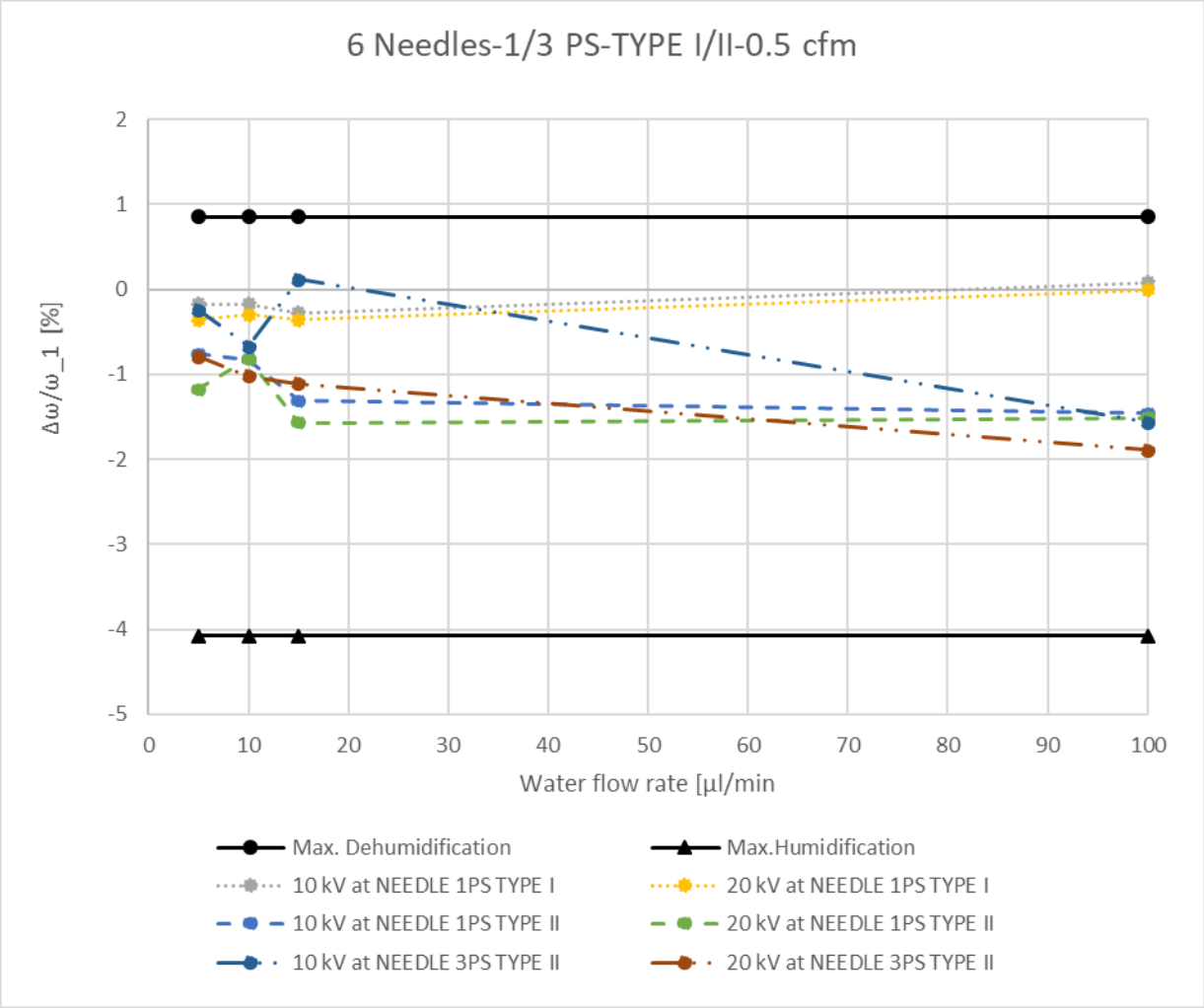

Fig. 51: Comparison between the actual dehumidification rates and the maximum dehumidification/humidification potential for 6 needles and 0.5 cfm

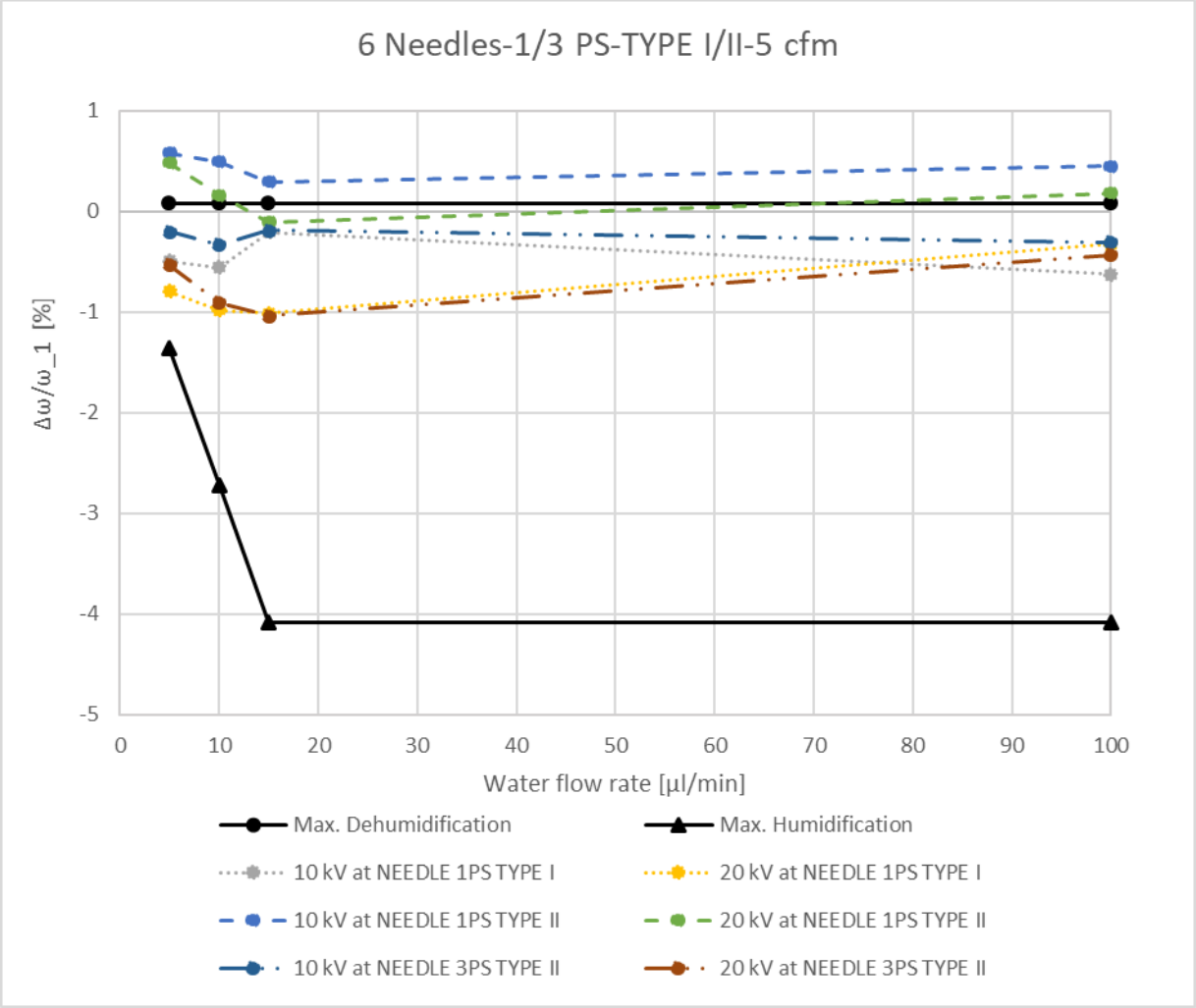

Fig. 52: Comparison between the actual dehumidification rates and the maximum dehumidification/humidification potential for 6 needles and 5 cfm

The solid black lines represent the two limits of maximum dehumidification and humidification. The actual dehumidification rates obtained with 6 needles and an air flow rate of 0.5 and 5 cfm are reported in the figures as well. The actual dehumidification rates were in general included between the two limits, with the exceptions of the dehumidification rates obtained with 5 cfm, 10 and 20 kV, one power supply and water type I. In these cases, the actual dehumidification rates were slightly higher than the predictions of the thermodynamic model. For all the air flow rates tested, the actual dehumidification

rates were always higher than the maximum humidification limit, showing that the electrical charge of the droplets prevented the complete evaporation of small droplets.

These preliminary data, in many cases negative or lower than the predictions of the model, may be attributed to many causes. In particular, in the actual spray injection tests, ideal conditions were not achievable. For instance, the relative humidity tested was equal to 90 % and not 100 %, and more likely the water droplets were not charged to their maximum limit. In addition, the size of the droplets, which was only estimated with correlations available in the literature, might not correspond to the desired one in the actual experimental tests.

Due to the absence of direct measurements of the size and charge of the droplets, some results were indeed difficult to explain with the current set up. For instance, it was counterintuitive that a better dehumidification rate was obtained with 5 cfm rather than with 0.5 cfm, when the same operating conditions were tested with six (6) electrospray heads and water type II. In this case it would have been fundamental the direct investigation and measurements of the droplets charge and size, key parameters for an improved dehumidification. A direct investigation would have allowed the comparison of the droplet size and charge between the two cases. It would have also allowed the assessment of the presence of disrupting or discharge phenomena in the conditions tested. This would have shed light of why a better dehumidification rate was not achieved for the highest electrospray current cases. In fact, the electrospray current was a good estimation of the charge droplets only if these disrupting phenomena did not occur. This kind of analysis is usually performed with phase doppler anemometry (PDA) devices, but their capital expenditure was too high to be justified for these exploratory tests. These exploratory tests were in fact carried out to find out that combination of working parameters to achieve a dehumidification rate similar to the one obtained in [16]**.** This target dehumidification was however never achieved for any of the conditions tested and a modification of the set up was made as a further attempt to get closer to the target dehumidification and replicate as closer as possible the set up in [16]**.** In particular, a smaller cross

section area was considered, and a positive high voltage was only applied at the plate electrode. The experimental tests carried out in the second campaign accommodated these modifications. Also, in this second campaign the direct measurements of droplet charge and size were not implemented and the main goal was to achieve a dehumidification rate such as to justify further analysis.

7.3 Second Experimental Campaign

The second experimental campaign was carried out after the first one to bring some major modifications, which were mainly inspired by the experimental set up described in [16]. In this set up, four (4) electrospray heads were installed on the bottom surface of the air duct, while the plate electrode was installed on the top surface of the air duct and it was electrified by a positive high voltage power supply, when a 10 $M\Omega$ resistor was connected to reduce the electrospray current. The heads were instead grounded. The air flow rate tested was extremely limited, i.e. 0.04 cfm (this was found out after a direct email communication with the authors of the paper), different inlet relative humidity, such as 70, 80 and 90 %, were tested and a dehumidification rate in terms of relative humidity of about 5 % was experienced in all the conditions tested, considering only the effect of negative corona discharge from charged water droplets. The levels of inlet humidity were achieved thanks to ultrasonic humidifiers. When also the effect of the water absorbing materials, placed on top of the plate electrode, was considered, a total reduction of about 10 % in terms of relative humidity was achieved.

These results, obtained without any need of cooling power but only with water absorbing materials, were extremely promising and the same conditions and set up were then replicated to obtain more conclusive results. In fact, the results obtained in the previous experimental campaign were often within the noise or uncertainty of the dew point sensors and it was premature to draw any conclusion. The only claim that could have been done, analyzing those results, was that the results did not contradict the thermodynamics model, which predicted very limited dehumidification even under ideal conditions.

To accommodate these modifications with the goal to achieve a 5 % dehumidification with 5 cfm, the position of the electrospray heads was moved from the inlet converging duct to the long straight square section duct. The main modifications with respect to the previous campaign were then the variation of the position along the test apparatus, i.e. to allow for a much smaller cross sectional area, the employment of four (4) grounded electrospray heads and a plate electrode at high voltage positive potential with a 10 $M\Omega$ resistor, and the use of water absorbing materials. The main challenge was that, only after a direct email exchange with the authors of the paper in Japanese, it was found out that the air flow rate tested was only 0.04 cfm, two order of magnitude lower than the target air flow rate for this research. This flow rate was not achievable or accurately measurable in our wind tunnel and test apparatus, which were thought for larger applications. It was then required to extrapolate the results obtained with 0.04 cfm for larger air flow rates, as shown in Table 15**,** and, after the extrapolation, the predicted dehumidification rates were way lower than the target for this project and resulted again within the noise or uncertainty of the dew point sensors. This extrapolation was however in good agreement with the predictions of the thermodynamics model.

Regardless the main challenge on the air flow rate, the tests with this new set up were still carried out in order to build more confidence on the previous results and have an additional verification of the limited dehumidification that can be achieved with this set up.

The tests were carried out with a positive high voltage potential of 10 kV applied at the plate electrode, both with the steam humidifier and the stream humidifier combined with the two ultrasonic humidifiers to reach a 90 $\%$ inlet relative humidity. To give more details on the air water content correction, Table 16 is provided.

Table 16: $\frac{\Delta\omega}{\omega_1}$ for multiple iso-ω tests carried out for each day when the spray injection tests were performed

Iso-ω tests	$\frac{\Delta\omega}{\omega_1}$ [%] **ratio (average of multiple iso-ω tests)**
Test 1	- 0.41
Test 2	0.43
Test 3	1.13

It represents the $\frac{\Delta\omega}{\omega_1}$ ratio of the multiple iso-ω tests carried out for each day when the spray injection tests were performed. This ratio was in general within the predicted uncertanty, as it is possible to see in the Table 16**.** Usually up to three iso-ω tests were carried out for each day of testing and the resulting average ratio for the iso-ω tests were subtracted from $\frac{\Delta\omega}{\omega_1}$ ratio obtained for each spray injection test.

Fig. 51 and 52 show the results for the only steam humidifier and for the stream humidifier combined with the two ultrasonic humidifier cases respectively.

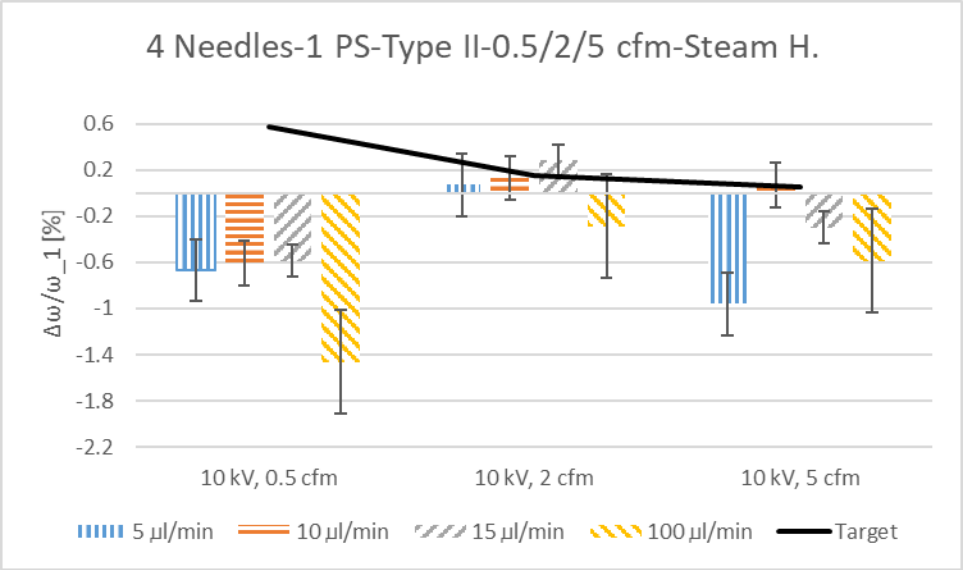

Fig. 53: Dehumidification results second experimental campaign (4 Needle – 1 PS (+) at electrode – Type II – 0.5/2/5 cfm), high voltage potential to the electrode (10 kV), only steam humidifier

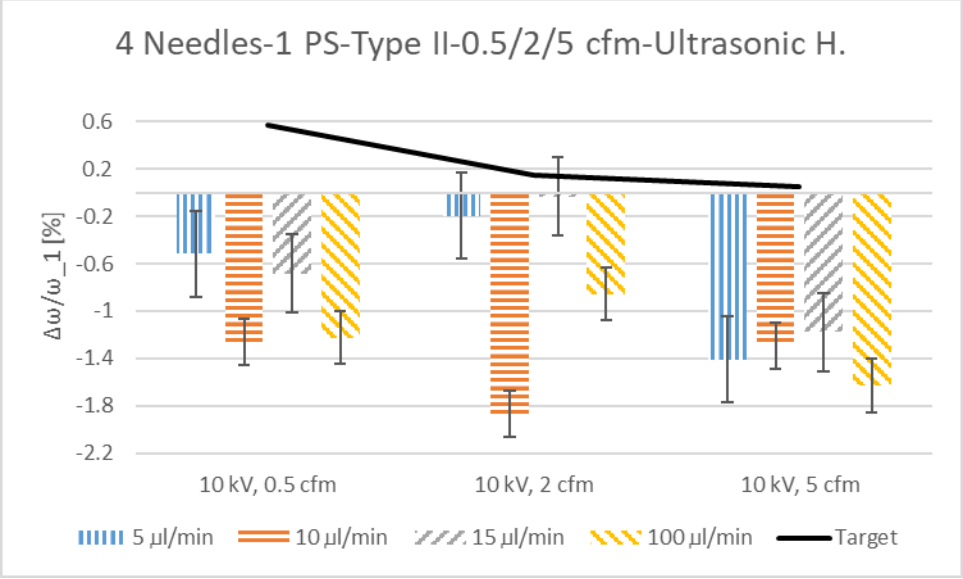

Fig. 54: Dehumidification results second experimental campaign (4 Needle – 1 PS (+) at electrode – Type II – 0.5/2/5 cfm), high voltage potential to the electrode (10 kV), steam and ultrasonic humidifier

The target black line, represented in Fig. 53 and Fig. 54, was a function of the air flow rates, when the number of injected droplets were fixed. In particular, the maximum dehumidification potential decreased as the air flow rate increased.

Also for these new set of tests, the dehumidification rate was in general negative, i.e. humidification of the air stream was actually occurring. A few dehumidification rates, close or higher to the predictions of the model, were experienced when only the steam humidifier was used with 2 and 5 cfm. All the results were higher than the maximum humidification limit. These results confirmed the trends of the previous results, where mainly negative bars, i.e. humidification, were experienced.

The electrospray current was also measured for both cases. Fig. 53 and 54 show the results for the only steam humidifier and for the stream humidifier combined with the two ultrasonic humidifier cases respectively.

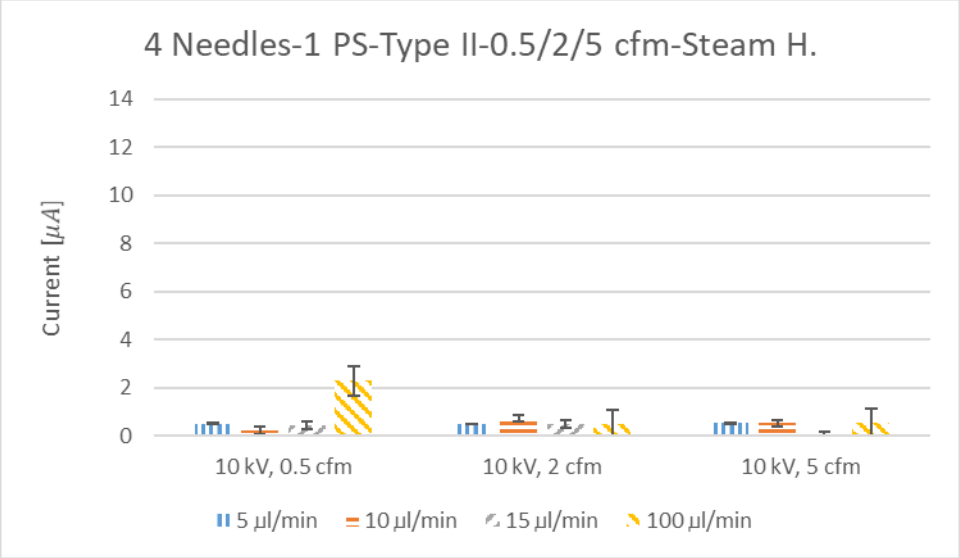

Fig. 55: Electrospray current second experimental campaign (4 Needle – 1 PS (+) at electrode – Type II – 0.5/2/5 cfm), high voltage potential to the electrode (10 kV), only steam humidifier

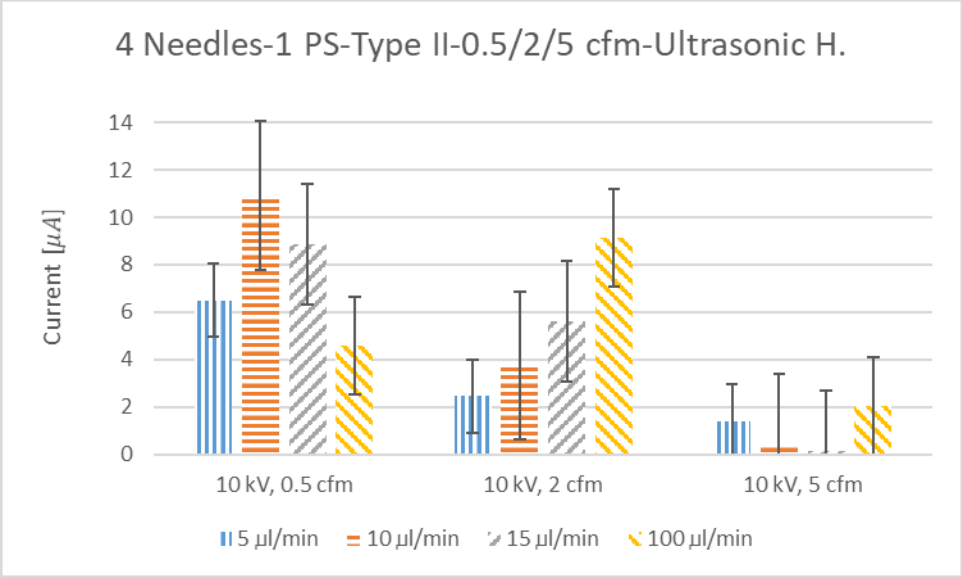

Fig. 56: Electrospray current second experimental campaign (4 Needle – 1 PS (+) at electrode – Type II – 0.5/2/5 cfm), high voltage potential to the electrode (10 kV), steam and ultrasonic humidifier

A particularly high difference in current level was registered passing from the only steam humidifier case to steam humidifier combined to the two ultrasonic humidifiers case. Slightly better dehumidification results with more positive bars were obtained when the current was lower, and, once again, a direct measurement of the droplets size and charge would have been essential for a good assessment of this interesting phenomenon.

Chapter 8: Conclusion

This research work investigated the potential of a new electrostatic based water vapor separation system for humidity control in buildings. Electrostatically enhanced condensation was considered and investigated to finely control humidity with limited energy consumption. In these electrostatically enhanced processes, water vapor was attracted and condensed on the surface of small highly charged droplets thanks to dielectrophoresis and diffusion.

This thesis showed the extremely demanding conditions for the droplets required for an enhanced dehumidification, and the experimental data highlighted the difficulties in obtaining considerable dehumidification under the laboratory conditions tested in the initial experimental investigation, that was presented in this thesis.

The thermodynamics model developed during this thesis predicted water vapor condensation for very small droplets at a high electrical charge. The optimal initial droplet diameter range promoting dehumidification resulted in about 2 to 4 μm, with an optimal at 3.6 μm when droplets were charged to their maximum limit and saturation air conditions were considered. Overall, electrospraying was shown to be a promising technology to generate small and highly electrically charged droplets, in the range predicted by the model. The cone jet mode was identified as the most suitable operational mode to produce droplets monodisperse in size and charge. Its stability was analyzed in detail and scaling laws available in the literature may be used to estimate the droplet size and charge in the stable cone jet mode. In terms of dehumidification rates, the model predicted very limited rates, and lower than the original target of this project, if up to six (6) electrospray heads were considered. This dehumidification rate could be improved increasing the number of droplets with the correct size and charge injected in the air stream

to dehumidify. However, the number of electrospray heads required to meet the target dehumidification rate was not possible to assemble in the laboratory during the period of this initial investigation.

In order to validate the model and with the goal to achieve a dehumidification rate of 5 % in terms of relative humidity with an air flow rate of 5 cfm, a new experimental test setup was designed, constructed and operated in order to facilitate these experiments. These experiments aimed to evaluate the air water content differential before and after the test section where the electrospray heads were installed. The air water content differential was evaluated in terms of the $\frac{\Delta\omega}{\omega_1}$ ratio, to eliminate the dependence on the dry bulb temperature along the test apparatus.

Working parameters, such as air and water flow rates, high voltage potentials and polarity, deionized water types with different electrical conductivity, were varied to find the best combination for an improved dehumidification. Two different experimental campaigns were carried out to explore mainly the effect of a different cross section area and a different high voltage electrical configuration. The inlet conditions to the test section were kept constant at about 68 °F and 90 % relative humidity, considering that higher dehumidification rates were predicted for saturated conditions. The dehumidification rates in terms of the air water content were then evaluated during thirty minutes spray injection tests. With the set up used and the conditions considered, limited dehumidification rates were achieved, and, in general, the dehumidification rate was lower than 1 % for the air flow rates considered in the present study. Frequently the dehumidification rate was negative, suggesting that humidification instead of dehumidification was actually occurring. These rates were within the uncertainty of the dew point sensors. For example, a negative dehumidification rate did not necessary mean humidification, if the measurement was within the uncertainty of the sensors.

The limited results gathered in the present thesis highlighted the complexity of the implementation of the electrostatically enhanced condensation processes, even in a laboratory setting. The reasons for these limited, frequently negative, results could be multiple. In particular, the already

limited predictions of the model were made under ideal conditions, such as saturation air conditions and droplets charged to their limit dictated by the Rayleigh model, which it was not possible to replicate in the spray injection tests, for practical reasons. Another additional explanation may be the fact the droplets did not have the right size and charge, and direct measurements of these parameters may then be useful.

As compared to the literature, the results obtained in some experimental investigations in previous published studies were not fully replicated in the work presented in this thesis. The main differences in this work were higher air flow rates and complete absence of any cooling power, which was implemented in one study in the literature to facilitate the vapor condensation.

This thesis provided the theoretical background and the preliminary experimental methodology for further investigations of electrostatically enhanced dehumidification processes. This thesis investigated water vapor attraction and condensation due to dielectrophoresis and diffusion, while additional features, such as the use of cooling power, may be necessary to reach a 5% dehumidification rate.

Chapter 9: Recommendations for Future Work

Together with the thermodynamics model for the prediction of the maximum dehumidification potential under ideal conditions, it would be beneficial to develop a dynamics model for electrostatically enhanced dehumidification processes. In particular, the dynamics model would be helpful to evaluate the droplets' growth and assess if the droplets have enough time to reach the limit predicted by the thermodynamics model. In addition, it may suggest some geometrical and flow features for the implementation of an effective dehumidification system. This analysis may be carried out with computational fluid dynamics (CFD) simulation software. This kind of analysis aimed to the development of a dynamics model is currently carried out in the same research group.

Some of the experimental results were difficult to evaluate and explain with the current set up and sensors. In particular, direct measurements of the droplet size and electrical charge, key parameters for an improved dehumidification, may facilitate a more comprehensive analysis and explanation of the results. PDA systems appear to be best candidates for these measurements. However, their high capital expenditure may be an obstacle for their adoption.

In this initial experimental investigation, it was not possible to achieve the target dehumidification rate of 5 % in terms of relative humidity with 5 cfm. In particular, the dehumidification rates obtained were limited and often within the uncertainty of the dew point sensors. Additional ways to increase these rates should be investigated. According to the thermodynamics model, this could be accomplished by increasing the number of droplets with the correct size and charge injected in the air stream. A higher number of electrospray heads or other kind of commercial spray nozzle may be investigated, provided that droplets with the correct size and charge can be produced. A number of electrospray heads so that

the measured dehumidification rate is outside the uncertainty of the sensors may be consider to obtain more conclusive results.

Additional features, such as the use of cooling coils or thermoelectric coolers, may be investigated to increase the dehumidification rates.

References

[1] C. T. R. Wilson, “Condensation of water vapor in the presence of dust free air and other gases,” Philos. Trans. R. Soc. Lond. A, vol. 189, pp. 265–307, Jan. 1897.

[2] C. T. R. Wilson, “On the comparative efficiency as condensation nuclei of positively and negatively charged ions,” Philos. Trans. R. Soc. Lond. A, vol. 193, pp. 289–308, Jan. 1900.

[3] A. I. Rusanov, “Thermodynamic theory of nucleation on charged particles,” J. Colloid Interface Sci., vol. 68, no. 1, pp. 32–47, Jan. 1979.

[4] M. D. Cohen, R. C. Flagan, and J. H. Seinfeld, “Studies of concentrated electrolyte solutions using the electrodynamic balance: 1. Water activities for single-electrolyte solutions,” J. Phys. Chem., vol. 91, no. 17, pp. 4563– 4574, Aug. 1987.

[5] J. J. Thomson, G.P. Thomson, Conduction of Electricity through Gases, Cambridge University Press, vol. 1, pp. 310-337, 1928.

[6] F. M. Kuni, A. K. Shchekin, and A. I. Rusanov, “Theory of nucleation on charged cores: 2. Thermodynamic parameters of an equilibrium nucleus,” Colloid J. USSR, vol. 44, no. 6, pp. 935–941, 1982.

[7] S. W. Thomson, “On the equilibrium of vapor at a curved surface of liquid,” Philos. Mag., ser. Series 4, vol. 42, no. 282, pp. 448–452, 1871.

[8] H. A. Pohl, Dielectrophoresis: The Behavior of Neutral Matter in Non-uniform Electric Fields (Cambridge Monographs on Physics). Cambridge, U.K.: Cambridge Univ. Press, 1978.

[9] F. Yu, “Modified Kelvin-Thomson equation considering ion-dipole interaction: Comparison with observed ion-clustering enthalpies and entropies,” J. Chem. Phys., vol. 122, no. 8, p. 084503, Feb. 2005.

[10] S. Sakataa and T. Okada, “Effect of humidity on hydrated cluster-ion formation in a clean room corona discharge neutralizer,” J. Aerosol Sci., vol. 25, no. 5, pp. 879–893, Jul. 1994.

[11] M. Alonso and F. J. Alguacil, “Particle size distribution modification during and after electrical charging: Comparison between a corona ionizer and a radioactive neutralizer,” Aerosol Air Qual. Res., vol. 8, no. 4, pp. 366–380, Dec. 2008.

[12] M. Reznikov, "Electrically Enhanced Condensation I: Effects of Corona Discharge," in IEEE Transactions on Industry Applications, vol. 51, no. 2, pp. 1137-1145, March-April 2015, doi: 10.1109/TIA.2014.2354734.

[13] M. Salazar, K. Minakata and M. Reznikov, "Electrically Enhanced Condensation II: Effects of the Electrospray," in IEEE Transactions on Industry Applications, vol. 51, no. 2, pp. 1146-1152, March-April 2015, doi: 10.1109/TIA.2014.2344508.

[14] M. Reznikov, M. Salazar, M. Lopez, and M. Rivera-Sustache, “Electrically enhanced harvesting of water vapor from the air,” in Proc. ESA Annu. Meeting Electrostatics, 2015.

[15] M. Reznikov, M. Salazar, M. Page and M. Rivera-Sustache, "Further Progress in the Electrostatic Nucleation of Water Vapor," in IEEE Transactions on Industry Applications, vol. 54, no. 1, pp. 591-598, Jan.-Feb. 2018, doi: 10.1109/TIA.2017.2755579.

[16] Y. Higashiyama, M. Kamada, Dehumidification using negative corona discharge from a water droplet, Proc. Annu. Electrostatics, 2017.

[17] H. Liu, H. Yang, R. Qi, “A review of electrically driven dehumidification technology for air-conditioning systems,” Applied Energy, vol 279, 2020.

[18] Zhao, Shaoxing, G. S. Peter Castle and Kazimierz Adamiak. “Comparison of conduction and induction charging in liquid spraying.” Journal of Electrostatics 63 (2005): 871-876.

[19] A. Jaworek, Micro- and nanoparticle production by electrospraying, Powder Tech., vol. 176, pp. 18-35, (2007).

[20] T. Gemci, R. Hitron, N. Chigier, Determination of individual droplet charge in electrosprays from PDPA measurements, Zaragoza, vol. 9, pp.11 (2002).

[21] Gu, Wenhua & Heil, Philip & Choi, Hyungsoo & Kim, Kyekyoon. (2007). Comprehensive model for fine Coulomb fission of liquid droplets charged to Rayleigh limit. Applied Physics Letters. 91. 064104 - 064104. 10.1063/1.2767774.

[22] M. Cloupeau, B. Prunet-Foch, Electrostatic spraying of liquids. Main functioning modes, J. Electrost. 25 (1990) 165–184.

[23] M. Cloupeau, B. Prunet-Foch, Electrohydrodynamic spraying functioning modes, a critical review, J. Aerosol Sci. 25 (6) (1994) 1121–1136.

[24] Chen, Da-Ren, David Y. H. Pui and Stanley L. Kaufman. “Electrospraying of conducting liquids for monodisperse aerosol generation in the 4 nm to 1.8 µm diameter range.” Journal of Aerosol Science 26 (1995): 963-977.

[25] K. Tang, A. Gomez, Generation by electrospray of monodisperse water droplets for targeted drug delivery by inhalation, J. Aerosol Sci. Vol. 25 No. 6 (1994) 1237-1249.

[26] K. Tang, A. Gomez, Generation of monodisperse water droplets from electrosprays in a corona-assisted cone-jet mode, J. of Colloid and Interface Science 175 (1995) 326-332.

[27] J.F. de la Mora, I.G. Loscertales, The current emitted by highly conducting Taylor cones, J. Fluid Mech., vol. 260, pp. 155-184, (1994).

[28] A.M. Gañan-Calvo, The surface charge in electrospraying: its nature and its universal scaling laws, J. Aerosol Sci., vol. 30, no. 7, pp. 863-872, (1999).

[29] J.F. de la Mora, I.G. Loscertales, The current emitted by highly conducting Taylor cones, J. Fluid Mech. 260 (1994) 155–184.

[30] L. de Juan, J.F. de la Mora, Charge and size distributions of electrospray drops, J. of Colloid and Interface Science 186 (1997) 280-293.

[31] Bigi, A. (2012). First Experimental Results of a Vortical Direct-contact Heat Exchanger for HVAC Systems. MS Thesis of work conducted under the direction of Dr. Lorenzo Cremaschi, Thesis is published at the Milan Polytechnic Institute, Milan, Italy.

[32] Cremaschi, L., Adanur, B. M., Harges, E., 2019. “Effect of humidity and airflow velocity on droplets elapsed time and radius at the onset of freezing and frost nucleation for super-hydrophilic and super-hydrophobic surfaces.” ASTFE Digital Library. Begel House Inc. doi: 10.1615/TFEC2019.phc.026880

[33] Adanur, B., Cremaschi, L., Harges, E., 2019. “Effect of mixed hydrophilic and hydrophobic surface coatings on droplets freezing and subsequent frost growth during air forced convection channel flows.” Science and Technology for the Built Environment 25(10), pp. 1302-1312. doi: 10.1080/23744731.2019.1648981.

[34] A. Jaworek, “Micro- and nanoparticle production by electrospraying.” Powder Technology, Volume 176, Issue 1, 2007, Pages 18-35.

[35] J.P. Borra, Y. Tombette, P. Ehouarn, “Influence of electric field profile and polarity on the mode of ehda related to electric discharge regimes.” Journal of Aerosol Science, Volume 30, Issue 7, 1999, Pages 913-925.

[36] J.-P. Borra, P. Ehouarn, D. Boulaud, “Electrohydrodynamic atomisation of water stabilised by glow discharge—operating range and droplet properties.” Journal of Aerosol Science, Volume 35, Issue 11, 2004, Pages 1313-1332.

[37] J.M López-Herrera, A Barrero, A Boucard, I.G Loscertales, M Márquez, “An experimental study of the electrospraying of water in air at atmospheric pressure.” Journal of the American Society for Mass Spectrometry, Volume 15, Issue 2, 2004, Pages 253-259.

[38] Jean-Pascal Borra, “Review on water electro-sprays and applications of charged drops with focus on the corona-assisted cone-jet mode for High Efficiency Air Filtration by wet electro-scrubbing of aerosols.” Journal of Aerosol Science, Volume 125, 2018, Pages 208-236.

[39] I Hayati, A Bailey, Th.F Tadros, “Investigations into the mechanism of electrohydrodynamic spraying of liquids: II. Mechanism of stable jet formation and electrical forces acting on a liquid cone.” Journal of Colloid and Interface Science, Volume 117, Issue 1, 1987, Pages 222-230.

Appendix

The bar charts reported in Chapter 7 represent the average dehumidification rates during the spray injection tests. When the CO_2 flow was tested, the iso-ω considered also the presence of the CO_2. In case of not repeated tests, the corrected, i.e. following the correction on the air water content procedure already described, average dehumidification rate during the single spray injection test was reported. In case of repeated tests, the average of all the dehumidification rates obtained in the repeated spray injection tests was reported.

As an example, the calculation required to obtain the bars for 5 and 10 $\mu l/min$ in Fig. 34, either with or without CO_2, is presented. First of all, an iso-ω test was carried out and the ratio $\frac{\Delta\omega}{\omega_1}$ was evaluated. This offset, evaluated during the iso-ω test, was subtracted from the ratio $\frac{\Delta\omega}{\omega_1}$, evaluated during the spray injection tests. The inlet and outlet air water content was evaluated with the average inlet and outlet dry bulb and dew point temperatures, during the 30 minutes tests. Table 17 shows sample calculations for the estimation of the average corrected dehumidification rates in Fig. 34, for 5 and 10 $\mu l/min$, 10 kV and 0.5 cfm.

Table 17: Sample calculations for the estimation of the average corrected dehumidification rates in Fig. 34, for 5 and 10 $\mu l/min$, 10 kV and 0.5 cfm.

	$T_{dry,in}$ [°F]	$T_{dew,in}$ [°F]	ω_{in} $[\frac{grains}{lbm}]$	$T_{dry,out}$ [°F]	$T_{dew,out}$ [°F]	ω_{out} $[\frac{grains}{lbm}]$	$\frac{\Delta\omega}{\omega_{in}}$ [%]	$\frac{\Delta\omega}{\omega_{in}}$ $cor.$ [%]
$\mathbf{iso-\omega}$ $\mathbf{5\ \mu l/min}$	66.05	65.58	94.42	66.12	65.42	93.88	0.57	-
$\boldsymbol{CO_2\ and}$ $\mathbf{10\ kV}$ $\boldsymbol{at\ NEEDLE}$ $\mathbf{5\ \mu l/min}$	65.56	65.29	93.46	65.71	65.09	92.79	0.72	0.15
$\mathbf{10\ kV}$ $\boldsymbol{at\ NEEDLE}$ $\mathbf{5\ \mu l/min}$	65.45	65.15	93.02	65.57	64.83	91.93	1.17	0.59
$\mathbf{iso-\omega}$ $\mathbf{10\ \mu l/min}$	66.99	65.53	94.27	67.00	65.68	94.75	-0.51	-
$\boldsymbol{CO_2\ and}$ $\mathbf{10\ kV}$ $\boldsymbol{at\ NEEDLE}$ $\mathbf{10\ \mu l/min}$	67.53	65.40	93.83	67.60	65.46	94.04	-0.22	0.05
$\mathbf{10\ kV}$ $\boldsymbol{at\ NEEDLE}$ $\mathbf{10\ \mu l/min}$	67.59	65.27	93.41	67.67	65.38	93.77	-0.38	-0.12

The last column shows the corrected average dehumidification rates during the spray injection tests, and these values are shown in the bar charts in Chapter 7.

As an additional example, Table 18 shows sample calculations for the estimation of the average corrected dehumidification rates in Fig. 44, for all the water flow rates considered, 10 kV and 5 cfm instead of 0.5 cfm.

Table 18: Sample calculations for the estimation of the average corrected dehumidification rates in Fig. 44, for 5/10/15/100 $\mu l/min$, 10 kV and 5 cfm.

	$T_{dry,in}$ [°F]	$T_{dew,in}$ [°F]	ω_{in} $[\frac{grains}{lbm}]$	$T_{dry,out}$ [°F]	$T_{dew,out}$ [°F]	ω_{out} $[\frac{grains}{lbm}]$	$\frac{\Delta\omega}{\omega_{in}}$ [%]	$\frac{\Delta\omega}{\omega_{in}}$ $cor.$ [%]
$\mathbf{iso-\omega\ (1)}$	68.10	65.11	92.89	68.28	64.29	90.19	2.90	-
$\mathbf{iso-\omega\ (2)}$	68.05	65.36	93.70	68.27	64.61	91.24	2.63	-
$\mathbf{10\ kV\ at\ NEEDLE\ 5\ \mu l/min}$	68.21	65.36	93.71	68.61	64.72	91.59	2.27	-0.50
$\mathbf{10\ kV\ at\ NEEDLE\ 10\ \mu l/min}$	68.12	65.39	93.81	68.27	64.77	91.74	2.21	-0.55
$\mathbf{10\ kV\ at\ NEEDLE\ 15\ \mu l/min}$	68.15	65.19	93.13	68.19	64.46	90.74	2.56	-0.20
$\mathbf{10\ kV\ at\ NEEDLE\ 100\ \mu l/min}$	68.12	65.32	93.57	68.79	64.71	91.56	2.14	-0.63

In this case, two iso-ω tests were carried out during the single day of experimental investigation. The average of the dehumidification rates obtained in these two tests were then used to implement the correction on the air water content procedure previously described. The last column shows again the corrected average dehumidification rates during the spray injection tests, and these values are shown in the bar charts in Chapter 7.